Engineering at the Limits of the Nanoscale

by

Farnaz Niroui

B.A.Sc. Nanotechnology Engineering, University of Waterloo (2011)
S.M. Massachusetts Institute of Technology (2013)

Submitted to the Department of Electrical Engineering and Computer Science
in partial fulfillment of the requirements for the degree of

Doctor of Philosophy in Electrical Engineering and Computer Science

at the

MASSACHUSETTS INSTITUTE OF TECHNOLOGY

September 2017

MASSACHUSETTS INSTITUTE OF TECHNOLOGY
OCT 26 2017
LIBRARIES
ARCHIVES

© Massachusetts Institute of Technology 2017. All rights reserved.

Author .... Signature redacted ...
Department of Electrical Engineering and Computer Science
~~August 31,~~ 2017

Certified by .... Signature redacted ....
Vladimir Bulović
Professor of Electrical Engineering and Computer Science
Thesis Supervisor

Certified by ... Signature redacted ....
Jeffrey H. Lang
Professor of Electrical Engineering and Computer Science
Thesis Supervisor

Accepted by .... Signature redacted ....
Leslie A. Kolodziejski
Professor of Electrical Engineering and Computer Science
Chair, Department Committee on Graduate Students

Engineering at the Limits of the Nanoscale

by

Farnaz Niroui

Submitted to the Department of Electrical Engineering and Computer Science
on August 31, 2017, in partial fulfillment of the
requirements for the degree of
Doctor of Philosophy in Electrical Engineering and Computer Science

Abstract

At the nanoscale, unique properties and phenomena emerge that can lead to scientific and technological paradigms beyond those classically envisioned. Exploring these opportunities at the few-nanometer regime requires unprecedented precision, resolution, control and uniformity, not readily feasible through conventional fabrication and metrology techniques. In particular, the dynamic, reliable and reversible structural tuning of such small dimensions remains a great challenge, yet a promising platform to enable devices of new and improved functionalities. To overcome these challenges, alternative techniques are necessary to push the frontiers of nanoscale processing.

In this thesis, the challenges and prospects of engineering active devices at the limits of the nanoscale are evaluated using a case study that focuses on developing a new platform for nanoelectromechanical (NEM) switches. The proposed NEM switches that rely on electromechanical modulation of the tunneling current in <5 nm switching gaps possess the potential to overcome the limitations of the conventional counterparts – minimizing stiction and lowering the actuation voltage.

Combined top-down and bottom-up fabrication methodologies are introduced for achieving active structures of the desired complexity with nanometer precision, resolution and control. Integration of device engineering and physics with chemistry and materials science leverages an understanding of material synthesis, surfaces and interfaces to achieve manipulation of matter in the nanometer regime with a precision and control otherwise not feasible. Accordingly, two example hybrid fabrication techniques are introduced allowing precise fabrication of electrically-active nanogaps.

Molecules are proposed as nanoscale structural components which can also control surface interactions and forces utilizing their chemical and mechanical properties. When used as interconnects between neighboring surfaces, they can precisely define nanoscale spacings. Uniquely, the mechanics of the molecular layer can be used to allow controlled and reversible tuning of the spacing where the elastic restoring force of the molecules balances the dominating surface adhesive forces to allow for stable yet mechanically active structures. Feasibility of molecules as nanoscale scaffolds and springs are demonstrated in this work in an electromechanically tunable molecular tunneling junction.

In such a junction, changes in the tunneling gap leads to an exponential modulation of the tunneling current. If sufficiently large, this modulation can serve as a NEM switching mechanism. The molecules provide precision in defining small switching gaps necessary to reduce the actuation voltage while the force control provided through the molecular layer's mechanics helps control the surface adhesion. These proposed tunneling-based switches, referred to as "squitches", form a promising platform towards a more energy-efficient operation. Two- and multi-terminal designs of squitches are proposed and experimentally demonstrated with example devices showing actuation voltages <2 V and current modulations $>10^4$.

The design of squitches pushes the limits of nanoscale processing and broadly helps reveal the challenges and prospects of engineering at dimensions few nanometers in size. By implementing a multidisciplinary approach, one can gain access to the limits of the nanoscale to investigate the emerging physical phenomena and develop next generation nanodevices beyond squitches. The key is continuous development of versatile processing techniques allowing nanoscale manipulation and characterization with high precision and control.

Thesis Supervisor: Vladimir Bulović
Title: Professor of Electrical Engineering and Computer Science

Thesis Supervisor: Jeffrey H. Lang
Title: Professor of Electrical Engineering and Computer Science

Acknowledgments

It is hard to believe that six years have passed since I first joined MIT – years filled with new experiences and changes in perspectives that have helped me in my personal and career development in ways well beyond the bounds of my imagination. As my graduate school journey comes to an end, I reflect back on my experiences at MIT with great fondness – experiences made possible by the presence and support of wonderful colleagues, mentors and friends. It is my pleasure to acknowledge those who made this journey possible.

First and foremost, I would like to acknowledge my advisors, Professor Vladimir Bulović and Professor Jeffrey Lang. Vladimir's enthusiasm and passion for science, his caring and cheerful character, and his leadership have always been very inspiring. I thank Vladimir for providing me with an opportunity to be able to pursue my broad research interests and most importantly, for helping me develop as a researcher by being a great role model. I am also very fortunate to have had the opportunity to be co-advised by Jeff. I have always been in admiration of Jeff's technical knowledge for its breadth and depth, and touched by his genuine interest in teaching. I am thankful to Jeff for being such a great mentor, for always so patiently advising me on research and my future career. I will always be grateful to both my advisors for all that they taught me over the past six years.

I would also like to deeply thank Professor Marc Baldo and Professor Timothy Swager for always providing me with great advice and perspective about my research. Moreover, I thank them for being great mentors and for all their guidance in helping me define my future career path.

I have been fortunate to have had the opportunity to interact and collaborate with great colleagues from across MIT and UC Berkeley. The work in this thesis would not have been possible without the help of Professor Timothy Swager, Professor Jing Kong, Ellen Sletten and Yi Song. I thank them and also Wen Jie Ong and Pan Wang from Tim's group for always sharing their chemistry expertise with me. It has also been a great pleasure to collaborate with and learn from Professor Tsu-

Jae King Liu, Professor Eli Yablonovitch, Professor Junqiao Wu, Bivas Saha and Benjamin Osoba from UC Berkeley. Beyond the collaborations related to the work presented in this thesis, I also had the privilege to be involved in other collaborations with Professors Jeffrey Grossman, Marin Soljačić, Marc Baldo, Karl Berggren and their groups. I especially thank Jan Onchoke Tiepelt, Grace Han, Yi Yang and Di Zhu from these groups, and Sam Stranks from the Organic and Nanostructured Electronics Laboratory (ONE Lab) for their collaborations and for providing me with an opportunity to learn from them about intriguing fields beyond my main research area.

One of the most rewarding aspects of my graduate studies has been mentoring high school and undergraduate research interns. Mayuran Saravanapavanantham, Jatin Patil, Dan Drew and Petar Todorović have been wonderful to work with. I thank them for enthusiastically contributing to many of the projects presented in this thesis.

It has been a great opportunity to be part of the ONE Lab for the past few years. While covering a wide breadth of research areas and expertise, ONE lab provided me with an ideal environment to pursue my research and develop my skills. I thank all the group members, past and present, for creating an enjoyable work environment and assisting with the progress of my research. I would like to especially thank Wendi Chang, Joel Jean, Mengfei Wu, Melany Sponseller, Anna Osherov, Annie Wang, Jinchi Han, Apoorva Murarka, Tom Mahony, Rich Swartwout, Roberto Brenes and Tony Zhu, for their continuous support and friendship.

My time at MIT was made a more fruitful and enjoyable adventure over the past few years because of the companionship of great friends. I thank Brian Modtland, Tony Wu, Phillip Nadeau, Mary Mu, Joel Yuen-Zhou, Jean Anne Incorvia, Dan Congreve, Saima Siddiqui, Megan Roberts, Ellen Sletten, Ritchie Chen, Josué López, Yi Song, Wenjing Fang, Xi Ling, Shengxi Huang, Katherine Song, Grace Han and Joy Yang. I am fortunate to have had their friendship and I am very thankful to them for providing me with a most memorable graduate experience.

Sometimes individuals leave lasting impressions; life lessons that help define new directions and perspectives, regardless of the brevity of the interactions. I have been lucky over the past few years to learn from such individuals who eased my concerns at the most critical of times, inspiring me to work hard towards achieving my goals. I thank Professors Kathryn Whitehead, Naomi Matsuura, Jim Plummer, Jing Kong and the late Mildred Dresselhaus for their inspiration.

I also would like to thank the funding agencies that have supported my research. I acknowledge financial support from the Natural Sciences and Research Council of Canada (NSERC). I would like to thank the NSF Center for Energy Efficient Electronics Science (E^3S) and all its faculty, staff, student and postdoctoral members. Beyond financial support, importantly, E^3S provided me with a vibrant intellectual community from whom I learned lessons that have helped me in both my research and professional development. I appreciate all the collaborations that I had through this center and the mentorship of the great colleagues with whom I interacted.

This thesis would not have been possible without the unconditional support of my family. I thank them for always being there for me, helping me put things into perspective, reminding me about the importance of compassion, patience and persistence, teaching me to value failures as much as successes, and encouraging me to strive to always achieve my dreams. I am forever thankful and I dedicate this thesis to them.

My journey, over the past few years, has been filled with invaluable learning experiences and friendships that I will always cherish and reflect upon as I move towards future adventures with great motivation and excitement.

Farnaz Niroui
August 2017
Cambridge, MA

Contents

1 **Introduction** **27**

1.1 Engineering at the Limits of the Nanoscale 27

1.2 Towards Low-Voltage and Stiction-Free NEM Switches – A Case Study 29

1.3 Thesis Organization 32

I Fabrication with Nanometer Precision, Control and Uniformity **34**

2 **Combining Top-Down and Bottom-Up Fabrication: Hybrid Nanotechnologies** **35**

2.1 Top-Down Fabrication 35

2.2 Bottom-Up Fabrication 40

2.3 Hybrid Top-Down and Bottom-Up Fabrication 41

2.4 Summary 43

3 **Controlled Fabrication of Nanoscale Gaps using Stiction** **45**

3.1 Design Principles 46

3.2 Fabrication Flow 47

3.3 Controlled Formation of Nanogap Electrodes 49

3.4 Example Applications 51

3.4.1 Electrostatically Tunable Nanogaps 51

3.4.2 Molecular Tunneling Junctions 52

3.5 Challenges and Outlook 54

3.6 Summary 55

4 Fabrication of Nanoscale Gaps with Nanometer Resolution and Surface Uniformity 57

4.1 Design Principles 58
4.2 Fabrication Flow 58
4.3 Electrically-Active Nanogaps with Nanometer Resolution and Uniformity 62
4.4 Example Application 64
4.5 Challenges and Outlook 65
4.6 Summary 66

II Nanoscale Force Control – A Molecular Approach 68

5 Molecules and their Applications in Nanoscale Processing 69

5.1 Molecules as Structural Components 70
5.2 Engineering Surface Interactions with Molecules 72
5.3 Molecules as Nanoscale Scaffolds and Springs 73
5.4 Summary 77

6 Controlled and Reversible Tuning of Nanogap Electrodes 79

6.1 Design Principle 79
6.2 Fabrication Flow 81
6.3 Results and Discussions 82
6.4 Summary 87

III Device Design – Tunneling Nanoelectromechanical Switches towards Low-Voltage and Stiction-Free Performance 88

7 Two-Terminal Tunneling Nanoelectromechanical Switches 89

7.1 Operating Principles of Tunneling NEM Switches 90
  7.1.1 Tunneling Switching Mechanism 90

7.1.2 Squitch Design 91
7.2 Two-Terminal Squitch Fabrication Flow 93
7.3 Results and Discussions 96
7.4 Summary 100

8 Multi-Terminal Tunneling Nanoelectromechanical Switches 103
8.1 Multi-Terminal Squitch Design 103
8.2 Multi-Terminal Squitch Fabrication Flow 104
8.3 Results and Discussions 109
8.4 Summary 111

9 Summary and Outlook 113
9.1 Summary 113
9.2 Outlook 116
9.2.1 Tunneling NEM Switches - Squitches 116
9.2.2 Engineering at the Limits of the Nanoscale - Beyond Squitches 120

A An Overview of NEM Switches 125

B Synthesis of Au Nanoplates and Nanorods 127
B.1 Au Nanoplate Synthesis 127
B.2 Au Nanorod Synthesis 128

C Theoretical Simulation and Fitting of Experimental Results 131

List of Figures

1-1 Schematic representation of the design and performance of a cantilever-based NEM switch. (a) An electrostatic force ($F_{\text{electrostatic}}$) induced through an applied voltage combined with the van der Waals forces (F_{vdW}) cause collapse of the cantilever onto the opposing electrode to turn ON the device as they come into contact. Once the voltage is removed, the elastic restoring force (F_{elastic}) overcomes the surface adhesive forces to turn OFF the device. (b) The switching mechanism leads to a near zero OFF-state leakage current and an abrupt switching behavior with a large ON-OFF current ratio. . . 30

1-2 Pictorial thesis overview: To enable engineering at the limits of the nanoscale, an interdisciplinary approach is necessary to develop alternative techniques for nanoscale fabrication and force control, leading to new paradigms of active devices. 33

2-1 Hybrid top-down and bottom-up fabrication techniques enable complex active structures with nanometer precision, resolution and control. Top-down fabrication involves use of processes including lithography to machine down bulk materials into nanostructures. Alternatively, bottom-up techniques involve nanoscale building blocks that assemble into larger functional entities. Example nanoscale building blocks are depicted here including chemically-synthesized molecules, nanoparticles and nanomaterials, and nanostructures formed through top-down fabrication. 36

2-2 An overview of various lithographic techniques. 39

2-3 Nanostructures formed through top-down lithography, thermal evaporation of Au and lift-off. The scanning electron micrograph (left) shows the nonuniform edges of the structure while the atomic force microscope topography scan (right) shows ~4 nm roughness associated with the thermally-evaporated Au film. 40

2-4 Comparison between self-assembly and directed-assembly of Au nanocubes. (a) Self-assembly promoted through surface interactions allows formation of an ordered layer of chemically-synthesized Au nanocubes. (b) The precise positioning of the cubes can be directed utilizing physical templates formed lithographically in a poly(methyl-methacrylate) (PMMA) layer. 42

3-1 Controlled fabrication of nanoscale gaps using stiction: (a) multilayer PMMA e-beam resist is spun onto Si/SiO_2 substrate and baked after each spin at 180°C, (b) resist is patterned using e-beam to define cantilever and opposing electrodes separated by a defined gap "g_{13}", (c) resist is developed in 1:3 solution of MIBK in isopropanol, rinsed in isopropanol bath and dried under a stream of nitrogen, (d) ~10 nm of Cr and ~100 nm of Au is evaporated onto the patterned structures defining the electrodes. The gap formed after stiction (g'_{13}) is smaller than that originally patterned (g_{13}). Upon evaporation of the metallic layers, the gap becomes even smaller ($g^*_{13} < g'_{13} < g_{13}$). . . 48

3-2 An undercut structure formed in PMMA to enable electrical isolation between different device components upon evaporation of the Au film. . . . 49

3-3 Stiction promotes formation of nanogaps smaller than patterned: (a) Scanning electron micrograph (SEM) of a cantilever with a gap of ~200 nm, (b) SEM of the same cantilever positioned closer to Electrodes 2 and 3. Larger capillary force in (b) causes collapse of the cantilever, leading to stiction and reducing the gap between Electrodes 1 and 3. 50

3-4 SEM of nanogaps fabricated using the scheme in Figure 3-1. Capillary forces during wet developing of the pattern cause stiction between Electrodes 1 and 2, while forming a gap of ~35 nm (a) and ~10 nm (b) between Electrodes 1 and 3. The smaller gap in (b) is achieved by positioning Electrode 3 closer to 2. 51

3-5 Optimizing device architecture and electrode placement relative to the point of stiction allow achieving nanogaps with controlled width, useful for fabrication of multi-terminal devices. 52

3-6 Electromechanically modulated nanogap formed using the stiction-based fabrication technique. (a) Through altering device geometry to achieve smaller gaps and more flexible cantilevers, nanogaps can be fabricated to undergo electromechanical modulation (blue compared to red), useful for applications in NEM switches. Insets show corresponding devices with the bottom cantilever (blue) ~20 nm thinner than the top (red). The voltage is applied across Electrodes 1 and 2 and the current between them is monitored. (b) Prototype design of a three-terminal NEM switch with a source-drain gap of ~50 nm. The electrodes are labeled as per a comparable field-effect transistor. 53

3-7 (a) Nanogap electrodes formed using the stiction-based fabrication technique involving self-assembled molecular layers. The molecules can serve as coatings on the electrodes to modify surface interactions or can bridge the gap between the two electrodes forming a metal-molecule-metal structure. (b) Chemical structure of fluorinated decanethiol molecule. (c) Current-voltage characteristics of three gaps of different sizes with molecular layers of fluorinated decanethiols self-assembled on the Au electrodes. Representative SEM image of the devices is shown. Nanogaps of different sizes are achieved by changing the original size of the gap patterned through electron-beam lithography. 54

4-1 SEM images of chemically-synthesized Au nanoplates with well-defined shapes, edges and thicknesses (a and b). The single-crystalline nature of the nanoplates is confirmed in the transmission electron microscopy diffraction pattern of (c) showing Au(111) plane. 59

4-2 Atomic force microscope surface topography scan of the single-crystalline Au nanoplate shows roughness of <1 nm (a), much smaller than ∼4 nm roughness expected for a thermally evaporated layer of Au (b). 60

4-3 Combined bottom-up self-assembly and top-down lithography formation of electrodes separated by nanogaps and with nanometer uniformity. (a) To self-assemble the nanogaps, nanoplates are surface functionalized with octadecanethiol to assume hydrophobic surface properties and then are assembled at the water-chloroform interface using hydrophobic-hydrophilic interactions and capillary forces as the solvents evaporate. (b) Nanogaps are formed using self-assembly of Au nanoplates (1) upon which wires and contacts are added using electron-beam lithography and lift-off (2). After anti-stiction treatment of the substrate surface (3) with trichloro(perfluorooctyl)silane, a UV-curable epoxy is used to peel off the nanogap and the interconnects onto a glass substrate to planarize the surface (4). (c) Chemical structure of trichloro(perfluorooctyl)silane used as anti-stiction coating in the planarization process. 61

4-4 The deposition technique used to fluorinate the substrate influences the molecular layer's uniformity which defines the roughness of the peeled epoxy surface. AFM topography scan of a surface containing a Au nanoplate peeled off a substrate fluorinated by vapor-phase assembly shows a rough surface (a). The surface roughness is minimized when trichloro(perfluorooctyl)silane is assembled in a liquid-phase instead (b). 63

4-5 Precisely defined nanogaps with nanometer resolution and surface uniformity formed through self-assembly of Au nanoplates based on the method shown in Figure 4-3a. 64

4-6 AFM surface topography shows a height variation of ~5 nm across the nanogap formed between the Au nanoplates due to the variations in thicknesses of the chemically-synthesized nanoplates. 65

4-7 (a) Optical image of a planarized electrically contacted nanogap formed in between Au nanoplates. (b) SEM of the corresponding nanogap with a width of ~30 nm. (c) The AFM surface topography of the structure shows uniform surfaces on the Au nanoplates and lithographically patterned Au wires achieved through the peeling technique. (d) A uniform AFM profile is observed across the nanogap. 66

4-8 Through dielectrophoretic positioning of Au nanoparticles coated with a molecular layer across the nanogap, vertical molecular tunnel junctions can be formed. The SEM image shows Au nanoparticles coated with cetylpyridinium chloride bridging a ~30 nm Au nanoplate electrodes. The current-voltage characteristic compares the current conduction before (blue curve) and after trapping (two consecutive measurements are shown in red). . . 67

5-1 Molecules which can be precisely engineered through chemical synthesis serve as nanoscale building blocks by helping define device design and surface interactions using their inherent structural, mechanical and chemical properties. 70

5-2 (a) Molecules can be engineered through chemical synthesis with the desired head, terminal and spacer groups where the functional end groups can be selected to allow spontaneous and selective assembly onto a desired surface, while the spacer group can help define the size, structure, chemical and mechanical properties. As an example, thiol functional groups in poly(ethylene glycol)dithiol allow self-assembly on Au. The transmission electron micrographs (TEM) in (b) show the surface of a Au nanocube without any molecular coating compared to that with ~3 nm-thick self-assembled layer of PEG-dithiol. The thickness of the molecular film is dependent on the polymer chain length. 72

5-3 (a) Layer-by-layer deposition of polyelectrolytes allows cyclic assembly of oppositely charged entities for example poly(allylamine hydrochloride) (PAH) and poly(sodium styrenesulfonate) (PSS) with precise thicknesses. The precision in forming nanoscale molecular layers is shown in (b) for the case of layer-by-layer deposition with PAH and PSS on a Au substrate and characterized with a scanning ellipsometer. 73

5-4 Modifying contacts of a NEM relay with low surface energy fluorinated molecules reduces stiction demonstrated through lowering of the hysteresis voltage, in this example design achieving ∼40% reduction on average. The NEM relay design is shown in the SEM image of (a) with the schematic cross-section of the device and the chemical structure of the molecular coating shown in (b) and (d) respectively. An example switching performance with and without molecular coating is included in (c), a hystereis <50 mV is achieved [11]. 74

5-5 The XPS spectrum of a tungsten (W) film with and without surface treatment by perfluorodecyltriethoxysilane confirms self-assembly of the molecular layer through use of silane end groups in a vapor-phase process. 75

5-6 Nanoscale force control using molecular layers as springs. An applied force (F_{applied}) compresses molecules connecting two neighboring surfaces. The elastic force (F_{elastic}) stored in compressed molecules overcomes the van der Waals forces (F_{vdW}) to make the process controlled and reversible. 75

5-7 A molecular layer that can define the spacing between two neighboring surfaces to allow dynamic tunability can be composed of (a) a single type of molecule, (b) engineered molecules with different components, (c) engineered thin-film composed of different molecular species, (d) active molecules that change conformation in response to an external stimulus. For example, dibenzocyclooctatetraene which has a tub conformation in the ground state flattens when reduced. 76

6-1 Molecules can help precisely define a nanogap electrode and allow its controlled and reversible electromechanical modulation by providing force control. If sufficiently small, conduction through quantum tunneling is observed where the tunneling current changes exponentially as a function of the tunneling gap. Here, α is an adjustable parameter that accounts for the effects of barrier shape and electron effective mass. In this example, α is selected to be 0.57, within the range reasonable for organic molecular layers. . . . 80

6-2 Fabrication process of the tunneling NEM switch: (a) multilayer PMMA electron-beam resist is spun on a Si/SiO_2 substrate and baked after each spin, resist is then electron-beam-patterned to define the switch components, (b) resist is developed in 1:3 solution of MIBK in isopropanol, (c) 100 nm of Au is evaporated over the substrate, (d) fluorinated decanethiol is self-assembled in vapor phase over Au, bridging the gap between Electrodes 1 and 2. 82

6-3 (a) Scanning electron micrograph of a laterally actuated cantilever formed based on the fabrication scheme in Figure 6-2. (b) Chemical structure of fluorinated decanethiol used in forming the molecular gap. The assembly process is executed in vapor-phase using thiol-chemistry. 83

6-4 (a) Current-voltage characteristics of a tunneling NEM switch in the absence of fluorinated decanethiol molecular layer showing device failure due to stiction after the first run; (b) Current-voltage characteristics of the switch after self-assembly of fluorinated decanethiol showing repeatable operation. Note that the highest value of current is set by the compliance of the measurement setup and is not a property of the device. 84

6-5 Experimental current-voltage characteristic of the tunneling NEM switch (blue) compared to the theoretical characteristics based on the Simmons model of tunneling with a constant gap (red) and a variable gap (green). 86

7-1 (a) Actuation voltage of an example two-terminal metal-molecule-metal squitch as a function of Young's modulus of the compressible molecular film showing an increase in the actuation voltage with an increase in the Young's modulus. (b) To achieve sub-1 V actuation in this example, a material with a Young's modulus <11 MPa is desired. 92

7-2 (a) Fabrication scheme for a two-terminal squitch with Au-(PEG-dithiol)-graphene switching gaps. (b) AFM topography of CVD-grown graphene transferred on a substrate showing sub-1 nm local roughness. (c) Chemical structure of PEG-dithiol used for the spacer layer. (d) The technique used to transfer the top graphene electrode onto the molecular layer. The transfer can either be done without an alignment over the entire substrate as a single sheet (Scheme I), or, the graphene can be first lithographically patterned into smaller features and transferred onto the bottom electrodes locally using an aligned transfer technique under an optical microscope (Scheme II). . . 95

7-3 (a) Optical image of an example two-terminal squitch. (b) Schematic cross-section of a two-terminal squitch with graphene top electrode, PEG-dithiol spacer layer and Au bottom electrodes. An applied voltage across the bottom electrodes induces an electrostatic force to compress the molecular layer and tune the tunneling gap through which the tunneling current is modulated. 96

7-4 Current-voltage characteristics of two-terminal squitches based on graphene-PEG-Au switching gaps. 97

8-1 An example design of a multi-terminal squitch. An applied voltage across gate electrodes 1 and 2 provides an electrostatic force to compress the molecular layer to tune the tunneling gap between the top electrode and the source/drain electrodes and consequently modulate the drain current (I_D). 104

8-2 Fabrication scheme for multi-terminal squitches. (a) Bottom electrode fabrication: A sacrificial layer made out of two-dimensional materials such as graphene is lithographically patterned to define the surface topography. Electrodes and interconnects are formed using electron-beam lithography. The substrate surface is fluorinated. Using an epoxy adhesive layer and a glass receiving substrate the structures are peeled off the surface. Sacrificial layer is etched, using O_2 plasma in the case of graphene, revealing the bottom electrode with the desired topography. (b) Molecular layers are self-assembled either on the bottom electrodes (Scheme I), top electrode (Scheme II) or a combination of the two (Scheme III). (c) Chemical structure of PEG-thiol used as the molecular spacer layer. (d) Top electrode is formed using chemically synthesized Au nanorods. The nanorod is precisely positioned on the bottom electrodes using a dielectrophoretic trapping approach. (e) SEM image of chemically-synthesized Au nanorods. 106

8-3 An example three-terminal bottom electrode formed using the fabrication technique of Figure 8-2a with Electrode 2 being recessed by $\sim$4 nm relative to Electrodes 1 and 3 using graphene as the sacrificial material, and evaporated Au as electrodes. 107

8-4 The peeling technique helps eliminate the edge defects imposed by the lift-off process. Here, an edge roughness $\sim$50 nm caused by the lift-off process (a) is eliminated through the peeling technique (b). The peeling also minimizes the surface roughness, achieving <1 nm average surface roughness on the peeled surface (d) compared to $\sim$4 nm roughness expected for the surface of an evaporated thin-film of Au (c). 108

8-5 (a) TEM image of the cross-section of a molecular gap with Au nanorod top electrode and peeled evaporated Au film as the bottom electrode. (b) The magnified image shows the well-defined uniform molecular layer formed between the Au nanorod facet and the peeled electrode, both surfaces exhibiting roughness <1 nm. 109

8-6 Current-voltage characteristics of an example multi-terminal squitch showing gated modulation of drain current. The experimental measurement is compared against the theoretically simulated performance showing a good fit when considering compression of the switching gap. To achieve the best-fit curve it is deduced that PEG-thiol layer has a Young's modulus of ~20 MPa. (b) Consecutive measurements of another device shows <50 mV hysteresis. 110

9-1 Schematic representation of strategies toward low-energy stiction-free NEM switches utilizing molecular layers. (a) In a conventional contact-based NEM switch, the elastic restoring force should exceed the surface adhesive forces to overcome the energy barrier (ΔE) to break the contact. (b) Low surface energy molecular layers reduce the surface adhesive forces at contact, decreasing the potential for stiction. (c) Additional minimization of stiction can be achieved using a metal-molecule-metal switching gap which further lowers the surface adhesive forces and allows nanoscale force control through compression of the molecular layer, while enabling formation of a few nanometer-thick gap for sub-1 V operation [102]. 115

9-2 Switching parameters including actuation voltage, switching energy and switching time change as a function of the mechanical properties of the molecular spacer. 118

9-3 In a Au-molecule-Au nanogap, the plasmon resonance shifts as the metal-metal gap decreases. Dark-field microscope images of Au nanocubes spaced from an underlying Au film at different distances using molecular layers show the gap-dependent resonance. 119

9-4 Engineering at the limits of the nanoscale, enabled through development of alternative fabrication techniques and by achieving control over surfaces and forces, makes feasible unique manipulation of properties including electronic transport, light-matter interactions, mechanics, magnetics, exciton and spin dynamics that can lead to new paradigms of active devices. 122

9-5 Alternative fabrication methodologies are needed to achieve resolution, control and uniformity required to promote engineering of active devices at the limits of the nanoscale. For the example of electromechanically tunable molecular junctions, conventional top-down lithography and thermal evaporation commonly lead to nonuniform molecular junctions with metal penetration through the molecular layer inducing damage (a) while hybrid top-down and bottom-up techniques help formation of well-defined molecular nanogaps with sub-nm precision, control and uniformity (b). The molecular junctions are outlined in dotted red lines. 123

B-1 SEM images of Au nanoplates synthesized in presence of PVP capping agent. 128

B-2 SEM images of Au nanorods of two different lengths with the length modified by the reaction conditions according to the procedure outlined in this section. 129

C-1 The distribution of Young's moduli extracted from modeling the three squitches of Figure 7-4a over 1 million simulation runs with the possible dielectric constant values being constrained to the range 1 to 5. The values of α and ϕ leading to this distribution are in the range of 0.4 to 1, and 1 to 5 eV, respectively. 133

List of Tables

A.1 Representative electrostatic NEM switches - design and performance. 125

B.1 The amounts of nitric acid (HNO_3) and solution B used in the synthesis of different nanorods and their corresponding average lengths. 130

Chapter 1

Introduction

"There's plenty of room at the bottom." *-Richard Feynman*

1.1 Engineering at the Limits of the Nanoscale

Consider the period at the end of this sentence – it is ~5×10^5 nm in diameter, or ~3×10^6 carbon atoms arranged next to each other. Two carbon atoms form a covalent bond approximately 0.15 nm in size. Eight of these carbon atoms can build up a small alkane molecule ~1 nm in length. Consider engineering devices at such small scale – unprecedented precision, resolution and uniformity would be essential. This thesis explores engineering at such small dimensions – at the limits of the nanoscale – where structures *single-digit nanometers* in size are needed towards development of active devices of unique functionalities.

At the nanoscale, properties and phenomena emerge that are classically unattainable. In past decades, these principles offered tremendous opportunities for interdisciplinary scientific and technological advancements, driving the field of nanotechnology. Exploiting these opportunities became feasible through innovations in nanoscale fabrication, visualization and characterization. However, despite vast improvements, these techniques become limiting in precision, control, resolution and uniformity as dimensions are further reduced towards the few-nanometer regime. In particular, the dynamic, controlled and reversible tuning of such small dimensions is a great challenge, often facing structural collapse due to the lack of control over surface adhesive forces. However, control over such dimensions, if implemented successfully, can lead to unexplored phenomena and device principles benefiting diverse areas of electronics, optics, spintronics, nanoelectromechanical systems and excitonics to name a few examples. To reach these potentials, alternative approaches are necessary to push the frontiers of nanoscale processing and control.

These alternative approaches should focus beyond incremental improvements in conventional fabrication tools, re-envisioning processing methodologies by bridging the boundaries between different disciplines. Integration of device engineering and physics with chemistry and materials science leverages an understanding of material synthesis, surfaces and interfaces to achieve manipulation of matter in the nanometer regime with a precision and control otherwise not feasible, down to <1 nm. When addressing the nanoscale from the bottom up through such an interdisciplinary approach, an extensive toolset emerges to develop new processing techniques and also redefine the limits of the conventional approaches by realizing new strategies of using them. However, given the small dimensions, processing is further challenged by the lack of resolution in visualization and characterization. In many cases, the needs are pushed well beyond the capabilities in reach of the state-of-the-art metrology techniques. Yet, detailed characterization of structures at the few nanometer dimensions and their performance are much needed to provide continuous feedback to guide engineering and scientific studies at this size scale. Thus, development of new metrology techniques and unique ways of utilizing conventional tools are as essential as new developments in processing.

As the processing and metrology methodologies advance to gain access to the few-nanometer regime and address the desired complexity of functional nanostructures, an important consideration is for these techniques to possess flexibility: the ability to readily reconfigure in operation and integrate with one another in such a way to accommodate a wide variety of material systems and functionalities that emerge at the nanoscale. Unlike conventional approaches which are often restricted in operation mode and capabilities, such versatile techniques are desired at the nanoscale to keep up with the demands of the continuously evolving field of nanotechnology and its multidisciplinary nature.

In this thesis, the challenges and prospects of engineering active devices at the limits of the nanoscale are evaluated. In doing so, a case study is considered through which a new platform for nanoelectromechanical (NEM) switches is introduced with the potential to overcome the limitations of their conventional counterparts. In demonstrating these devices, various processing techniques are developed to allow: 1) nanoscale fabrication with nanometer precision, control and uniformity, and 2) nanoscale force control for dynamic tuning of dimensions in a controlled and reversible manner. Engineering approaches are consequently realized which can extend in application beyond NEM switches to broadly enable active devices with critical features nanometer in size.

1.2 Towards Low-Voltage and Stiction-Free NEM Switches – A Case Study

A nanoelectromechanical (NEM) switch in the simplest form is composed of a movable electrode, such as a cantilever, faced opposing stationary electrodes to form a capacitor structure as shown in Figure 1-1a. An applied voltage across the capacitor provides an electrostatic force to attract the top electrode towards the bottom. Once reaching the pull-in, the point at which the combined electrostatic and surface adhesive forces overwhelm the elastic restoring force, the deflected electrode collapses to come into physical contact with the opposing electrode to turn the device ON. As the applied voltage is removed, the elastic restoring force in the deflected electrode overcomes the surface adhesive forces causing it to return to its original position, turning the device OFF. This switching mechanism allows NEM switches to exhibit a near-zero off-state leakage current and abrupt switching behavior with an effectively infinite sub-threshold slope [1, 2], schematically shown in Figure 1-1b. Consequently, NEM switches have the potential to achieve more energy-efficient performance than

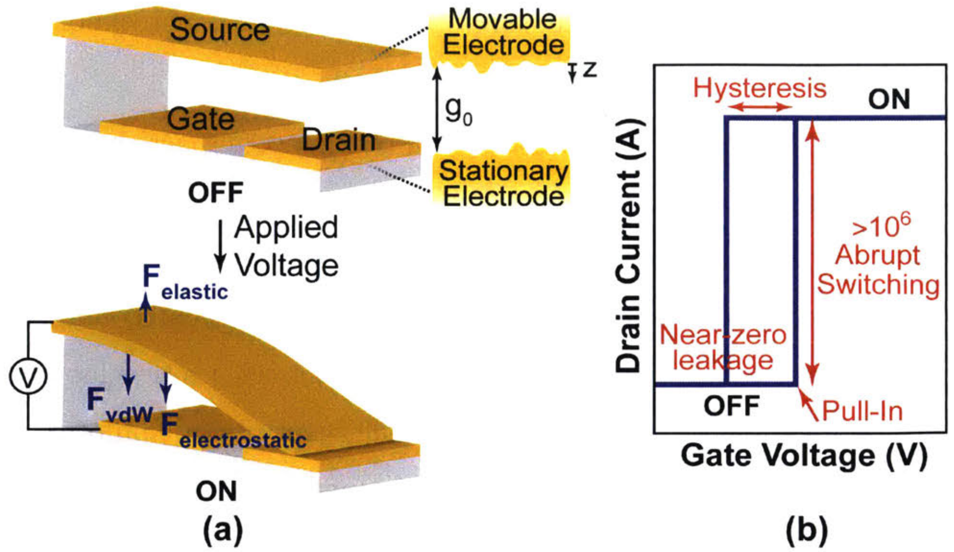
Source
Movable Electrode
z
g_0
Gate
Drain
Stationary Electrode
OFF
Applied Voltage
$F_{elastic}$
V
F_{vdW}
$F_{electrostatic}$
ON
(a)
Hysteresis
ON
Drain Current (A)
$>10^6$ Abrupt Switching
Near zero leakage
OFF
Pull-In
Gate Voltage (V)
(b)

Figure 1-1: Schematic representation of the design and performance of a cantilever-based NEM switch. (a) An electrostatic force ($F_{electrostatic}$) induced through an applied voltage combined with the van der Waals forces (F_{vdW}) cause collapse of the cantilever onto the opposing electrode to turn ON the device as they come into contact. Once the voltage is removed, the elastic restoring force ($F_{elastic}$) overcomes the surface adhesive forces to turn OFF the device. (b) The switching mechanism leads to a near zero OFF-state leakage current and an abrupt switching behavior with a large ON-OFF current ratio.

their complementary metal-oxide-semiconductor (CMOS) counterparts that are limited to a 60 mV/decade sub-threshold swing [1, 2].

Approaching an energy-efficient reliable performance for ultra-low power applications though requires overcoming two of the main challenges faced by the current NEM switches: large actuation voltage and stiction which refers to the adhesion between the contacting electrodes [1, 2]. To examine these challenges, one should focus on the switching gap of such a device, shown in Figure 1-1a.

Assuming a near zero off-state leakage, the dynamic energy consumption (E) in a switching cycle is approximated by $E \sim CV_{actuation}^2$ where C is the capacitance. A lowering of the actuation voltage ($V_{actuation}$) is necessary to reduce the switching energy [2]. With switching gaps typically >10 nm, current electrostatic NEM switches commonly exhibit operating voltages >1 V [1, 2]. Assuming a simplified design based on a parallel plate capacitor, $F_{electrostatic} \propto V^2/(g_0 - z)^2$ where V is the applied voltage, g_0 is the initial switching gap and z is the displacement. Accordingly, to move towards millivolt actuation, the switching gaps need to be reduced in width – in a relay $V_{actuation} \propto (g_0)^{3/2}$ where the actuation voltage is considered to be equal to the pull-in voltage [2]. Miniaturization of such a mechanically-active structure to a few-nanometer regime is not trivial as the surface adhesive forces, including the van der Waals forces, increase drastically with a reduction in the separation distance between the approaching electrodes ($F_{vdW} \propto 1/(g_0 - z)^3$). These dominating surface adhesive forces can cause collapse of the structure and adhesion between the contacting surfaces, referred to as stiction, during fabrication and operation [3–7]. Reducing the switching gap size is further challenged by the roughness of the contacts, inherent to the processing techniques conventionally employed, as schematically shown in Figure 1-1a , limiting the extent of miniaturization.

Over the past years, extensive research has focused on developing new designs and fabrication schemes enabling low-voltage NEM switches with an operating voltage of ~400 mV, the lowest reported to date without any pre-biasing and with a switching gap of ~4 nm [8]. An overview of some representative NEM switches are outlined in Table A.1 (Appendix A) [8–26]. Despite various developments, overcoming these challenges is yet to be fully realized beyond proof of principle. The surface adhesive forces remain a challenge, causing unstable electrostatic modulation of the gap, leading to unreliable performance and often premature failure due to permanent stiction. Beyond unreliable performance, contact stiction also leads to hysteresis in switching (Figure 1-1b). The hysteresis limits the lowest operating voltage and active power consumption achievable [11]. To acquire a more energy-efficient operation, the hysteresis voltage should also be minimized by reducing the surface adhesion.

While developing techniques to scale down device dimensions, methodologies should also be devised to provide nanoscale force control to minimize stiction and allow controlled electrostatic modulation of nanogap electrodes to enable energy-efficient yet reliable performance. In designing such a switch, engineering a stable electromechanically active nanogap becomes the main challenge. As this thesis works towards addressing this objective, three considerations are made: 1) miniaturization of the switching gap, 2) reduction in surface roughness, and 3) force control to reduce hysteresis and allow controlled mechanical tuning. The end result is a switching gap <10 nm wide, formed with nanometer precision and uniformity, capable of controlled and reversible electromechanical modulation.

1.3 Thesis Organization

As discussed, this thesis studies the challenges of engineering at the limits of the nanoscale and introduces approaches to address them by focusing on the design of electromechanically active nanogaps. By developing new fabrication techniques and methodologies for force control, this work then introduces and experimentally demonstrates a switching mechanism for low-voltage and stiction-free NEM switches as an example device concept enabled by the ability to manipulate features single-digit nanometers in size. In doing so, three interdependent areas are investigated as outlined below.

Part I - Fabrication with Nanometer Precision, Control and Uniformity

To allow engineering of active nanostructures with features few nanometers in size, Chapter 2 introduces fabrication techniques which combine top-down and bottom-up approaches. These techniques can be versatile, capable of integrating with novel and existing platforms, while allowing structures of desired complexity to be designed with nanometer resolution, control, and uniformity as building blocks of active nanoscale devices. Two example fabrication methodologies developed for formation of <10 nm electrically active gaps are reported in Chapters 3 and 4. The technique in Chapter 3 complements top-down fabrication with bottom-up engineering of surfaces and forces to achieve unprecedented resolution while the method in Chapter 4 utilizes top-down fabrication to assist bottom-up assembly of nanogaps.

Part II - Nanoscale Force Control – A Molecular Approach

Molecules are introduced in Chapter 5 as building blocks that contribute precision in fabrication while also providing nanoscale force control through their chemical and mechanical properties. It is proposed that when used as nanoscale springs between neighboring surfaces, the molecule's mechanical compression provides an elastic restoring force to overcome surface adhesive forces to allow dynamic tunability in a controlled and reversible manner. This is shown in an electromechanically tunable molecular tunneling junction in Chapter 6.

Part III - Device Design – Tunneling Nanoelectromechanical Switches towards Low-Voltage and Stiction-Free Performance

Electromechanical modulation of the tunneling current in a molecular nanogap is used to propose a tunneling-based NEM switch. The molecular layer helps define switching gaps much smaller than that feasible through conventional fabrication techniques while helping avoid stiction, enabling a more energy-efficient alternative to common electromechanical switches. An example two-terminal design of such a NEM switch is demonstrated in Chapter 7, while Chapter 8 discusses a proposed multi-terminal architecture.

Lastly, Chapter 9 summarizes the thesis while reflecting on the NEM switch case study to provide a general perspective on the challenges of engineering at the limits of the nanoscale. The extension of the toolset developed in this thesis and the lessons learned in designing the switch to other device applications at the few-nanometer regime is discussed. A pictorial summary of this thesis is shown in 1-2.

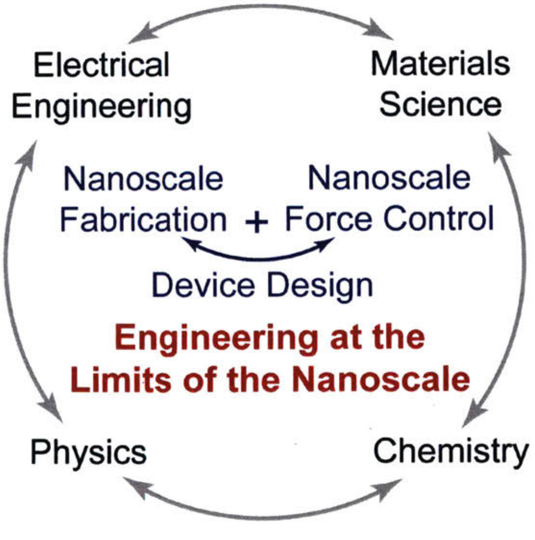
Electrical Engineering
Materials Science
Nanoscale Fabrication
+
Nanoscale Force Control
Device Design
Engineering at the Limits of the Nanoscale
Physics
Chemistry

Figure 1-2: Pictorial thesis overview: To enable engineering at the limits of the nanoscale, an interdisciplinary approach is necessary to develop alternative techniques for nanoscale fabrication and force control, leading to new paradigms of active devices.

Part I

Fabrication with Nanometer Precision, Control and Uniformity

Chapter 2

Combining Top-Down and Bottom-Up Fabrication: Hybrid Nanotechnologies

Fabrication technologies have continuously evolved over the past decades driven by the progress in the semiconductor electronics industry to keep up with the need for continuous device miniaturization. These predominantly top-down methodologies are often optimized for particular applications and material systems. In addition to the lack of versatility in processing, these techniques become limiting in resolution, precision and uniformity as dimensions continue to scale down. Therefore, they are not broadly suited for manufacturing of the various unconventional structures of unique functionalities that emerge at the nanoscale. Alternative methodologies are necessary to promote engineering of active devices in the few-nanometer regime.

2.1 Top-Down Fabrication

Conventionally, nanoscale features are fabricated through top-down approaches in which bulk components are patterned into miniaturized entities (Figure 2-1). Lithography is the most commonly used top-down approach with the resolution mainly limited by the exposure wavelength. The schematic overview of the process is shown in Figure 2-2. In this process, a polymeric resist responsive to the wavelength of the exposure source is deposited onto the substrate. Once exposed through a photomask or by direct-write, the desired pattern is transferred onto the resist. In this process the chemical properties of the resist alter where exposed. Once rinsed through the development process, a resist-based mask forms on the substrate. Following a deposition or etching step and after removing the resist, the desired features form on the underlying surface. Exposure wavelengths transitioning from visible to extreme ultraviolet and soft x-ray have allowed improvements in resolution from micron-scale features, when using conventional photo-lithography, to sub-100 nm [27–30]. Reduction in wavelength combined with improvements in optical and processing techniques can further improve resolution to <10 nm. Ion and electron-beam lithography techniques have been implemented that allow features as small as a few nanometers [31–33]. However, widespread use of the next generation lithography processes is a technological challenge, having a low throughput while being costly and time-consuming.

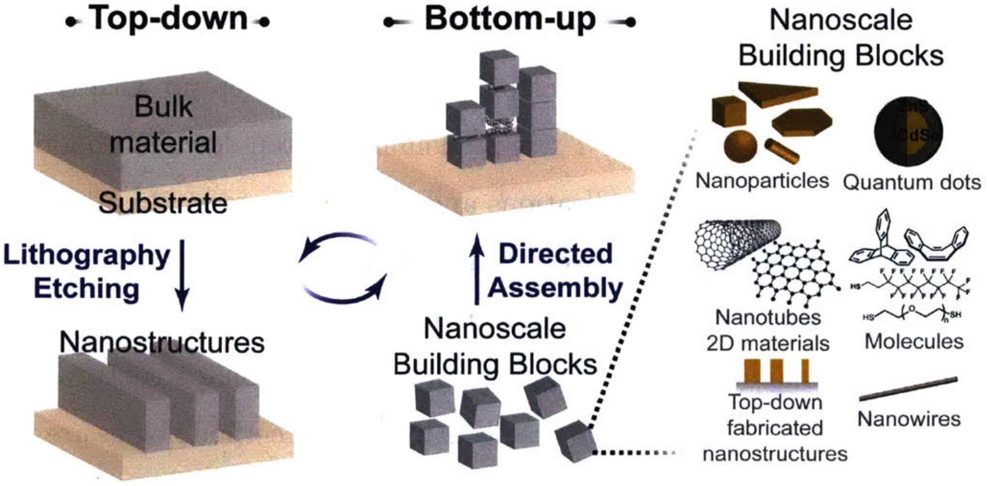
Top-down
Bottom-up
Nanoscale Building Blocks
Bulk material
Substrate
Nanoparticles
Quantum dots
CdSe
Lithography Etching
Directed Assembly
Nanostructures
Nanoscale Building Blocks
Nanotubes
2D materials
Molecules
HS
SH
Top-down fabricated nanostructures
Nanowires

Figure 2-1: Hybrid top-down and bottom-up fabrication techniques enable complex active structures with nanometer precision, resolution and control. Top-down fabrication involves use of processes including lithography to machine down bulk materials into nanostructures. Alternatively, bottom-up techniques involve nanoscale building blocks that assemble into larger functional entities. Example nanoscale building blocks are depicted here including chemically-synthesized molecules, nanoparticles and nanomaterials, and nanostructures formed through top-down fabrication.

Alternative techniques have also been developed to be used in conjunction with these lithographic approaches to allow for high-throughput and low-cost processing of a wide variety of materials beyond conventional semiconductors, and on versatile surfaces including those nonplanar and pliant. A widely studied category of these techniques are soft lithography methodologies. Broadly, these techniques rely on using an elastomeric mold or stamp, commonly made out of polydimethylsiloxane (PDMS), to transfer desired patterns of a particular ink onto a receiving substrate. The patterns are defined by the topography of the stamp. Soft lithography processes typically involve printing, molding and embossing [34–36]. Figure 2-2 summarizes example techniques in the simplest forms, but it should be noted that variations of each have been developed for optimized performance and to accommodate different needs.

Amongst these techniques, microcontact printing is a versatile soft lithography approach through which an elastomeric stamp formed using a lithographically patterned master is used to transfer an ink onto a substrate. Example inks include molecules such as alkane thiolates, silanes, or biomolecules. The patterned molecular layer can then be used as an etching mask, or as a seed layer to promote spatially-selective growth or deposition of a material such as a metallic or semiconducting thin-film [35, 37, 38]. Similarly, nanotransfer printing utilizes an elastomeric stamp to transfer patterns of a solid ink, such as thin-films of metals, onto a substrate with shapes defined by the surface topography of the stamp while layer-by-layer stacking enables three-dimensional arrangements [39–41].

In addition to printing, molding is also a common soft lithography technique. In the simplest form, replica molding allows fabrication of a replica of the original master by solidifying a liquid precursor (prepolymer) against the elastomeric mold [35]. In a variation of this technique, known as microtransfer molding, the patterned features on the stamp are filled with a liquid precursor and are transferred onto a substrate in contact with the mold upon curing of the prepolymer [35]. It is possible to use capillary forces to fill the channels formed in the mold with the prepolymer, leading to a technique referred to as micromolding in capillaries [35]. In another emerging technique, referred to as nanoimprint lithography, the topographic patterns in a rigid mold are transferred to a thermoplastic polymer film placed on the substrate heated above its glass-transition temperature under an applied pressure [35, 42, 43]. Such high-throughput techniques have shown to allow sub-100 nm features applicable to a wide range of materials. However, fabrication of structures with high spatial complexity that requires multiple processing steps with precision in alignment and relative placement while maintaining high spatial density remains an ongoing challenge.

Focused ion beam milling which develops the desired features by direct sputtering of the material using a focused ion beam, such as gallium or helium ions, has also been shown effective in high resolution fabrication with features <10 nm reported [44–47]. This maskless and resistless process can be implemented in a single step with precise positioning of arbitrary-shaped high resolution features. Despite its efficacy for planar fabrication, complex three-dimensional features are challenging to form. With the need for direct manipulation of the beam to individually pattern each component, large area processing is time consuming and not effective. The process is also not compatible to all material types as high energy ion beam can cause damage, in particular, to organic components.

Top-down techniques and their variations provide sufficient control over deterministic positioning of the features with the desired spatial variation and complexity. The fabricated nanostructures can also be easily accessed externally such that they can be electrically, optically or mechanically activated for the desired function. However, for further miniaturization, these techniques become limiting in resolution, precision and uniformity. Most notably, surface and edge imperfections are inevitable. At the few-nanometer regime, such irregularities, though small, can be on the order of the device critical dimensions and will hinder the desired function. To highlight these challenges, an example structure fabricated through top-down lithography and lift-off is shown in Figure 2-3 capturing the resulting edge defects and ~3 nm surface roughness. When building complex nanoscale devices with features only few nanometers in size and requiring multiple processing steps, such topographical non-uniformities will accumulate to challenge fabrication and impede successful device functionality.

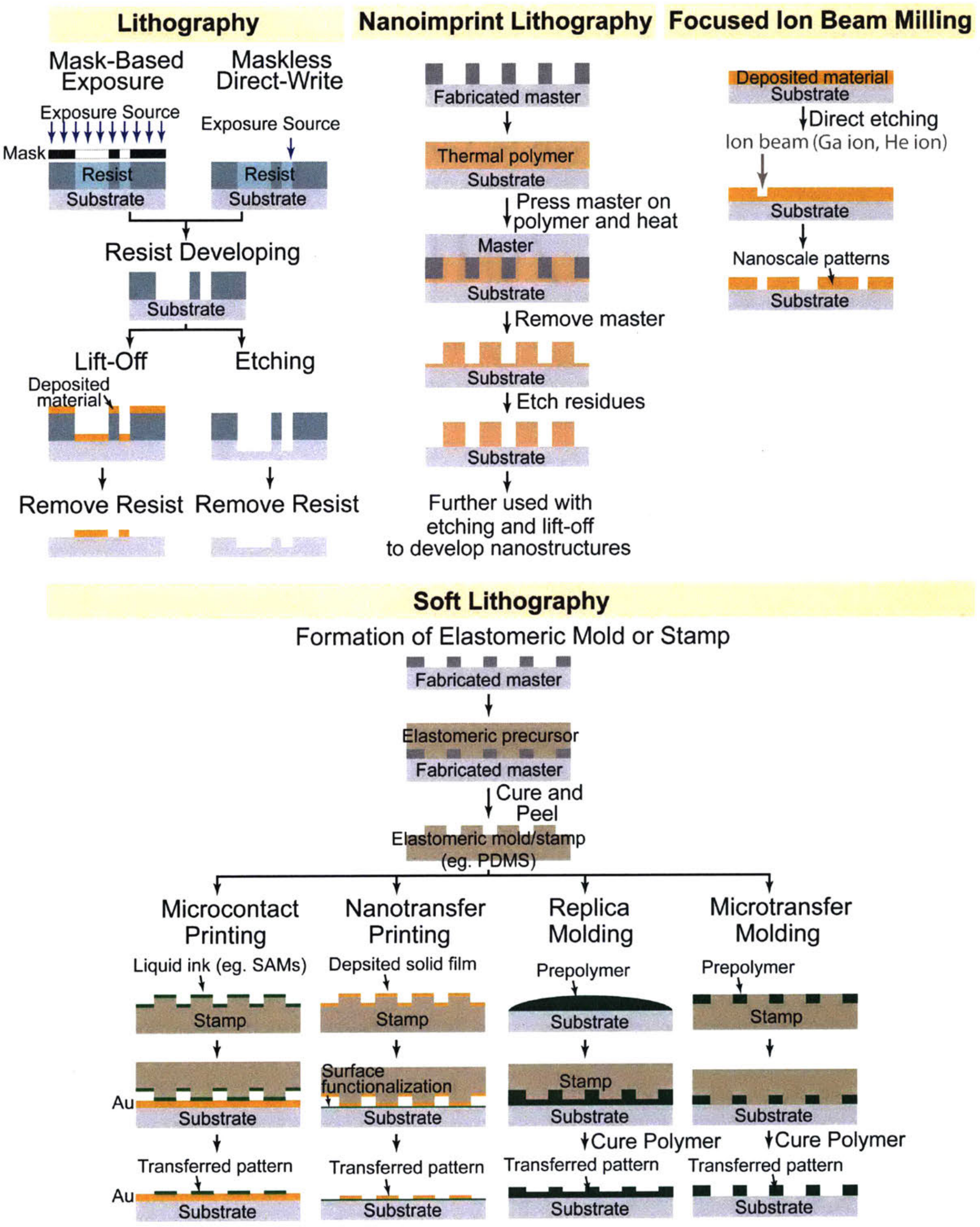

Lithography
Mask-Based Exposure
Maskless Direct-Write
Exposure Source
Mask
Exposure Source
Resist
Substrate
Resist
Substrate
Resist Developing
Substrate
Lift-Off
Etching
Deposited material
Remove Resist
Remove Resist
Nanoimprint Lithography
Fabricated master
Thermal polymer
Substrate
Press master on polymer and heat
Master
Substrate
Remove master
Substrate
Etch residues
Substrate
Further used with etching and lift-off to develop nanostructures
Focused Ion Beam Milling
Deposited material
Substrate
Direct etching
Ion beam (Ga ion, He ion)
Substrate
Nanoscale patterns
Substrate
Soft Lithography
Formation of Elastomeric Mold or Stamp
Fabricated master
Elastomeric precursor
Fabricated master
Cure and Peel
Elastomeric mold/stamp (eg. PDMS)
Microcontact Printing
Nanotransfer Printing
Replica Molding
Microtransfer Molding
Liquid ink (eg. SAMs)
Depsited solid film
Prepolymer
Prepolymer
Stamp
Stamp
Substrate
Stamp
Au
Substrate
Surface functionalization
Substrate
Stamp
Substrate
Substrate
Cure Polymer
Cure Polymer
Transferred pattern
Transferred pattern
Transferred pattern
Transferred pattern
Au
Substrate
Substrate
Substrate
Substrate

Figure 2-2: An overview of various lithographic techniques. Conventional lithography involves use of an illumination source to expose through a photomask or direct-write a polymeric resist layer sensitive to the exposure wavelength. Once developed, the resist-based mask is used with a deposition or etching step to transfer the patterns onto the substrate. Nanoimprint lithography transfers the topographical patterns on a solid master onto a heated thermal polymer under an induced pressure. Focused ion-beam milling utilizes high energy ion-beam to directly write the patterns by sputtering. Soft lithography involves techniques through which elastomeric molds or stamps are used to transfer onto the substrate an ink in form of the patterns defined by the topography of the master.

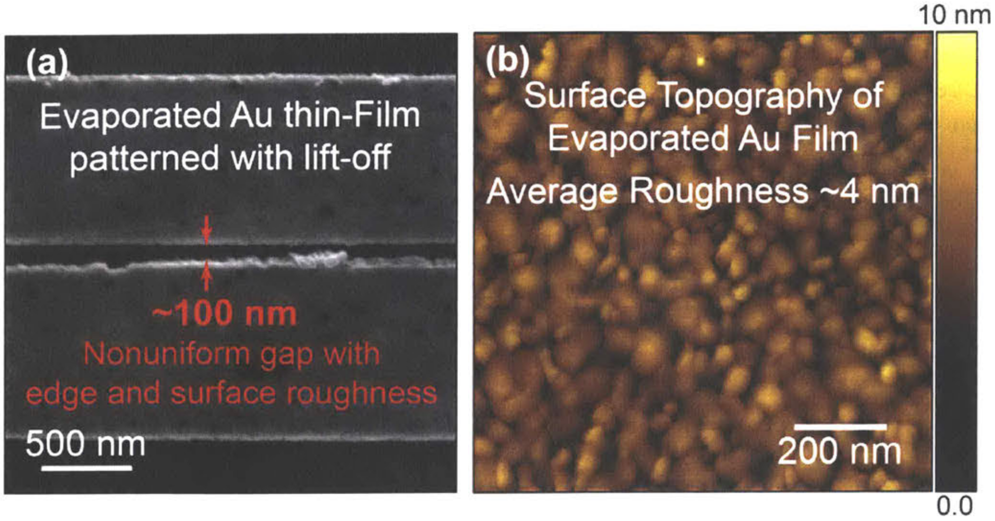
(a)
Evaporated Au thin-Film patterned with lift-off
~100 nm
Nonuniform gap with edge and surface roughness
500 nm
(b)
Surface Topography of Evaporated Au Film
Average Roughness ~4 nm
200 nm
10 nm
0.0

Figure 2-3: Nanostructures formed through top-down lithography, thermal evaporation of Au and lift-off. The scanning electron micrograph (left) shows the nonuniform edges of the structure while the atomic force microscope topography scan (right) shows $\sim$4 nm roughness associated with the thermally-evaporated Au film.

2.2 Bottom-Up Fabrication

Bottom-up fabrication, schematically shown in Figure 2-1, is an additive multidisciplinary technique where nanostructured building blocks are assembled to form larger functional entities with atomic precision [48–50]. These nanoscale building blocks include atoms, molecules, nanoparticles and other nanomaterials that are commonly chemically synthesized with sub-nanometer control over dimensions, surface topography and geometry. The chemical nature of the bottom-up methodologies also accommodates broad material systems much larger than that tolerated by the top-down approaches, making them suitable for engineering of emerging nanoscale devices. The building blocks can also be formed from nanostructures patterned through conventional top-down lithography techniques as will be discussed in the following chapter. In bottom-up assembly, controlled local interactions defined by surface properties are induced to rearrange the building blocks until the desired structure which corresponds to the lowest energy state of the system is assumed. Such thermodynamically-driven assembly leads to well-defined planar structures with nanometer resolution and uniformity but is insufficient to form complex, asymmetric and three-dimensional features.

Structures of higher complexity however, can also be realized by utilizing directed-assembly methodologies in which asymmetric and directional interactions are used to promote directionality and specificity in assembly. A widely studied technique allowing controlled fabrication of complex three-dimensional nanostructures utilizes deoxyribonucleic acid (DNA) to induce programmable assembly [51–53]. The DNA strands can be designed with desired nucleotide sequence ensuring pre-determined complementary base pairing in such a way that desired three-dimensional structures can be spontaneously formed. Nanostructures decorated with such DNA strands can also be selectively assembled into desired custom shapes as complementary base pairing occurs.

When developing nanoscale devices, precise positioning of the components is also important but not readily feasible through a self-assembly process. The deterministic positioning of the building blocks can be enhanced utilizing external stimuli including physical and chemical guides, electric and magnetic fields, and light [54–57]. Collectively, a versatile approach emerges to assemble structures with nanoscale precision and resolution in a controlled and predictive manner. Figure 2-4 compares planar self-assembly of Au nanocubes with their directed-assembly where top-down fabricated physical templates direct the nanocubes' precise positioning.

2.3 Hybrid Top-Down and Bottom-Up Fabrication

Bottom-up programmable assembly provides nanometer precision, resolution and uniformity desired for engineering at the limits of the nanoscale. However, these techniques alone can be insufficient to develop structures for functional devices and their integration into existing platforms. This typically requires higher order complexity and connectivity between individual components and external accessibility to provide driving input and extract output signals, particularly important for electrically-active devices. On the other hand, top-down techniques provide control over large-area processing of features of arbitrary shapes and complexity with the necessary interconnections. However, they lack the much needed nanometer precision, resolution

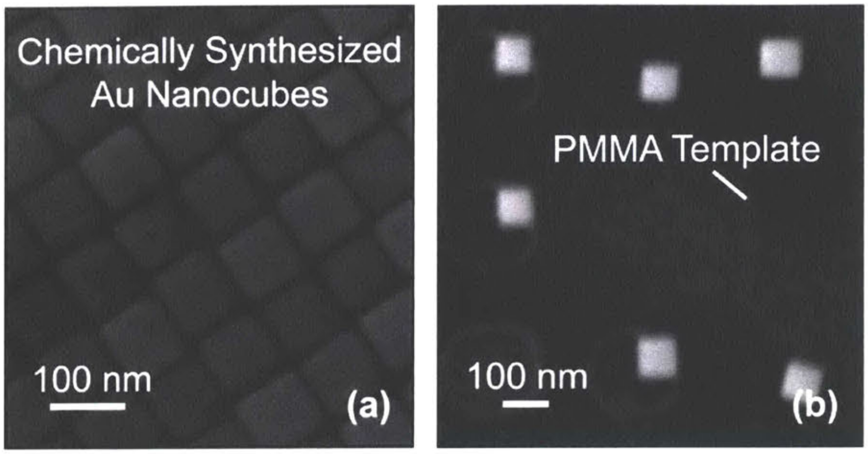

Figure 2-4: Comparison between self-assembly and directed-assembly of Au nanocubes. (a) Self-assembly promoted through surface interactions allows formation of an ordered layer of chemically-synthesized Au nanocubes. (b) The precise positioning of the cubes can be directed utilizing physical templates formed lithographically in a poly(methyl-methacrylate) (PMMA) layer.

and uniformity. The two methodologies can be cohesively combined to allow parallel integration of heterogeneous nanocomponents into higher order structures to yield complex active devices bearing features and uniformity in the nanometer scale [58, 59].

In one scheme, the bottom-up techniques can be complemented with the conventional top-down approaches to enable assembly of more complex structures. Concurrently, this integrative technique can add to the design components including interconnects needed for transforming the structures into active devices and systems – linking the nanoscale to the micro- and macroscale. Alternatively, top-down fabricated structures can undergo bottom-up engineering of surfaces and forces to evolve into desired architectures possessing critical dimensions of few nanometers. In combining these techniques complementary assistive fabrication techniques are needed. The objective of these techniques is to: 1) maintain the nanometer precision and uniformity throughout the processing, 2) ensure successful integration of top-down and bottom-up schemes, and 3) provide versatility such that the fabricated structures can be incorporated into novel and existing platforms regardless of the infrastructure.

Building on this premise, two techniques for controlled fabrication of electrically-active nanogaps are introduced in Chapters 3 and 4. Extensions of these multidisciplinary techniques are then used in the following chapters in the design of low-voltage and stiction-free nanoelectromechanical switches.

2.4 Summary

With continuous need for miniaturization, top-down fabrication techniques become limiting in resolution and uniformity. To overcome these limitations, chemistry has been used to formulate alternative bottom-up techniques through which nanometer control over manipulation of matter is feasible. Despite providing nanometer precision and uniformity, these processes lack the ability to achieve the complexity needed for functional nanodevices. To engineer active devices at the limits of the nanoscale hybrid top-down and bottom-up techniques appear promising as they can leverage the advantages of each methodology to enable complex active devices with nanometer precision, control and uniformity. Such integrative fabrication techniques should also provide sufficient flexibility to accommodate the diverse material systems, beyond conventional semiconductors, that are relevant to device engineering at the nanoscale. This in turn opens up a wide range of material properties and functionalities that would not have been available if only relying on top-down fabrication.

Chapter 3

Controlled Fabrication of Nanoscale Gaps using Stiction

Electrodes separated by nanometer-thin gaps are important building blocks of functional nanoscale devices and a platform for studying fundamental properties of materials with applications in molecular electronics, plasmonics and nanoelectromechancal systems, to name a few. Current methods of fabricating such nanogaps include electrochemical plating, focused ion-beam milling, electromigration, mechanical break junctions, nanosphere lithography, molecular junctions, adhesion lithography, atomic layer lithography, oblique-angle shadow evaporation and selective etching of well-defined sacrificial layers [47, 60–69]. Even though successful in forming individual sub-10 nm gaps, these approaches which involve multiple processing steps do not allow high throughput fabrication. The resulting devices typically lack robustness and exhibit unstable operation due to the inherent nonuniformities. These techniques also commonly used for two-terminal devices lack the versatility to be effectively incorporated into more complex, multi-terminal designs necessary for practical applications in integrated systems.

Here, we propose the use of stiction, an otherwise irreversible failure mode, to

---

Chapter 3 is adapted with permission from [F. Niroui, E. M. Sletten, P. B. Deotare, A. I. Wang, T. M. Swager, J. H. Lang and V. Bulović, Controlled fabrication of nanoscale gaps using stiction, *Micro Electro Mechanical Systems (MEMS), 28th IEEE International Conference*, 85–88, 2015]. Copyright 2015 IEEE.

promote controlled fabrication of nanogap electrodes [70]. In this integrative approach, top-down fabricated metallic nanostructures will undergo structural changes induced by bottom-up modulation of surface interactions such that nanogaps smaller than originally patterned are achieved. The feasibility of this approach and example applications are discussed in this chapter.

3.1 Design Principles

Stiction is a common mode of failure in electromechanical systems. It arises when the surface adhesive forces, including capillary, van der Waals, and electrostatic, overwhelm the elastic restoring force of the mechanically-active component, leading to its collapse and permanent adhesion. The drastic increase in adhesive forces with the decrease in the separation distance between approaching surfaces makes stiction increasingly more prominent as dimensions are scaled down. This failure mode however if induced in a controlled manner can be leveraged to assist formation of nanogap electrodes with a separation much smaller than that possible through conventional fabrication, as will be discussed in the following sections [70, 71].

In the scheme proposed here, laterally-actuated cantilevers and other device components are first formed using a one-step top-down lithography process. The design involves cantilevers facing opposing stationary structures such that a gap is formed between them. Capillary forces exerted on these mechanically-active cantilevers during a liquid phase processing step can induce deflection and eventual collapse. As the cantilever deflects due to the induced surface adhesive forces, the separation gaps can be modulated. The eventual stiction between the cantilever and a support structure stabilizes the system and enables formation of gaps smaller than originally patterned between the cantilever and additional electrodes located relative to the point of stiction. Through changes to the structures and liquid phase processing, surface adhesive forces caused by the capillary action, as well as van der Waals forces, can be adjusted to allow for precise tuning of the gap size.

3.2 Fabrication Flow

The fabrication scheme for the stiction-induced formation of nanogap electrodes is shown in Figure 3-1. Five layers of poly(methyl-methacrylate) (PMMA), a positive electron-beam resist, are spun over a silicon (Si) substrate with 2 μm-thick thermal oxide (SiO_2). Each layer is spun at 2000 rpm for 45 s and baked at 180°C for 90 s. The initial three layers of PMMA have molecular weight of 495 kg/mol (PMMA 495 A6) followed by two layers of molecular weight 950 kg/mol (PMMA 950 A4). Next, the cantilever and other electrodes are patterned onto the PMMA film using electron-beam (e-beam) lithography. The resist is developed in 1:3 dilution of methyl isobutyl ketone (MIBK) in isopropanol for 3 min, thoroughly rinsed in clean isopropanol and dried under a gentle stream of nitrogen. Finally, about 10 nm of chromium (Cr) and 100 nm of gold (Au) are deposited over the substrate using thermal evaporation to form the electrodes.

The five layers of PMMA of two different molecular weights with a total thickness of about 1.5 μm allow fabrication of large aspect ratio features with an undercut profile, a thinner base and a thicker top as shown in Figure 3-2. The undercut is achieved due to the differential dissolution rate of PMMA of varying molecular weights in MIBK – lower molecular weight PMMA has a faster dissolution rate than the higher molecular weight PMMA. The undercut prevents sidewall coverage during metal deposition and ensures electrical isolation between the electrodes such that functional devices can be achieved.

During the wet-developing process, a capillary force is exerted onto the cantilever, labelled as Electrode 1 in Figure 3-1. This force can cause deflection of the cantilever. If sufficiently large to overcome the spring restoring force, the cantilever collapses on to an opposing PMMA support structure (Electrode 2) and undergoes stiction. The deflection and stiction reduce the gap between the cantilever and opposing electrodes, leading to the formation of nanogaps smaller than originally patterned. The spring constant of the cantilever can be adjusted by altering its geometry and constituent material. At the same time, the surface adhesive forces experienced by the cantilever can be changed by the material selection, solvent and temperature used in the processing, and the placement and geometry of the stationary structures. By adjusting the surface adhesive forces, one can control the extent of deflection and its profile such that desired gap dimensions are achieved. The nanogaps further reduce in size when evaporating a thin-film of metal onto the PMMA to define the conductive electrodes with the reduction in the size depending on the thickness of the deposited film.

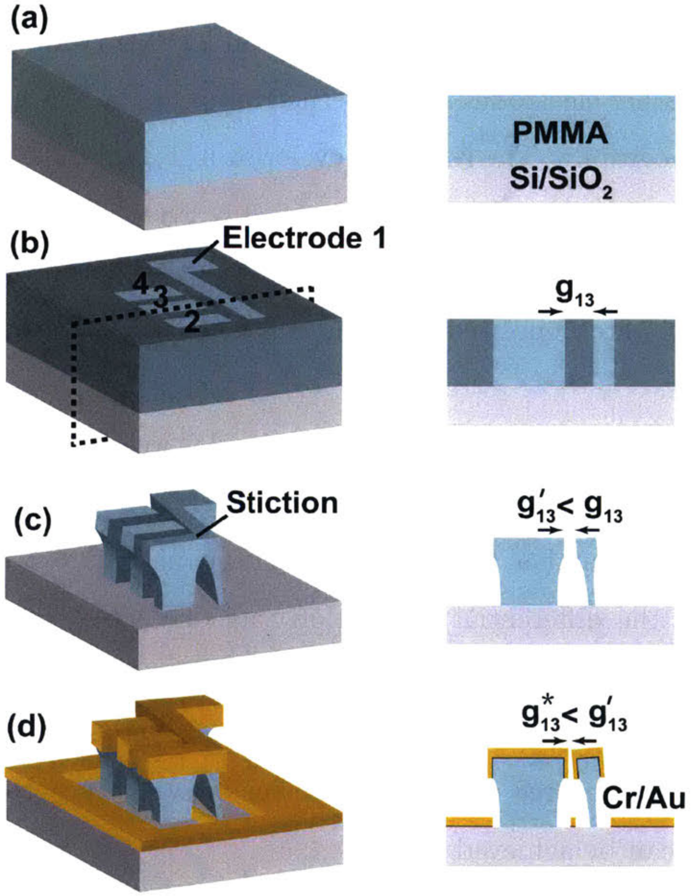

Figure 3-1: Controlled fabrication of nanoscale gaps using stiction: (a) multilayer PMMA e-beam resist is spun onto Si/SiO$_2$ substrate and baked after each spin at 180°C, (b) resist is patterned using e-beam to define cantilever and opposing electrodes separated by a defined gap "g_{13}", (c) resist is developed in 1:3 solution of MIBK in isopropanol, rinsed in isopropanol bath and dried under a stream of nitrogen, (d) ~10 nm of Cr and ~100 nm of Au is evaporated onto the patterned structures defining the electrodes. The gap formed after stiction (g'_{13}) is smaller than that originally patterned (g_{13}). Upon evaporation of the metallic layers, the gap becomes even smaller ($g^*_{13} < g'_{13} < g_{13}$).

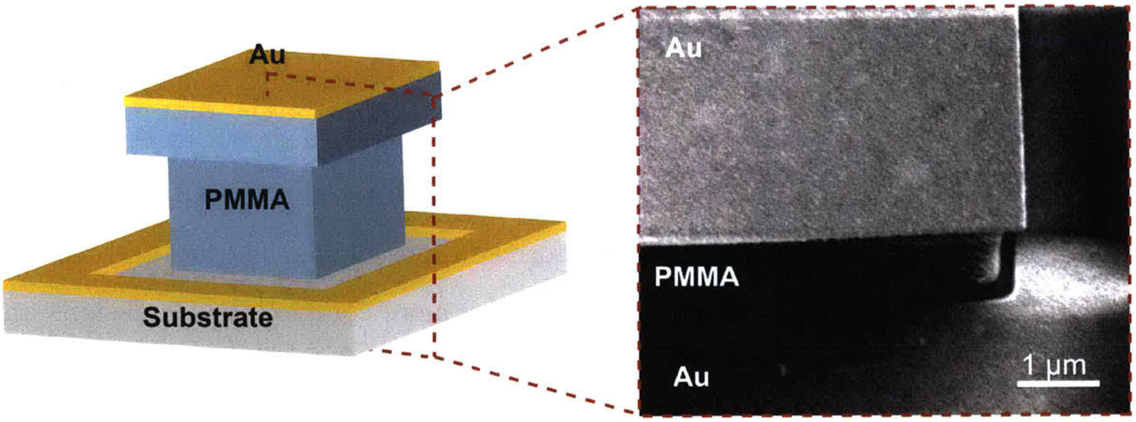

Figure 3-2: An undercut structure formed in PMMA to enable electrical isolation between different device components upon evaporation of the Au film.

3.3 Controlled Formation of Nanogap Electrodes

Figure 3-3 shows the feasibility of the proposed stiction-assisted fabrication scheme to form nanoscale gaps through a single lithography step. As mentioned previously, the surface adhesive forces induced can be modulated by controlling the design and processing conditions including the dimensions of the cantilever, gap size, and the solvent and temperature involved in the liquid-phase fabrication step. If the surface adhesive forces are sufficient to overcome the elastic restoring force, the cantilever collapses onto the support structure where stiction makes this deformation irreversible. The cantilevers of Figure 3-3 are formed based on the scheme shown in Figure 3-1. To promote stiction in this design, the gap size between Electrode 1 and the opposing electrodes is decreased by approximately 30 nm in the cantilever of Figure 3-3b compared to that in Figure 3-3a. Once collapsed, an effective gap of ~50 nm is achieved between Electrodes 1 and 3 at the point closest to the stiction region compared to the 200 nm gap in a similar cantilever that has not undergone collapse and stiction. The proposed fabrication technique is also applicable to material sets beyond those investigated here for the proof of principle demonstration. Changes in the constituent materials and surface engineering using additional coatings can also help modify the adhesive forces to further tune the nanogaps.

Through engineering of the spring constant of the cantilever, and the geometry and relative placement of the electrodes, the size of the nanogaps can be controlled. An example ~35 nm gap is shown in Figure 3-4a. By positioning Electrode 3 closer to the point of stiction, a smaller gap ~10 nm is achieved as shown in Figure 3-4b. The tunability of the gap dimension is further demonstrated in Figure 3-5 where gaps ranging from about 10 nm to 170 nm are formed on a single substrate and through a single lithography step providing a platform for more complex device designs and concepts. With versatility to use a broad set of materials to achieve complex nanostructures over large areas, the stiction-induced fabrication is a promising method for developing functional nanoscale devices that require controlled formation of nanogap electrodes.

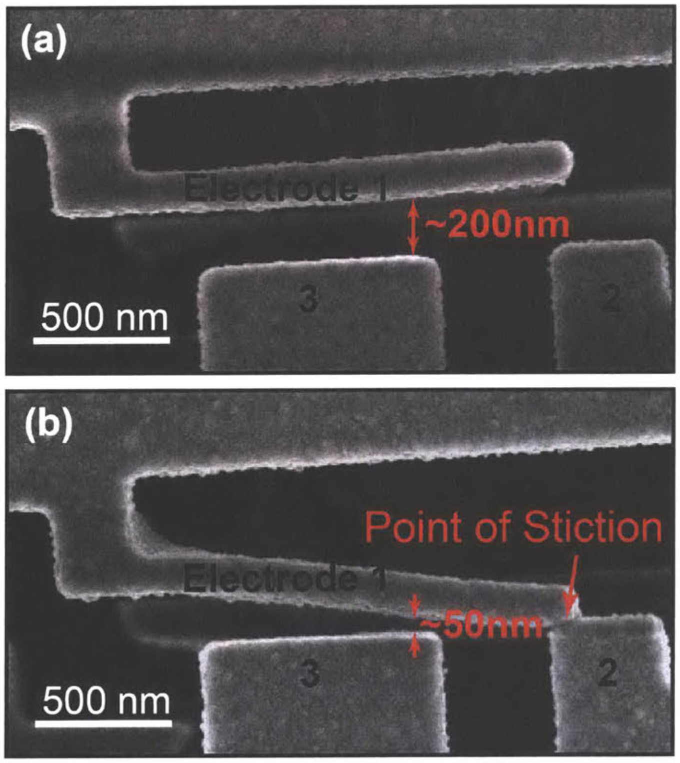

Figure 3-3: Stiction promotes formation of nanogaps smaller than patterned: (a) Scanning electron micrograph (SEM) of a cantilever with a gap of ~200 nm, (b) SEM of the same cantilever positioned closer to Electrodes 2 and 3. Larger capillary force in (b) causes collapse of the cantilever, leading to stiction and reducing the gap between Electrodes 1 and 3.

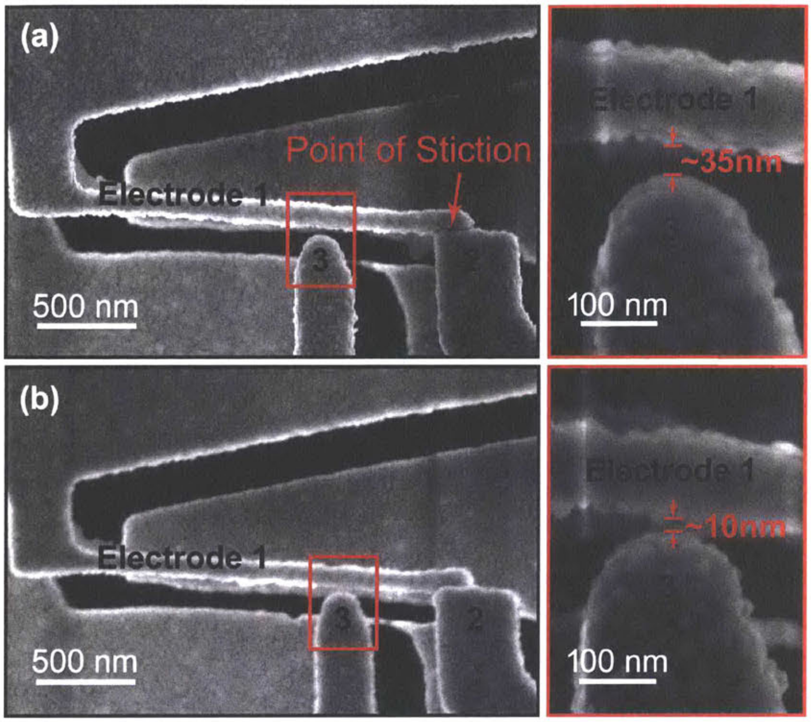

Figure 3-4: SEM of nanogaps fabricated using the scheme in Figure 3-1. Capillary forces during wet developing of the pattern cause stiction between Electrodes 1 and 2, while forming a gap of ~35 nm (a) and ~10 nm (b) between Electrodes 1 and 3. The smaller gap in (b) is achieved by positioning Electrode 3 closer to 2.

3.4 Example Applications

3.4.1 Electrostatically Tunable Nanogaps

A potential application of the proposed nanogap fabrication is in the development of NEM switches where stiction, a common mode of NEM switch failure, is used to promote device miniaturization. To design a NEM switch, the nanogap needs to be electrostatically tunable. In forming the nanogap, depending on the design, the collapsed electrode can be made to remain stationary or undergo mechanical motion in response to electrostatic actuation. As shown in Figure 3-6a, a smaller gap and a more flexible cantilever allow electromechanical modulation of the gap. In this two-terminal example, a current modulation $>10^{11}$ is achieved within 3 V applied bias. The switching performance can be optimized by modifying the device design achieved through changes in the fabrication process. This approach can also be extended to multi-terminal NEM switches that more closely resemble the operation of conventional

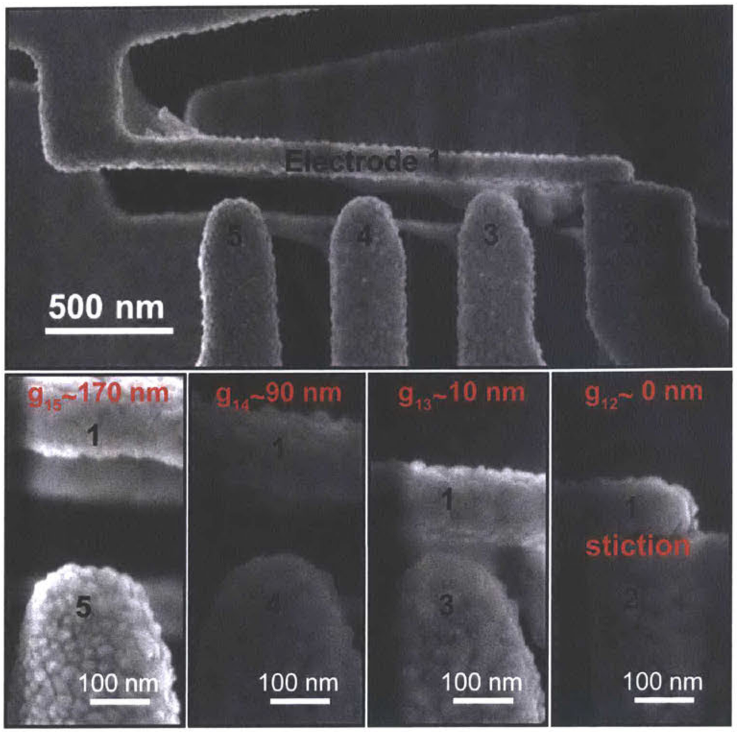

Figure 3-5: Optimizing device architecture and electrode placement relative to the point of stiction allow achieving nanogaps with controlled width, useful for fabrication of multi-terminal devices.

transistors. A prototype design is shown in Figure 3-6b.

3.4.2 Molecular Tunneling Junctions

Nanogap electrodes have also been widely desired for applications in molecular electronics that rely on metal-molecule-metal building blocks. These molecular junctions are conventionally formed using techniques such as direct deposition of metallic contacts, nanotransfer printing of top electrodes and break junctions [63]. The resulting devices commonly lack stability, uniformity and robustness. Additionally, high-throughput fabrication and integration into more complex designs and systems to extend practical applications are limited.

The proposed stiction-induced nanogap fabrication introduces an alternative approach to forming molecular junctions. In this approach, damage to the molecular layer can be avoided and device stability improved as the molecules are introduced into the gap after formation of the electrodes through techniques such as vapor de-

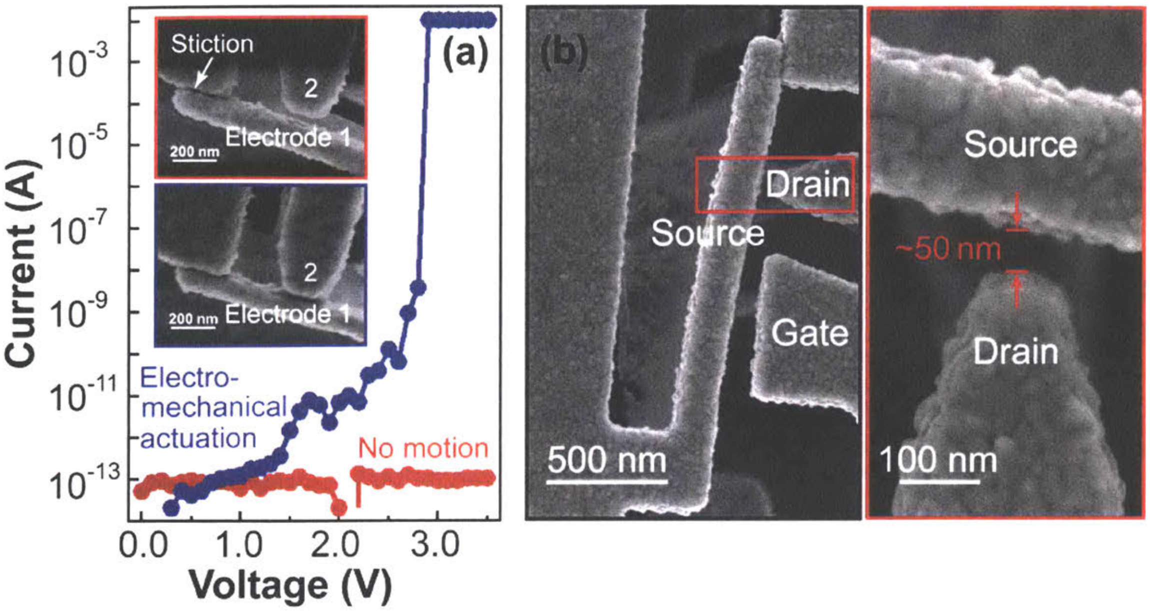

Figure 3-6: Electromechanically modulated nanogap formed using the stiction-based fabrication technique. (a) Through altering device geometry to achieve smaller gaps and more flexible cantilevers, nanogaps can be fabricated to undergo electromechanical modulation (blue compared to red), useful for applications in NEM switches. Insets show corresponding devices with the bottom cantilever (blue) ~20 nm thinner than the top (red). The voltage is applied across Electrodes 1 and 2 and the current between them is monitored. (b) Prototype design of a three-terminal NEM switch with a source-drain gap of ~50 nm. The electrodes are labeled as per a comparable field-effect transistor.

position or liquid-phase self-assembly. In self-assembly, molecules are functionalized with terminal groups that enable selective attachment onto the electrode surfaces, as will be discussed further in Chapter 5. For example, thiolated molecules readily self-assemble on gold.

Figure 3-7 shows the current-voltage characteristics of nanogaps of different sizes with thin-films of fluorinated decanethiol self-assembled on the Au surface using vapor-phase deposition. As expected, a general increase in current is observed with the decrease in gap size. Further analysis of the data to understand the specifics of the molecular gap requires more detailed experimentation. It is speculated that as molecular layers are formed, further decrease in the gap size can be achieved through changes in the surface adhesive forces imposed by changes in the surface properties. Integration of molecular layers in the nanogaps can also be useful for applications in NEM devices where anti-stiction coatings can be introduced to enhance operation reliability. With the versatility to accommodate various metallic electrodes, this fabrication technique can be compatible to a wide set of molecular layers, allowing fundamental analysis of their properties while extending functionalities.

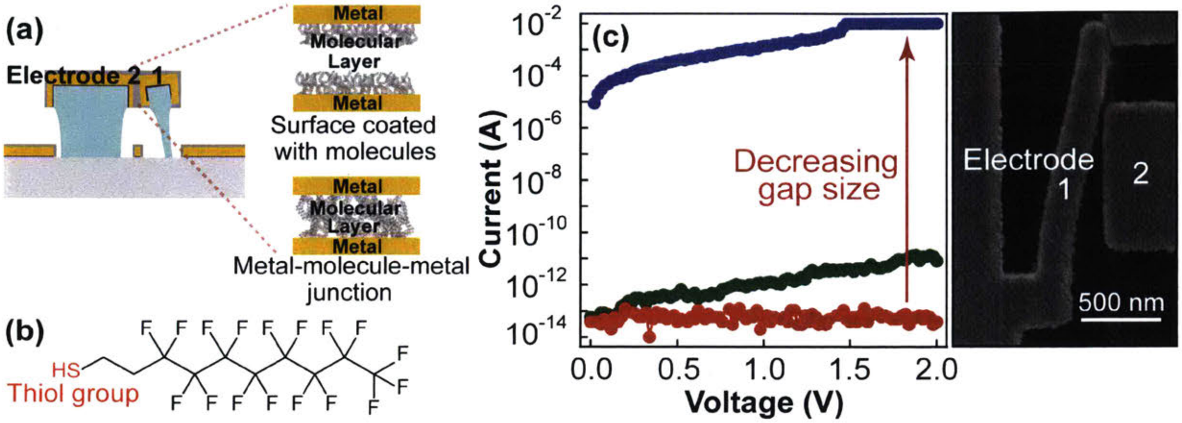

Figure 3-7: (a) Nanogap electrodes formed using the stiction-based fabrication technique involving self-assembled molecular layers. The molecules can serve as coatings on the electrodes to modify surface interactions or can bridge the gap between the two electrodes forming a metal-molecule-metal structure. (b) Chemical structure of fluorinated decanethiol molecule. (c) Current-voltage characteristics of three gaps of different sizes with molecular layers of fluorinated decanethiols self-assembled on the Au electrodes. Representative SEM image of the devices is shown. Nanogaps of different sizes are achieved by changing the original size of the gap patterned through electron-beam lithography.

3.5 Challenges and Outlook

Despite providing a promising platform for controlled fabrication of nanogap electrodes, the proposed technique faces some challenges. As seen in the SEM images, the metal electrodes have a large surface roughness, which introduces inhomogeneity in the gap size, making the device performance less stable and susceptible to electrical shorting. These topographical nonuniformities can also accumulate through potential subsequent processing steps, making this a less ideal basis for fabrication of more complex nanoscale devices and systems. To overcome this challenge, materials alternative to Au and PMMA or techniques such as atomic layer deposition which leads to atomically smooth surfaces should be implemented. In addition, some functional devices can be envisioned that require nanogaps with asymmetric metal electrodes of different materials. Enabling such structures requires modifications to the fabrication scheme that may increase the process complexity. It should be noted that in these electrically-active nanogaps, the induced electrostatic force through an applied voltage can provide yet another mechanism to tune the nanogap post-fabrication to achieve the desired size.

3.6 Summary

A stiction-assisted fabrication is proposed and demonstrated as a promising technique for controlled formation of precisely defined nanogap electrodes. In this approach, top-down lithography is facilitated by the bottom-up engineering of forces to gain nanometer control and precision in fabrication. Capillary forces induced during liquid phase processing of the lithographically patterned sample cause deflection of the mechanically movable electrodes and subsequent stiction to the opposing stationary support structures. The deflection caused by modulation of surface adhesive forces leads to a reduction in the gap size to achieve a width less than originally patterned. The experimental results support the feasibility of the proposed method to fabricate nanogaps, with controlled widths smaller than 15 nm being demonstrated. Further optimization of this versatile fabrication platform allows development of nanogap electrodes for applications including plasmonic, electromechanical and molecular devices.

Chapter 4

Fabrication of Nanoscale Gaps with Nanometer Resolution and Surface Uniformity

When engineering at the limits of the nanoscale, in addition to nanometer control and resolution in fabrication, nanometer surface uniformity is essential. In developing nanogap electrodes, a fundamental component of active nanoscale devices such as nanoelectromechanical switches, many of the techniques developed to date including that introduced in Chapter 3 lack the desired surface uniformity. The resulting irregularities which can be on the order of the device critical dimensions can hinder the expected function. Furthermore, some of these techniques suffer from inefficient scalability to larger areas and lack versatility in the choice of compatible materials and substrates.

As discussed in Chapter 2, bottom-up techniques promise to achieve nanometer precision, resolution and uniformity beyond the limits feasible through top-down approaches. Importantly, they are well suited for large-area processing with minimal limitations on the choice of substrate or the materials employed. However, the re-

---

Chapter 4 is adapted with permission from [F. Niroui, M. Saravanapavanantham, T. M. Swager, J. H. Lang and V. Bulović, Fabrication of nanoscale structures with nanometer resolution and surface uniformity, *Micro Electro Mechanical Systems (MEMS), 30th IEEE International Conference*, 659–662, 2017]. Copyright 2017 IEEE.

sulting structures often lack the infrastructure needed to function as independent electrically-controlled entities, a feature required for many device applications. To overcome the limitations of bottom-up assembly while leveraging their benefits, here we propose a hybrid approach in which bottom-up assembly is assisted by the top-down lithographic techniques [72].

4.1 Design Principles

The integrative fabrication methodology proposed here consists of three main steps. First, bottom-up assembly is used to promote controlled formation of well-defined nanogaps using chemically-synthesized single-crystalline Au nanoplates shown in Figure 4-1. These Au nanoplates have surface uniformity significantly better than Au thin-films formed through thermal evaporation. While an evaporated Au film exhibits roughness ~4 nm, single-crystalline Au nanoplates posses roughness <1 nm (Figure 4-2). Second, top-down lithography is used to integrate interconnects with the nanogaps such that they can be electrically-activated. Third, a technique is implemented to planarize the step height that is introduced across the nanogap by the nonuniform thicknesses of the chemically-synthesized nanoplates. The planarization also helps eliminate the edge imperfections and reduce surface roughness of the lithographically patterned electrical connections. The latter will be discussed in more detail in Chapter 8 where a variation of this method is implemented in another device design.

4.2 Fabrication Flow

The fabrication scheme used for formation of nanogap electrodes using the single-crystalline nanoplates is shown in Figure 4-3. Au nanoplates are synthesized by reducing gold(III) chloride hydrate ($HAuCl_4$) with ethylene glycol in presence of aniline and using polyvinylpyrrolidone (PVP) as the capping agent [73]. The synthesis protocol is outlined in Appendix B. The self-assembly of the nanoplates is driven by

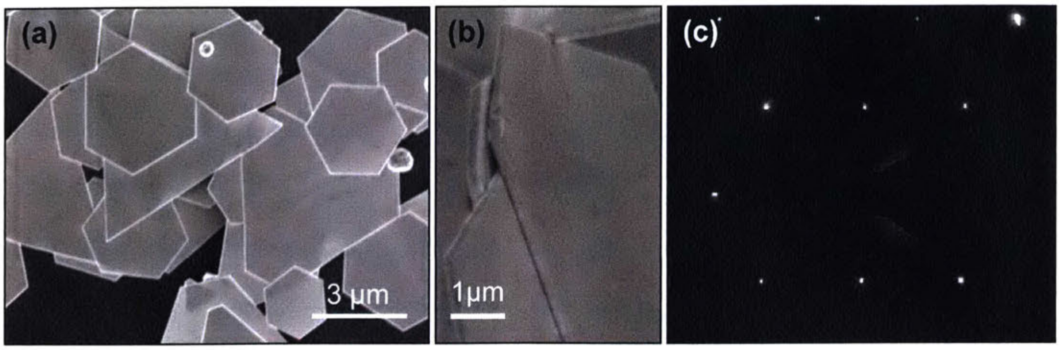

Figure 4-1: SEM images of chemically-synthesized Au nanoplates with well-defined shapes, edges and thicknesses (a and b). The single-crystalline nature of the nanoplates is confirmed in the transmission electron microscopy diffraction pattern of (c) showing Au(111) plane.

engineering the surface interactions between the plates such that they come together to form the nanogaps (Figure 4-3a). The as-synthesized Au nanoplates are functionalized with octadecanethiol to assume a hydrophobic surface, and then are phase transferred into chloroform. A $\sim$20 μL droplet of the functionalized Au nanoplates is then dispensed on a thin layer of deionized water coating a SiO_2 substrate of about 1 cm^2. Chloroform is immiscible in water. The hydrophobic surfaces of the Au plates allow them to disperse in chloroform but prevent them from entering the hydrophilic phase, enabling them to be suspended at the water-chloroform interface. Chloroform, having a higher density than water, exerts a downward force on the plates to stabilize them at the interface. As the solvents evaporate, a force is exerted laterally to bring the Au plates together to form nanogaps that adhere onto the substrate once the solvents are completely evaporated.

Upon assembly, the substrate containing the nanogaps is briefly sonicated in ethanol to remove the undesired aggregated Au nanoplates and spherical Au particles that are formed as byproducts of the synthesis. To remove the residual PVP and octadecanethiol molecules, the substrate is then rinsed in a piranha solution. Once cleaned, interconnects and contact pads are added to the nanogaps using electron-beam lithography and a lift-off process based on thermally evaporated Au. It should be noted that the commonly used Cr adhesion layer is not used here. This ensures that the Au electrodes have a weak adhesion to SiO_2 to enable future processing steps, as will be discussed.

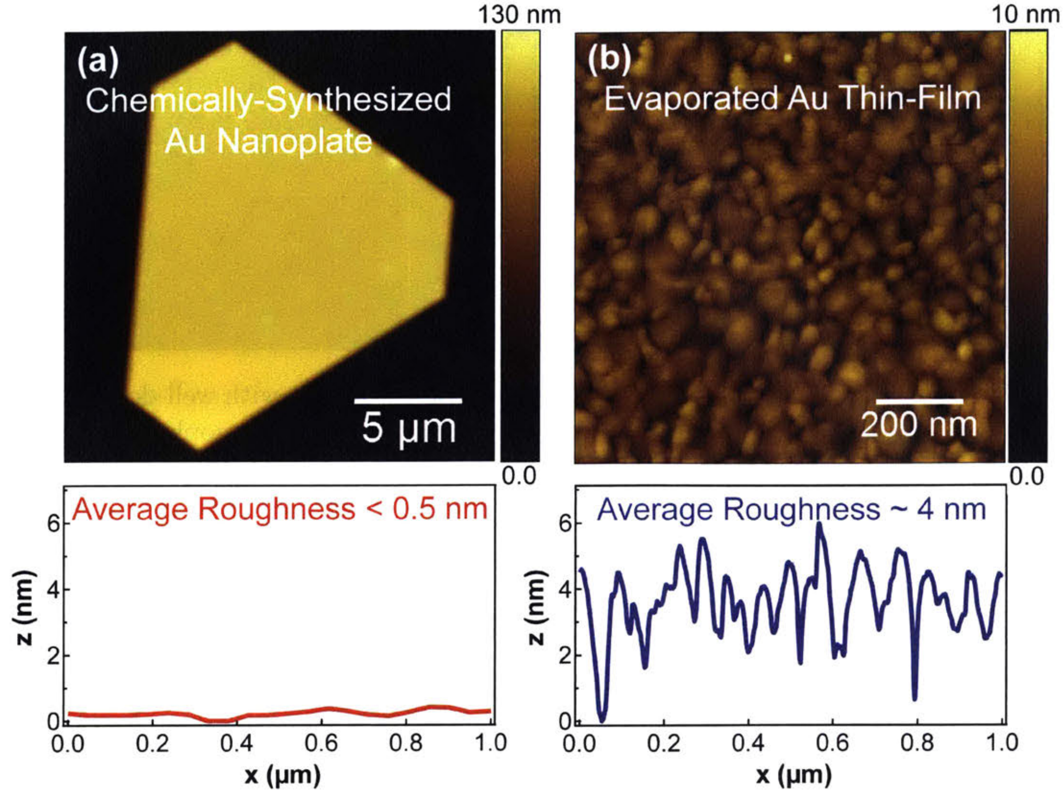

Figure 4-2: Atomic force microscope surface topography scan of the single-crystalline Au nanoplate shows roughness of <1 nm (a), much smaller than ~4 nm roughness expected for a thermally evaporated layer of Au (b).

At this point, electrically accessible well-defined nanogaps are achieved. However, due to nonuniformities in the thicknesses of the Au nanoplates, a step height across the nanogap may be present. If a planarized profile is required, the height variation must be eliminated. This is achieved through peeling the Au nanoplates and the electrical contacts using a receiving surface covered with an adhesive layer. The peeling reveals the coplanar side of the plates originally in contact with the substrate. To do so, first, the substrate is functionalized with a layer of low surface-energy trichloro(1H,1H,2H,2H-perfluorooctyl)silane through vapor or liquid-phase growth. The molecular structure is depicted in Figure 4-3b. The functional silane end-groups of the molecules allow assembly on the SiO_2 such that surfaces not covered by the Au acquire an anti-stiction property promoted by the fluorinated chains of the molecular coating. Then, a ~30 μL drop of an ultraviolet light (UV) curable epoxy (Norland Optical Adhesive 61) is dispensed onto the substrate, following which, a receiving

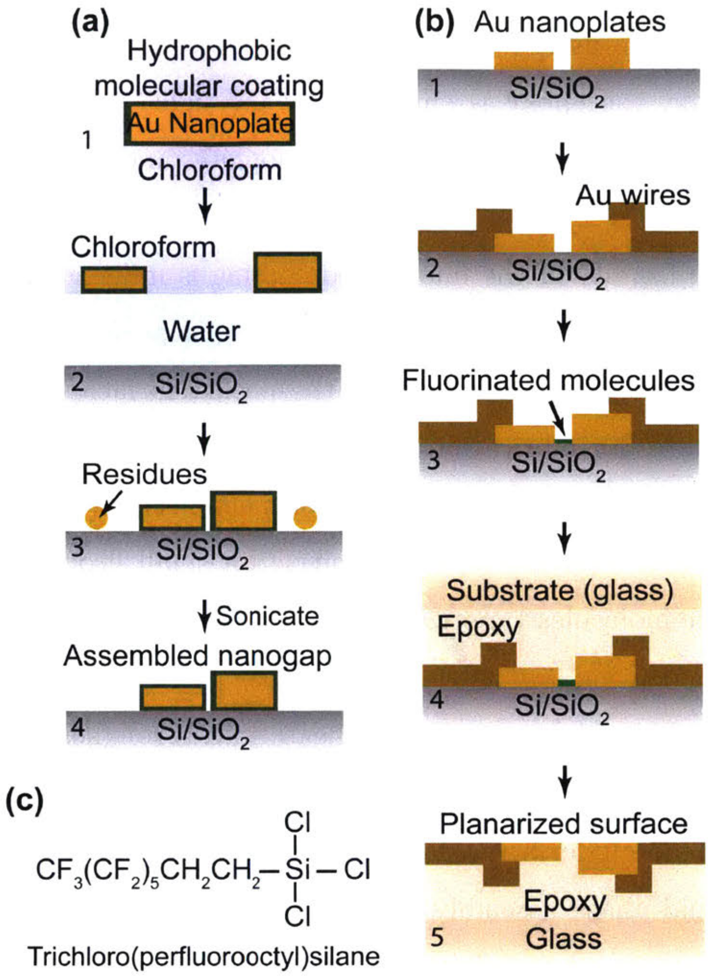
(a)
Hydrophobic molecular coating
Au Nanoplate
1
Chloroform
Chloroform
Water
2
Si/SiO2
Residues
3
Si/SiO2
Sonicate
Assembled nanogap
4
Si/SiO2
(b) Au nanoplates
1
Si/SiO2
Au wires
2
Si/SiO2
Fluorinated molecules
3
Si/SiO2
Substrate (glass)
Epoxy
4
Si/SiO2
Planarized surface
Epoxy
5
Glass
(c)
CF3(CF2)5CH2CH2–Si–Cl
Cl
Cl
Trichloro(perfluorooctyl)silane

Figure 4-3: Combined bottom-up self-assembly and top-down lithography formation of electrodes separated by nanogaps and with nanometer uniformity. (a) To self-assemble the nanogaps, nanoplates are surface functionalized with octadecanethiol to assume hydrophobic surface properties and then are assembled at the water-chloroform interface using hydrophobic-hydrophilic interactions and capillary forces as the solvents evaporate. (b) Nanogaps are formed using self-assembly of Au nanoplates (1) upon which wires and contacts are added using electron-beam lithography and lift-off (2). After anti-stiction treatment of the substrate surface (3) with trichloro(perfluorooctyl)silane, a UV-curable epoxy is used to peel off the nanogap and the interconnects onto a glass substrate to planarize the surface (4). (c) Chemical structure of trichloro(perfluorooctyl)silane used as anti-stiction coating in the planarization process.

glass substrate is placed on top of the adhesive layer. Capillary forces cause the epoxy to spread, forming a uniform layer in between the original substrate and the receiving surface. The uniformity of the epoxy layer is further improved by placing the sample inside a vacuum desiccator. Pulling vacuum also assists in eliminating the small air bubbles that might be introduced in the epoxy. If not removed, these bubbles can add to the undesired surface roughness. After removing the substrate from the desiccator, the epoxy is cured under UV light. Once cured, the glass is detached from the SiO_2, peeling off the Au nanoplates and electrical connections as a uniform layer.

The surface uniformity of the fluorinated coating is influenced by the deposition technique and its roughness translates into the roughness of the peeled epoxy layer. It is desired to minimize the roughness of the peeled surface such that it is suited to serve as a platform for fabrication of nanoscale devices and systems upon further processing steps. For vapor-phase deposition of the molecules, the substrate is placed inside a vacuum desiccator in close proximity to a small droplet of the molecules. Under vacuum, the molecules vaporize and assemble onto the substrate. This process can lead to polymerization and formation of thicker and nonuniform molecular films. The roughness of these films can then replicate into a rougher epoxy surface upon peeling as shown in Figure 4-4a. This roughness can be minimized if the substrate is rinsed in fresh ethanol under brief sonication upon the vapor-phase assembly process. Alternatively, liquid-phase assembly of the fluorinated coating leads to a uniform surface, shown in Figure 4-4b. To promote liquid-phase assembly, the substrate is placed inside a 5 mM solution of fluorinated molecules in anhydrous ethanol in a nitrogen glovebox environment. After 4 hours, the substrate is removed from the solution of molecules, rinsed in fresh ethanol and dried under a stream of nitrogen.

4.3 Electrically-Active Nanogaps with Nanometer Resolution and Uniformity

The self-assembly of Au nanoplates leads to formation of well-defined nanogaps with nanometer resolution and precision. Figure 4-5 shows nanogaps of various widths as small as ~10 nm formed through this bottom-up approach with a resolution, and edge and surface uniformity not feasible through conventional top-down fabrication.

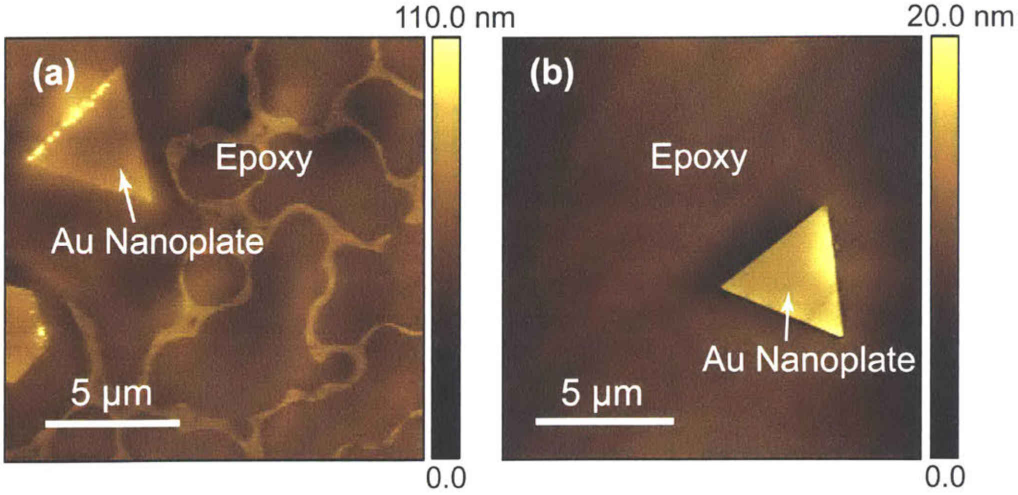

Figure 4-4: The deposition technique used to fluorinate the substrate influences the molecular layer's uniformity which defines the roughness of the peeled epoxy surface. AFM topography scan of a surface containing a Au nanoplate peeled off a substrate fluorinated by vapor-phase assembly shows a rough surface (a). The surface roughness is minimized when trichloro(perfluorooctyl)silane is assembled in a liquid-phase instead (b).

The gap width is influenced by factors including the substrate surface properties, types of immiscible solvents used, molecular coating on the nanoplates, density of Au nanoplates, and temperature used for the assembly process. The smallest nanogap possible is limited by the thickness of the molecular layer that functionalizes the nanoplates. However, to reach this limit other experimental conditions, mentioned above, need to be controlled as they influence the assembly process.

As mentioned previously, due to variations in thicknesses of the nanoplates chemically synthesized, there typically exists a step height and nonuniform profile across the nanogap. An example is shown in Figure 4-6 where ~5 nm height variation is observed across the gap. Depending on the application, it might be desired to planarize this profile. Figure 4-7 illustrates an electrically accessible, ~30 nm gap with <1 nm surface roughness and a planarized surface fabricated using the scheme of Figure 4-3. In this example, peeling is used to ensure the step height across the nanogap is removed. The peeling also eliminates the edge defects on the lithographically patterned electrical wires and pads, associated with the lift-off process, by exposing the side originally in contact with the SiO_2 substrate. The bottom surfaces of the patterned structures

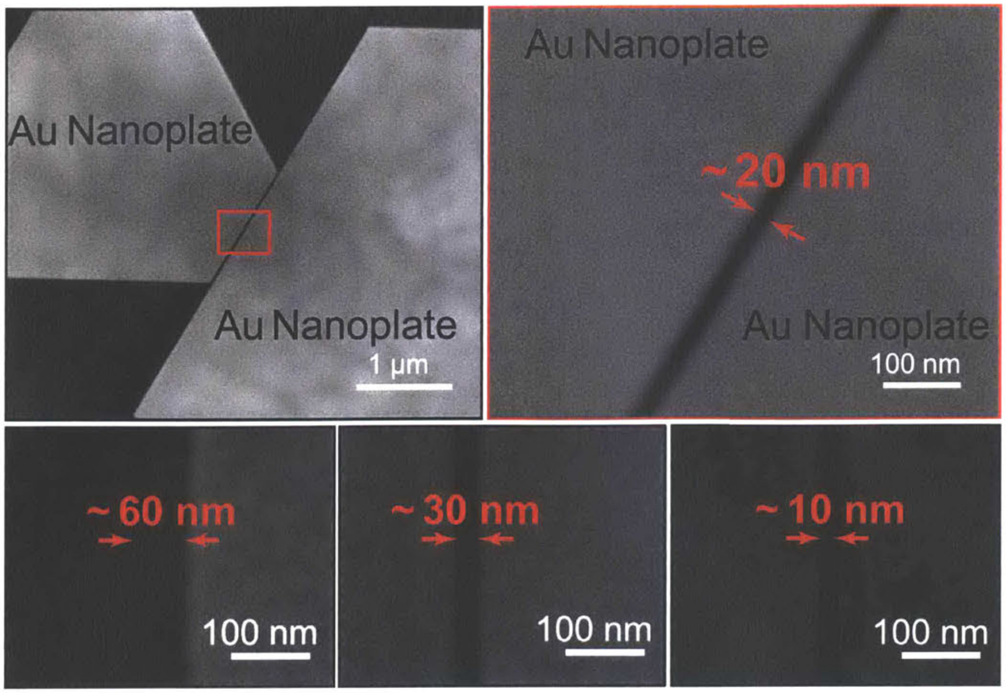

Figure 4-5: Precisely defined nanogaps with nanometer resolution and surface uniformity formed through self-assembly of Au nanoplates based on the method shown in Figure 4-3a.

assume the surface roughness of the underlying substrate. By revealing this surface after peeling, the electrical connections acquire a roughness much smaller than that associated with the top surface of the evaporated Au thin-film.

4.4 Example Application

The fabricated electrically-driven nanogaps can be used as building blocks of nanoscale devices with applications in nanoelectromechanical systems, molecular electronics and active plasmonics. They serve as a platform where further processing can be used to form more complex nanoscale structures with tailored functionalities.

An example application is shown in Figure 4-8. Here, Au nanoparticles coated with a layer of cetylpyridinium chloride (CPC) are dielectrophoretically trapped across the gap to form a vertically-defined molecular junction [74–77]. The current-voltage characteristics of Figure 4-8 show an increase in conduction through the molecular junction formed based on the nanoparticle, compared to the current conduction through the

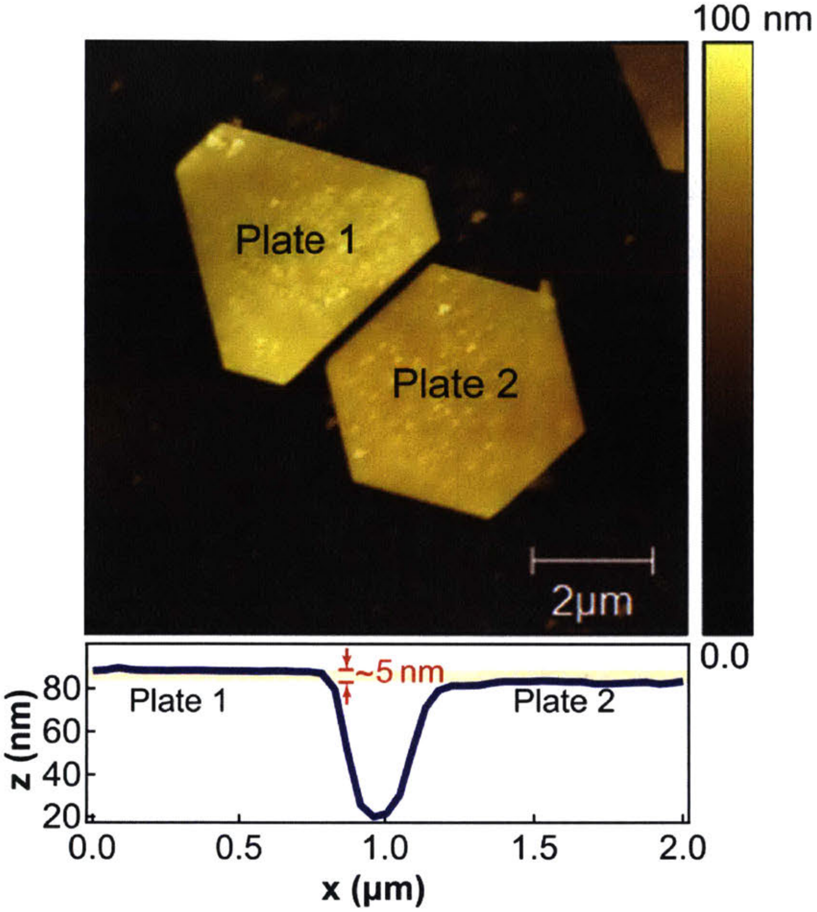

Figure 4-6: AFM surface topography shows a height variation of ~5 nm across the nanogap formed between the Au nanoplates due to the variations in thicknesses of the chemically-synthesized nanoplates.

laterally aligned nanogap prior to nanoparticle trapping. By tailoring the thickness and the type of molecular coating employed in functionalizing the nanoparticle or the Au nanoplate surfaces, molecular junctions of varying electronic performance emerge. Subsequently, a range of applications in molecular devices can be realized.

4.5 Challenges and Outlook

The proposed fabrication technique is demonstrated with Au nanoplates and interconnects. However, this process can be extended to other materials and their combinations to accommodate various applications. Currently, due to the relatively large size distribution that is present in the synthesized nanoplates, the assembly is of-

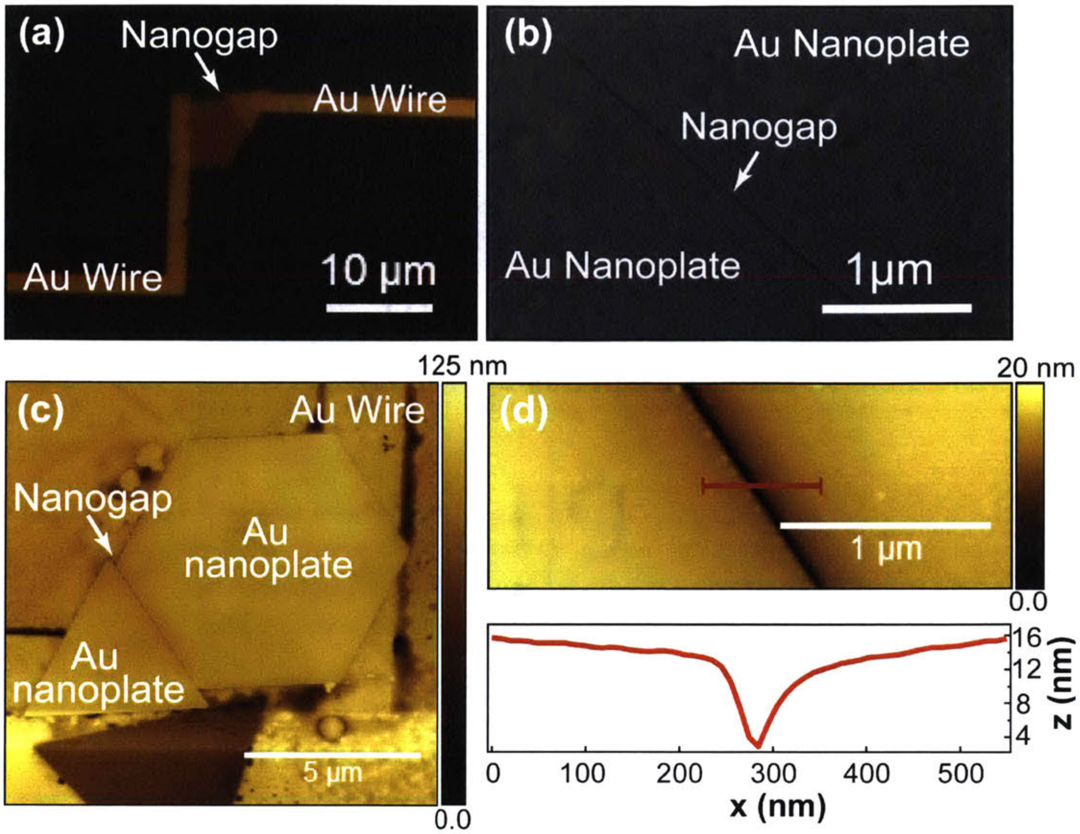

Figure 4-7: (a) Optical image of a planarized electrically contacted nanogap formed in between Au nanoplates. (b) SEM of the corresponding nanogap with a width of ~30 nm. (c) The AFM surface topography of the structure shows uniform surfaces on the Au nanoplates and lithographically patterned Au wires achieved through the peeling technique. (d) A uniform AFM profile is observed across the nanogap.

ten localized. Further optimization is necessary to enable uniform self-assembly over larger areas with precise control over spatial positioning. This can be achieved by improving the synthetic approach to yield nanoplates with a smaller size distribution, and by optimizing the assembly conditions. To allow for deterministic positioning of the nanogaps, directed assembly methodologies can also be implemented, for example, through use of physical guides formed using conventional lithography.

4.6 Summary

The unprecedented precision and resolution of bottom-up assembly is combined with the versatility of top-down lithography to develop a technique for fabrication of

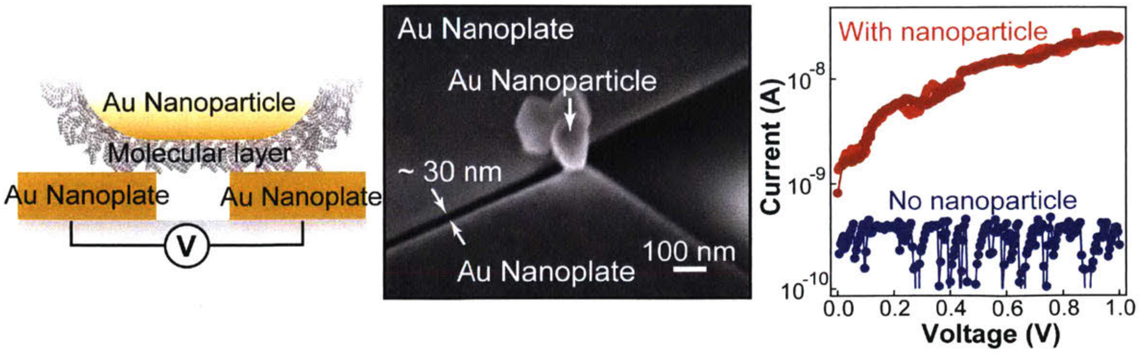

Figure 4-8: Through dielectrophoretic positioning of Au nanoparticles coated with a molecular layer across the nanogap, vertical molecular tunnel junctions can be formed. The SEM image shows Au nanoparticles coated with cetylpyridinium chloride bridging a ~30 nm Au nanoplate electrodes. The current-voltage characteristic compares the current conduction before (blue curve) and after trapping (two consecutive measurements are shown in red).

electrically-active well-defined nanogaps <10 nm. By engineering surfaces and interfaces, chemically-synthesized gold nanoplates, with <1 nm surface roughness, are assembled to form nanogaps. Interconnects and electrical contact pads are added using top-down lithography to introduce electrical functionality to the assembled nanogaps. A planarization technique is employed to eliminate nanometer-scale height variations across the gap due to the thickness inhomogeneity inherent to synthesized nanoplates. This is achieved by peeling the nanoplate electrodes as a uniform layer off the original substrate using an adhesive receiving surface, revealing the coplanar side originally in contact with the substrate. The peeling also eliminates edge defects and minimizes the surface roughness inherent to features formed through lithography. Overall, a platform to enable nanoscale devices of various functionalities including those relevant to molecular electronics, plasmonics, and nanoelectromechanical systems is achieved.

Part II

Nanoscale Force Control – A Molecular Approach

Chapter 5

Molecules and their Applications in Nanoscale Processing

The field of molecular electronics, dating back to nearly 50 decades ago, has been dominantly focused on the study of molecules as the building blocks of electronic devices and corresponding transport phenomena. Progress in the field has been continuously challenged by the limitations in fabrication and measurement capabilities. Given the nanometer scale dimensions of the molecular devices, the performance reliability is notably sensitive to any nonidealities, even though small, in the fabricated structures and the measurement methodologies. With rapid progress in fabrication and characterization over the past years, the field of molecular electronics has expanded beyond electronic transport to explore other intrinsic features and their utility in functional devices [78–84]. Examples of emerging applications include molecular spintronics, plasmonics, thermoelectrics, optoelectronics, and quantum optics. Despite rapid progress in the field, an in-depth understanding of the underlying physical phenomena and full exploration of the technological opportunities are in their infancy and a topic of active research. In particular, integration of emerging device concepts into more complex functional systems remains a challenging prospect.

The atomic control over molecular design achieved through chemical synthesis provides a versatile approach to engineer molecule's inherent properties. The result is a large library of molecular units that can chemically or physically interact with one another or other nanostructures to build active devices and systems. In addition to the possibility of possessing unique properties such as electrical, optical or thermal, importantly, molecules can serve as structural units to facilitate engineering of nanoscale structures in the few-nanometer regime with atomic resolution. Their mechanical properties and induced surface interactions defined by their chemical composition further assist in controlling nanoscale forces towards structural robustness and tunability. With the ability to serve as chemically-engineered nonlinear springs, molecules can offer a new dimension to the properties of restoring springs that are needed in mechanically-active structures. Thus, when designing emerging molecular devices, the molecules' structure, chemical composition and mechanical properties are important in nanoscale processing (Figure 5-1).

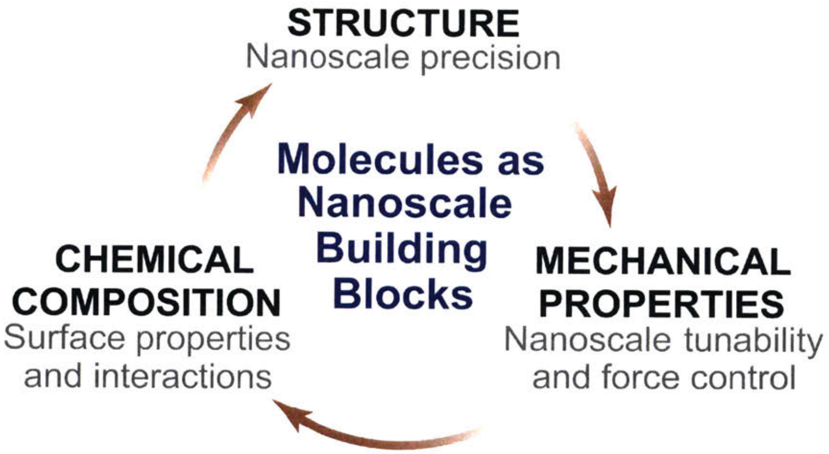
STRUCTURE
Nanoscale precision
Molecules as Nanoscale Building Blocks
CHEMICAL COMPOSITION
Surface properties and interactions
MECHANICAL PROPERTIES
Nanoscale tunability and force control

Figure 5-1: Molecules which can be precisely engineered through chemical synthesis serve as nanoscale building blocks by helping define device design and surface interactions using their inherent structural, mechanical and chemical properties.

5.1 Molecules as Structural Components

As discussed in Part I, fabrication of structures few nanometers in size is often limited by the resolution of the processing techniques. In particular, defining nanometer-thin spacing between neighboring structures is a challenge as the dominating surface adhesive forces at such small spacing can cause collapse of the structures. Molecules which can be precisely defined in conformation using chemical synthesis can serve as interconnects between neighboring surfaces. The atomic precision in defining the size of the molecule leads to an unprecedented precision in defining the spacing. Additionally, the molecules provide a restoring force to help balance out the surface adhesive forces to provide structural stability. In simplest form, this can help develop stable nanogaps, a topic of interest in this thesis, but more complex structures can also be facilitated.

Molecules can form into a thin-film using a self-assembly process. Through chemical synthesis, molecules can be designed with functional end groups that allow specific and spontaneous assembly onto the desired surface (Figure 5-2). Such self-assembly of molecular layers have been widely studied through which functional groups suitable for assembly by covalent or noncovalent interactions onto a wide range of materials have been identified. Thiol-chemistry for example, through which sulfhydryl (thiol) functional group (-SH) adsorbs to surfaces including Au, Ag, Pt, Ru and Ni, has been extensively studied and employed in molecular electronics [85].

Through engineering of the spacer group, the length of the molecules can be tuned to precisely control the molecular layer thickness and consequently the spacing between neighboring surfaces. Figure 5-2b shows an example where poly(ethylene glycol)dithiol (PEG-dithiol) is self-assembled using thiol-chemistry on the surface of Au nanocubes. By changing the polymer chain length, reflected in its molecular weight, the effective thickness of the self-assembled layer can be modified.

Beyond self-assembly, other techniques including thermal evaporation, spin-coating, molecular layer deposition, and layer-by-layer deposition can also be used in the formation of nanometer-thin molecular layers. Among these techniques, layer-by-layer deposition which relies on cyclic deposition of alternatively charged molecules through electrostatic interactions provide nanometer precision in defining thicknesses, over large areas and applicable to a wide range of materials. The control over thickness is shown in Figure 5-3 for the case of layer-by-layer deposited films of poly(sodium styrenesulfonate) (PSS) and poly(allylamine hydrochloride) (PAH) on Au substrates and measured with a spectroscopic ellipsometer. Here, PSS serves as the polyanion and PAH forms the polycation needed in the assembly process.

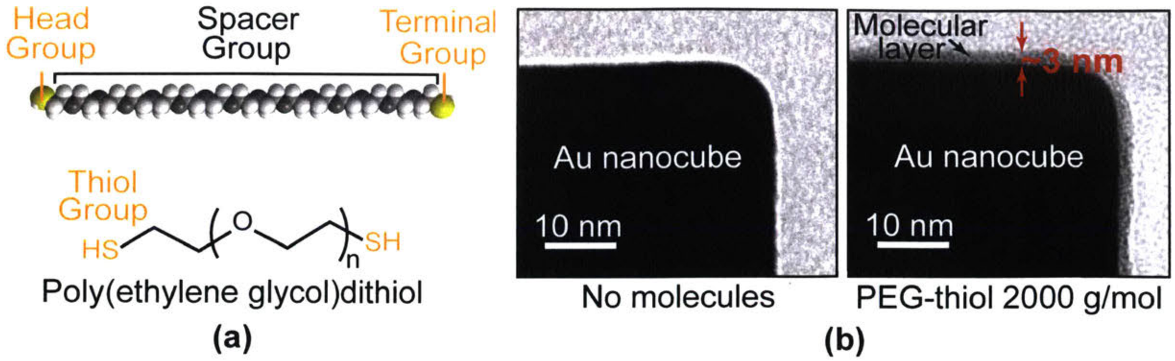

Figure 5-2: (a) Molecules can be engineered through chemical synthesis with the desired head, terminal and spacer groups where the functional end groups can be selected to allow spontaneous and selective assembly onto a desired surface, while the spacer group can help define the size, structure, chemical and mechanical properties. As an example, thiol functional groups in poly(ethylene glycol)dithiol allow self-assembly on Au. The transmission electron micrographs (TEM) in (b) show the surface of a Au nanocube without any molecular coating compared to that with ~3 nm-thick self-assembled layer of PEG-dithiol. The thickness of the molecular film is dependent on the polymer chain length.

5.2 Engineering Surface Interactions with Molecules

The spacer and functional end groups of a molecule can also help define its chemical properties, determining its interactions with the surrounding. By coating surfaces with the molecules, consequently, the surface properties can be modified. This has made molecular layers a versatile approach for surface and interface engineering to either enhance or reduce the surface interactions with the surrounding components. By controlling the surface interactions, the molecules help provide control over nanoscale processes from bottom up and hence yield higher precision. For example, by enhancing compatibility between typically incompatible surfaces, their uniform integration into multi-component structures can be improved using molecular coatings. On the other hand, molecular layers can be used as anti-stiction coatings to avoid adhesion between neighboring or approaching surfaces. Beyond providing structural stability, this technique can assist with the controlled and reversible dynamic tunability. An important application of the latter will be in nanoelectromechanical systems that involve electromechanically tunable nanogaps.

By modifying the contacts in an electromechanically active nanogap with a low surface energy molecular layer, the interactions between the approaching electrodes

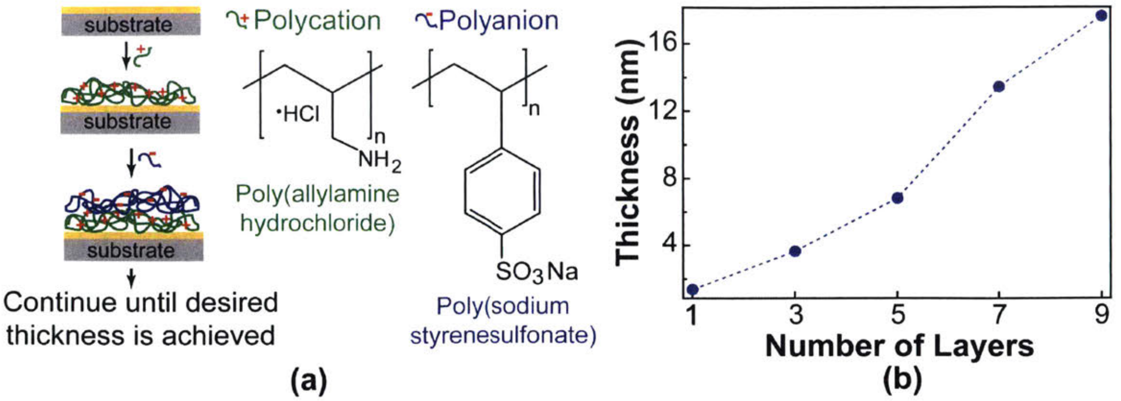

Figure 5-3: (a) Layer-by-layer deposition of polyelectrolytes allows cyclic assembly of oppositely charged entities for example poly(allylamine hydrochloride) (PAH) and poly(sodium styrenesulfonate) (PSS) with precise thicknesses. The precision in forming nanoscale molecular layers is shown in (b) for the case of layer-by-layer deposition with PAH and PSS on a Au substrate and characterized with a scanning ellipsometer.

can be minimized [11, 86, 87]. This will not only help improve the device reliability and robustness but can help lower the hysteresis. The area within the hysteresis curve in a NEM switch corresponds to the lost switching energy. Reducing the hysteresis is therefore necessary to reduce the switching energy to move towards a more energy-efficient operation. The importance of molecular coatings in reducing surface adhesive forces is evident in Figure 5-4 where the hysteresis voltage of the NEM relay is reduced by $\sim$40% to $<$50 mV when contacts are treated with fluorinated alkane molecules (1H,1H,2H,2H-perfluorodecyltriethoxysilane) [11]. The fluorocarbon backbone lowers the surface energy and the surface adhesive forces while the silane functional group is used to promote the self-assembly onto the W contacts. The x-ray photoemission spectrum (XPS) in Figure 5-5 confirms successful self-assembly of the molecules which is performed in vapor phase.

5.3 Molecules as Nanoscale Scaffolds and Springs

As discussed, molecules can serve as scaffolds to define the spacing between neighboring nanostructures with nanometer precision and control. The mechanical properties of the molecules can further be leveraged to promote controlled and reversible tuning

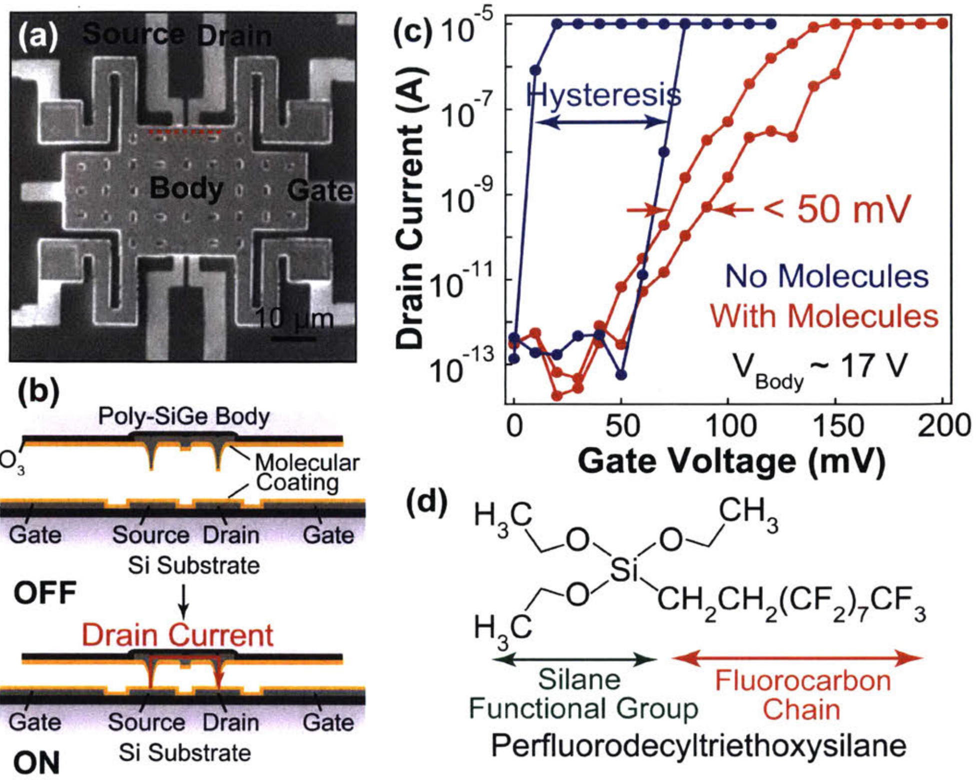

Figure 5-4: Modifying contacts of a NEM relay with low surface energy fluorinated molecules reduces stiction demonstrated through lowering of the hysteresis voltage, in this example design achieving ~40% reduction on average. The NEM relay design is shown in the SEM image of (a) with the schematic cross-section of the device and the chemical structure of the molecular coating shown in (b) and (d) respectively. An example switching performance with and without molecular coating is included in (c), a hystereis <50 mV is achieved [11].

of the defined dimensions. In this scheme, shown in Figure 5-6, an applied external force can compress the molecules as the two surfaces approach each other. The elastic restoring force in the deformed molecules can help balance the surface adhesive forces during this process. Once the applied force is removed, the surface adhesive forces are overcome by the elastic restoring force of the deformed molecules to avoid stiction, transition back to the original dimensions, promoting controlled and reversible operation. This nanoscale force control in particular is important at the few-nanometer regime where controlling large surface adhesive forces is a great challenge.

The key is precise engineering of the mechanical response to achieve continuous balancing of the surface attractive forces throughout the tuning process. The mechan-

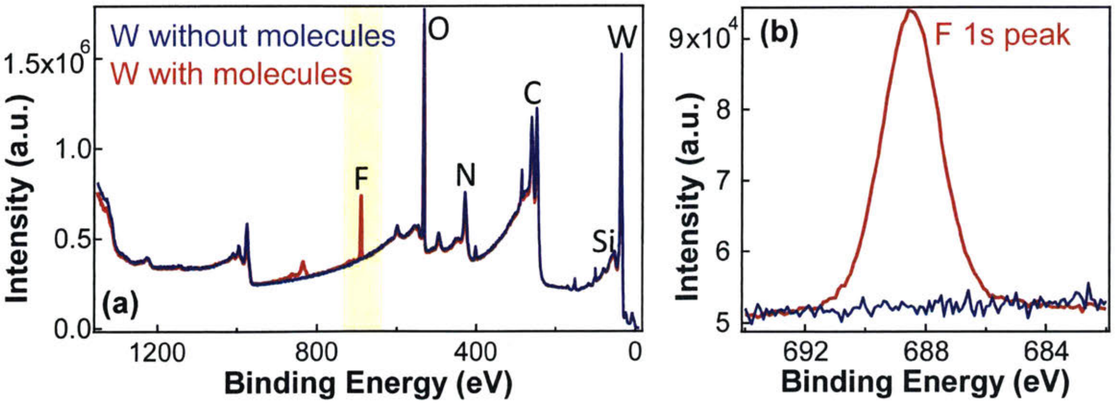

Figure 5-5: The XPS spectrum of a tungsten (W) film with and without surface treatment by perfluorodecyltriethoxysilane confirms self-assembly of the molecular layer through use of silane end groups in a vapor-phase process. This is confirmed as a fluorine (F) peak is detected when characterizing the sample with the self-assembled fluorinated molecules while no F peak is observed for the sample without exposure to the molecules.

ical properties and their deformation-dependent dynamics can be engineered through chemical composition and physical form. This can be achieved at two levels: the design of individual molecules through chemical synthesis or collective engineering of the molecular layer by modifying its morphology and incorporating molecular entities of different properties. Such engineering of molecular mechanics is feasible but lacks the comprehensive knowledge-base needed for the design due to the limited studies executed to date concerning mechanics at molecular level. Tunability of dimensions can also be achieved by utilizing electrically-active molecules that change conformation in response to introducing a charge imbalance [88, 89]. The different approaches to

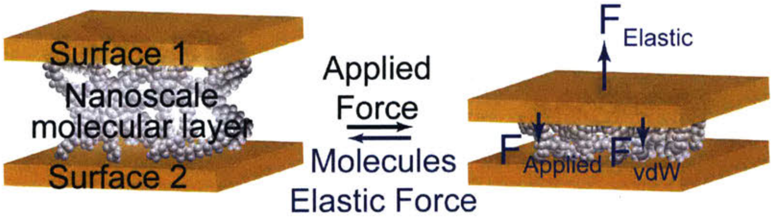

Figure 5-6: Nanoscale force control using molecular layers as springs. An applied force (F_{applied}) compresses molecules connecting two neighboring surfaces. The elastic force (F_{elastic}) stored in compressed molecules overcomes the van der Waals forces (F_{vdW}) to make the process controlled and reversible.

engineering mechanically conformal spacers are outlined in Figure 5-7. Few research efforts have fundamentally studied mechanical performance of molecules, effects of molecular deformation on the electronic transport, and conformational changes in molecules due to optical or electrical stimuli [90–93]. However, utility of mechanical properties in developing active yet autonomously functioning molecular devices has not been well explored. The field remains to be an ongoing area of research while many opportunities for devices of unique functionalities can be envisioned given the added degree of freedom provided by nanomechanics to promote engineering at the limits of the nanoscale.

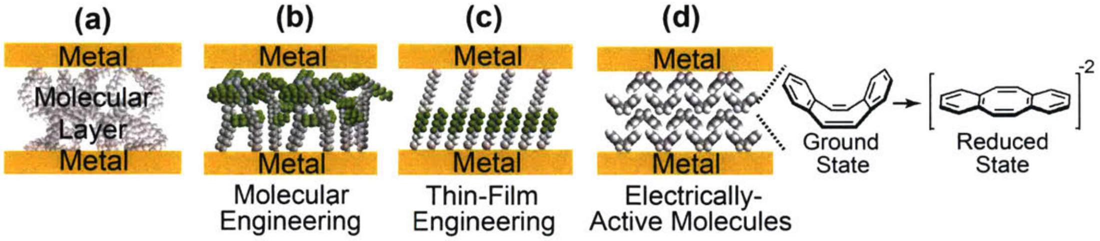

Figure 5-7: A molecular layer that can define the spacing between two neighboring surfaces to allow dynamic tunability can be composed of (a) a single type of molecule, (b) engineered molecules with different components, (c) engineered thin-film composed of different molecular species, (d) active molecules that change conformation in response to an external stimulus. For example, dibenzocyclooctatetraene which has a tub conformation in the ground state flattens when reduced.

Force control using molecules as nanoscale springs provides a promising platform to develop precisely defined sub-10 nm nanogaps that can be dynamically tuned electromechanically. The structure is composed of an insulating molecular layer sandwiched between metallic contacts. In this metal-molecule-metal junction, an applied voltage across the electrodes provides an electrostatic force which can attract the top electrode towards the bottom, compressing the molecules in the process. The compressed molecules provide elastic restoring force that balances the surface adhesive forces. The feasibility of this mechanism to produce stiction-free controlled and reversible electromechanically tunable nanogaps is explored in the following chapter.

5.4 Summary

Molecules can serve as structural building blocks to facilitate nanoscale processing. Atomic resolution feasible through chemical synthesis provides precise control over the structure and chemical composition. Consequently, molecules can precisely define the spacing between neighboring surfaces with resolution superior to that feasible through conventional fabrication techniques. By engineering surfaces, molecular coatings can adjust surface interactions to assist with structural robustness and controlled tunability. The mechanical properties of the molecules are proposed to further provide means of controlled and reversible tuning of the spacing between the structures. This is achieved by predictive conformational changes in molecules defined by their customizable mechanical response.

Chapter 6

Controlled and Reversible Tuning of Nanogap Electrodes

Previous chapter discussed the utility of molecules as building blocks of nanoscale structures providing nanometer precision, control and resolution in processing. We proposed use of molecules as nanoscale springs to precisely tune the distances between the neighboring surfaces. Here, using an electromechanically tunable molecular junction, the feasibility of molecules in precisely defining nanoscale gaps and providing force control is investigated [94].

6.1 Design Principle

The desired design will be composed of a molecular layer sandwiched between two conducting electrodes where one can be mechanically mobile, as shown in Figure 6-1. The width of the gap is defined by the thickness of the molecular film. An applied voltage across the contacts induces an electrostatic force to cause the top electrode to approach the bottom by compressing the molecules. As the voltage is removed, the elastic force of the deformed molecules provides the restoring force necessary to

---

Chapter 6 is adapted with permission from [F. Niroui, P. B. Deotare, E. M. Sletten, A. I. Wang, E. Yablonovitch, T. M. Swager, J. H. Lang and V. Bulović, Nanoelectromechanical tunneling switches based on self-assembled molecular layers, *Micro Electro Mechanical Systems (MEMS), 27th IEEE International Conference*, 1103–1106, 2014.]. Copyright 2014 IEEE.

overcome the surface adhesive forces such that the gap recovers to its original width. Given the small dimensions involved and the fragility of the organic materials, direct and reliable probing of the nanogap's mechanical tunability is not trivial using the conventional imaging and characterization techniques.

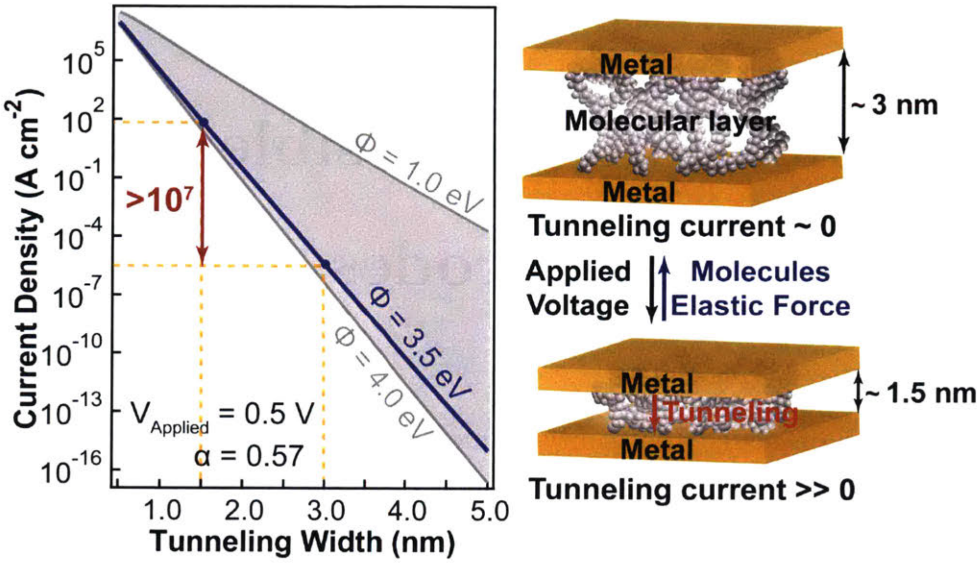

Figure 6-1: Molecules can help precisely define a nanogap electrode and allow its controlled and reversible electromechanical modulation by providing force control. If sufficiently small, conduction through quantum tunneling is observed where the tunneling current changes exponentially as a function of the tunneling gap. Here, α is an adjustable parameter that accounts for the effects of barrier shape and electron effective mass. In this example, α is selected to be 0.57, within the range reasonable for organic molecular layers.

If the molecular gap is sufficiently small, it allows conduction through the junction due to quantum tunneling in response to the applied voltage. The conduction mechanism through self-assembled monolayers of organic molecules has been extensively studied and can be explained based on the Simmons model for $V < \phi/q$ [95–100]:

$$\begin{aligned} I = \left(\frac{qA}{4\pi^2\hbar G^2}\right) \quad & \{(\phi - \tfrac{qV}{2})exp[-\tfrac{2(2m)^{1/2}}{\hbar}\alpha(\phi - \tfrac{qV}{2})^{1/2}G] \\ & -(\phi + \tfrac{qV}{2})exp[-\tfrac{2(2m)^{1/2}}{\hbar}\alpha(\phi + \tfrac{qV}{2})^{1/2}G]\} \end{aligned} \tag{6.1}$$

where m is the electron mass, q is the electron charge, G is the tunneling distance, A is the overlapping area between the electrodes, ϕ is the molecular layer tunneling barrier height, and α is an adjustable parameter that accounts for the effects of barrier shape and electron effective mass. The exponential dependence of the tunneling current on the tunneling distance, as depicted in Figure 6-1, can serve as a suitable approach to probe electromechanical changes in the gap size with sub-nanometer precision. As will be discussed in Part III, this current modulation which can be tuned by the mechanical properties of the molecular layer can develop a new platform for low-voltage and stiction-free NEM switches.

6.2 Fabrication Flow

To acquire an electromechanically active metal-molecule-metal structure, a fabrication scheme similar to that presented in Chapter 3 is implemented using a laterally-actuated cantilever design. The process flow is outlined in Figure 6-2. In brief, a cantilever and opposing electrodes are formed using electron-beam lithography in $\sim$1.5 μm thick layer of poly(methyl-methacrylate) (PMMA) spun over a silicon (Si) substrate with 2 μm-thick thermal oxide (SiO_2). Once the structures are formed, 100 nm of Au is deposited over the substrate using thermal evaporation to define the electrodes. Upon deposition of the Au film, the nanogap width is reduced in size with the reduction determined by the thickness of the film. The device fabrication is completed by self-assembly of fluorinated decanethiol molecules in vapor phase onto the Au surfaces through the use of thiol chemistry. The molecular film forms uniformly over the entire substrate including inside the nanogap. Results indicate that through the assembly process Electrodes 2 collapses onto Electrode 1 with the molecules sandwiched between the electrodes, forming a gap narrower than originally patterned and leading to a metal-molecule-metal junction $\sim$1 nm wide with a movable electrode. A scanning electron micrograph of a fabricated cantilever and the chemical structure of the fluorinated decanethiol molecule are shown in Figure 6-3a and b, respectively.

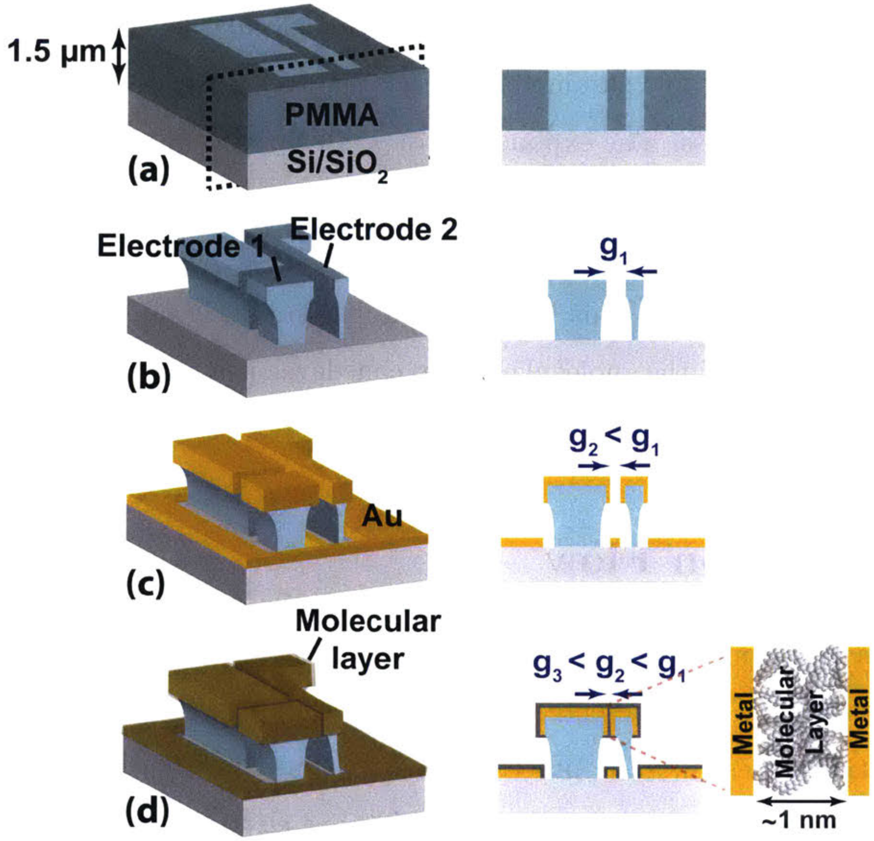

Figure 6-2: Fabrication process of the tunneling NEM switch: (a) multilayer PMMA electron-beam resist is spun on a Si/SiO_2 substrate and baked after each spin, resist is then electron-beam-patterned to define the switch components, (b) resist is developed in 1:3 solution of MIBK in isopropanol, (c) 100 nm of Au is evaporated over the substrate, (d) fluorinated decanethiol is self-assembled in vapor phase over Au, bridging the gap between Electrodes 1 and 2.

6.3 Results and Discussions

The fabricated cantilever has a gap of ~15 nm after the deposition of the Au film and prior to the self-assembly of fluorinated alkane molecules. When electrically actuated, this structure which resembles a conventional relay relies on the elastic restoring force of the cantilever to overcome the surface adhesive forces to ensure repeatable operation. The current-voltage (I-V) characteristic of such a device in the absence of a molecular layer is shown in Figure 6-4a. A successful initial actuation is followed by subsequent electrical shorting of the device due to stiction. This irreversible operation arises since the surface adhesive forces in this design have overcome the elastic

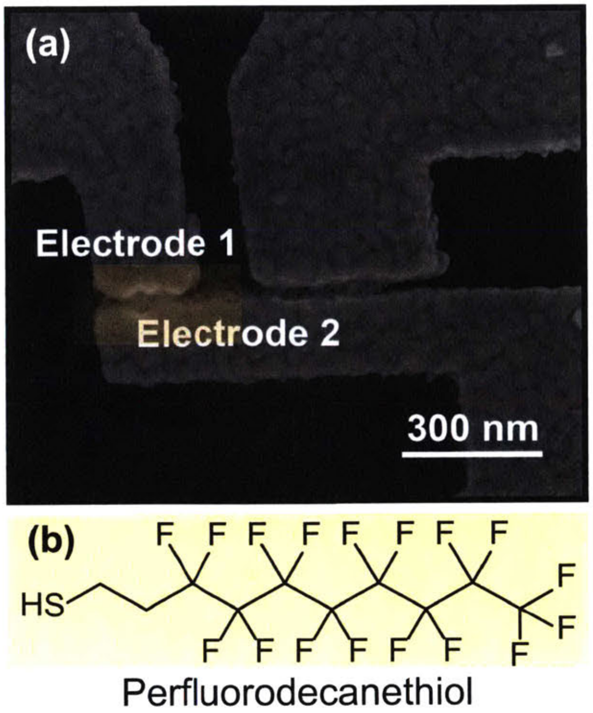

Figure 6-3: (a) Scanning electron micrograph of a laterally actuated cantilever formed based on the fabrication scheme in Figure 6-2. (b) Chemical structure of fluorinated decanethiol used in forming the molecular gap. The assembly process is executed in vapor-phase using thiol-chemistry.

restoring force of the cantilever, causing cantilever collapse and permanent adhesion between the contacting electrodes.

On the other hand, a similar device characterized after the self-assembly of fluorinated decanethiol molecules exhibits repeatable operation as shown in Figure 6-4b. The presence of the molecular layer helps reduce the possibility of stiction. This reversible operation can be attributed to the reduction in surface energy and the introduction of an elastic restoring force by the molecules while also avoiding direct contact between the electrodes. Figure 6-4b shows a distribution in the measured results over multiple runs. The nonuniformity in operation may be caused by the irregular topography of the electrodes as seen on the SEM image of Figure 6-3a. The surface uniformity and consequently the performance stability can be improved by using alternative materials and deposition techniques. For example changing the PMMA support structure to SiO_2 or utilizing atomic layer deposition are expected to improve surface uniformity.

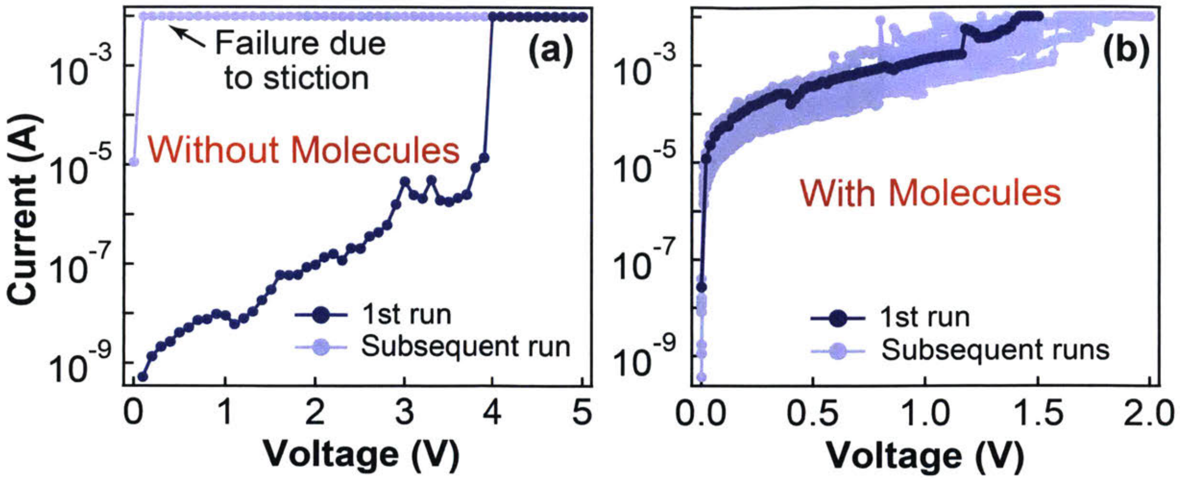

Figure 6-4: (a) Current-voltage characteristics of a tunneling NEM switch in the absence of fluorinated decanethiol molecular layer showing device failure due to stiction after the first run; (b) Current-voltage characteristics of the switch after self-assembly of fluorinated decanethiol showing repeatable operation. Note that the highest value of current is set by the compliance of the measurement setup and is not a property of the device.

Notably, the current-voltage characteristics before and after molecular layer deposition are distinct, with the behavior obtained after incorporation of the molecules resembling that of quantum tunneling. The Simmons model is used to compare the experimental results with the theoretically expected behavior. Here, to acquire a close fit to the experimental data, ϕ of 1.4 eV and α of 0.6 are selected, within the range of values reported in the literature for similar molecular layers [96, 97]. Even though the selected values of ϕ and α are reasonable approximates, note that the exact values can vary depending on the specifics of the tunneling junction. Based on the experimental data, the initial thickness of the tunneling gap is estimated to be $\sim$1.0 nm, which is consistent with the expected thickness of a monolayer of decanethiol [92]. Accordingly, it is deduced that Electrode 1 and Electrode 2 collapse onto each other through the self-assembly of the molecules to form a metal-molecule-metal structure with a gap smaller than $\sim$15 nm that was originally patterned. This is an example hybrid fabrication technique where top-down fabrication of nanostructures is combined with bottom-up self-assembly of molecules, and engineering of surfaces and forces to allow controlled formation of electromechanically-active molecular gaps.

When compared to the theoretical expected behavior assuming a constant tunneling distance (nanogap width) throughout the actuation process, a close fit with the experimental data is obtained at lower voltage values but a larger discrepancy is observed as the voltage increases. The comparison is shown in Figure 6-5. The faster increase in current than expected at larger voltage values may be accounted for by a reduction in the tunneling width throughout the actuation process. Applying a voltage across the metal-molecule-metal structure induces an electrostatic force. If sufficient to overcome the elastic restoring force of the molecular layer, it can compress the molecular layer and reduce the gap between Electrodes 1 and 2. The decrease in the electrode-electrode tunneling distance results in a faster increase in the tunneling current than that expected for a constant gap. To evaluate this possibility, the theoretical model is modified by taking into account the electromechanical modulation of the molecular junction.

To do so, the balance of electrostatic, van der Waals and spring restoring forces at equilibrium are used to determine the electrode-electrode distance at each applied voltage. Subsequently, the extracted gap size is used within the Simmons model to evaluate the tunneling current. The force balance equation is given by

$$M\frac{d^2z}{dt^2} = \frac{\epsilon_r \epsilon_0 A V^2}{2(G_0 - z)^2} + \frac{A_H A}{6\pi (G_0 - z)^3} - k(L - G_0 + z) \tag{6.2}$$

where M is the mass of Electrode 2, G_0 is the initial distance between the electrodes, z is the displacement of Electrode 2, L is the initial thickness of the molecular layer, A is the overlapping area between the electrodes, A_H is the Hamaker constant, ϵ_0 is the permittivity of free space, ϵ_r is the dielectric constant of the molecular layer, and k is the spring constant of the layer related to the Young's modulus Y by $k = YA/L$. The relative permittivity of the molecular layer is assumed to be 2.0, within the range of values reported for alkanethiols [100]. The Hamaker constant is considered to be 3×10^{-19} J based on the values reported for capacitive structures with Au electrodes [101]. Considering the structural profile of Electrode 2, its spring constant is estimated to be orders of magnitude smaller than that expected for the molecular layer; thus, its contribution to the force balance equation is neglected.

The green curve in Figure 6-5 shows the simulated current-voltage characteristic using the modified model. By taking into account electromechanical compression of the molecular layer a closer fit to the experimental result is obtained compared to the case of a constant switching gap. In this case, electromechanical modulation of the fluorinated molecular layer leads to about 10-fold increase in current within the voltage range considered. To achieve the best-fit curve it is deduced that the molecular gap underwent ~26% or ~3 Å decrease in the tunneling distance. The theoretical model suggests a Young's modulus of approximately 0.23 GPa for fluorinated decanethiol, in agreement with the measurements reported in the literature for alkanethiols of similar molecular structure [92]. It is worth noting that this device platform provides a suitable approach for studying mechanical properties of molecular layers which would be difficult to study using conventional metrology tools due to the small dimensions involved.

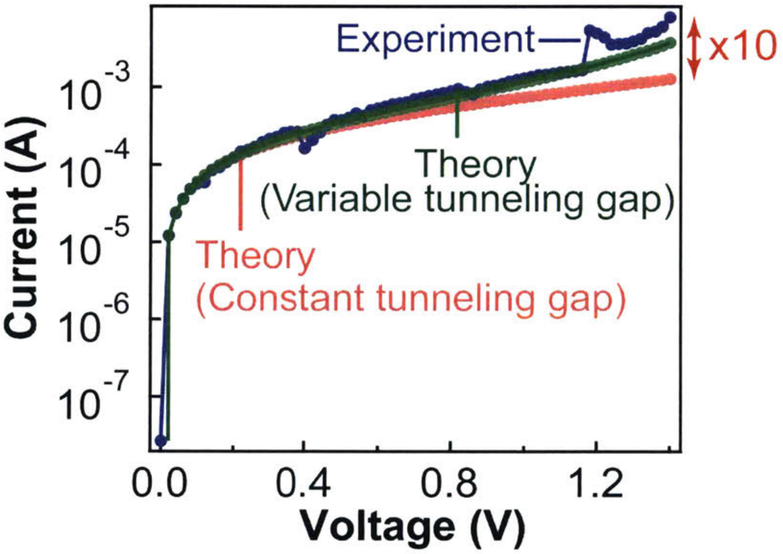

Figure 6-5: Experimental current-voltage characteristic of the tunneling NEM switch (blue) compared to the theoretical characteristics based on the Simmons model of tunneling with a constant gap (red) and a variable gap (green).

The results imply that in addition to providing precision in defining dimensions between surfaces, molecular layers can provide control of surface adhesive forces necessary to achieve dynamic and reliable tuning of these dimensions. This feature which relies on the mechanical properties of the molecular layer is in particular helpful for the design of active devices only few nanometers in scale which would commonly face premature failure due to stiction. To emphasize the prospects, the following section introduces a new platform for low-voltage and stiction-free NEM switches using the proposed electromechanically tunable molecular junctions.

6.4 Summary

Molecules can serve as structural components to allow precise formation and dynamic tuning of nanogap electrodes with unprecedented nanometer precision and control. The feasibility of this concept is investigated based on a metal-molecule-metal junction formed using a laterally actuated cantilever and fluorinated alkanethiol molecules. In this design, ~1 nm molecular gap undergoes controlled electromechanical compression, modulating the electrode-electrode distance and consequently the tunneling conduction. With versatility in design of the structure and mechanical properties of the molecular films, an engineering approach emerges to support the development of active nanoscale devices in the sub-10 nm regime that would otherwise not be easily feasible due to stiction-induced failures. More fundamentally, this platform can also serve as a metrology tool for studying the combined electrical and mechanical properties of molecular thin-films.

Part III

Device Design – Tunneling Nanoelectromechanical Switches towards Low-Voltage and Stiction-Free Performance

Chapter 7

Two-Terminal Tunneling Nanoelectromechanical Switches

Reversible conformational changes in engineered nanostructures due to external stimuli can lead to modulation of characteristics including light-matter interaction, electrical conduction and optical properties. This controlled alteration of properties creates a foundation for a broad range of active nanoscale devices. Electromechanical devices, which involve movable structures with electrostatically tunable spacing, are an extensively studied example with applications such as switches, memory units, tunable optical filters, light modulators and sensors to name a few. Most commonly studied structures have tunable dimensions larger than tens of nanometers. Miniaturization to smaller dimensions can lead to improved device performance including energy-efficiency while also introduce unique functionalities that are not feasible at larger scale. As discussed previously however, miniaturization to the few-nanometer regime is challenged by limited resolution of the fabrication techniques and the large surface adhesive forces causing stiction.

In previous sections, various processes were discussed to enable nanometer precision, control and uniformity in fabrication and mechanical tuning of dimensions to

---

Chapter 7 is adapted with permission from [F. Niroui, A. I. Wang, E. M. Sletten, Y. Song, J. Kong, E. Yablonovitch, T. M. Swager, J. H. Lang and V. Bulović, Tunneling nanoelectromechanical switches based on compressible molecular thin films, *ACS Nano*, 9(8): 7886-7894, 2015]. Copyright 2015 American Chemical Society.

promote engineering at the limits of the nanoscale. A scheme was proposed in Part II where molecules help define electromechanically tunable nanogap electrodes with nanometer resolution and with alleviated stiction despite the small dimensions. This mechanism can form a platform for electromechanical systems with critical dimensions <10 nm and without stiction. With the ability to create nanogaps only few nanometers in size and with controlled and reversible electromechanical modulation such tunable metal-molecule-metal structures are proposed here as a platform for low-voltage and stiction-free NEM switches [102]. The NEM switch to be discussed is only one of many devices that could benefit from hybrid fabrication techniques and molecular engineering, and so serves as an illustrative example.

7.1 Operating Principles of Tunneling NEM Switches

7.1.1 Tunneling Switching Mechanism

Unlike conventional NEM switches which rely on direct contact between electrodes [1, 2], the proposed switching mechanism relies on electromechanical modulation of tunneling current in a metal-molecule-metal switching gap. This tunneling-based NEM switch, named a squeezable switch or a "squitch", has the potential to overcome two of the main challenges of current NEM switches: large actuation voltage and stiction-induced premature device failure, while maintain the benefits that NEM switches offer: near-zero off-state leakage and abrupt switching behavior. Through the use of molecules to form the switching gap, nanogaps can be defined with dimensions much smaller than conventionally feasible, leading to a lowering of the actuation voltage. Furthermore, through the reversible electromechanical compression of these molecules, an approach for controlling surface adhesive forces is introduced to prevent stiction during fabrication and operation.

The exponential dependence of tunneling current on tunneling distance can ensure large ON-OFF current ratio if sufficient modulation of the switching gap is facilitated. In the example in Chapter 5, a 10-fold increase in current is observed for

~3 Å compression of a nanogap composed of a fluorinated decanethiol layer with a large Young's modulus of ~0.23 GPa. To ensure current modulation $>10^6$, a larger modulation of the tunneling gap is necessary. For example, in reference to Figure 6-1, a 50% modulation of a 3 nm gap with ϕ of 3.5 eV and α of 0.57 leads to $>10^6$ ON-OFF current ratio. The OFF-state switching gap should be selected to ensure low leakage current while the gap should be sufficiently small such that the actuation voltage can be kept at the lowest possible. To further allow for a low actuation voltage, the Young's modulus of the molecular layers should be kept at the lowest tolerable by the design. The Young's modulus should be sufficiently low to allow low-voltage actuation while be large enough to provide adequate restoring force to ensure reversible stiction-free performance. This means that the elastic restoring force provided by the compressed molecular layer should exceed the van der Waals forces while being less than the combined van der Waals and applied electrostatic forces ($F_{vdW} < F_{elastic} < [F_{vdW} + F_{electrostatic}]$). Figure 7-1 shows the dependence of the actuation voltage on the Young's modulus for an example switch. In this particular architecture, a modulus of <11 MPa provides an actuation in the sub-1 V regime.

7.1.2 Squitch Design

The main component of the design is the metal-molecule-metal switching gap composed of an electrically insulating compressible molecular layer sandwiched between conductive electrodes. For the proof-of-concept design investigated here, an off-state switching gap of ~3 nm is deemed suitable. To ensure a large modulation of the switching gap, a low Young's modulus self-assembled layer of poly(ethylene glycol)dithiol (PEG-dithiol) is incorporated in the design. The self-assembled layer of the polymeric material is expected to form a thin-film composed of void space which can yield a lower effective Young's modulus compared to a well-packed film of shorter alkane molecules. Such nanometer-thin polymeric layer is susceptible to the damage imposed by the fabrication technique in particular that of the top electrode. For example, the most widely used deposition techniques are not adequate for this design as direct deposition onto the molecular layer can cause penetration of metallic

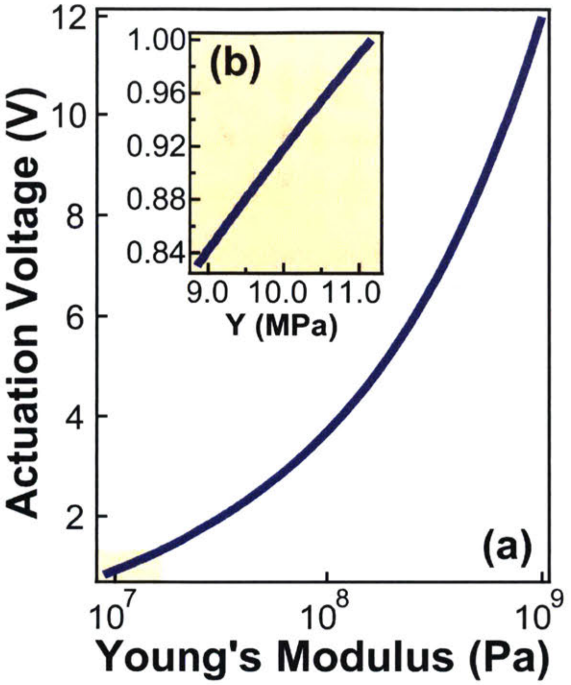

Figure 7-1: (a) Actuation voltage of an example two-terminal metal-molecule-metal squitch as a function of Young's modulus of the compressible molecular film showing an increase in the actuation voltage with an increase in the Young's modulus. (b) To achieve sub-1 V actuation in this example, a material with a Young's modulus <11 MPa is desired.

filaments into the layer causing nonuniform switching gap and electrical shorting. The resulting nonuniformities even though small are significant given the <3 nm width of the switching gap. Hence, these can correlate to large perturbations in the device reliable and stable operation.

In Chapter 5, a fabrication technique is introduced to form electromechanically tunable molecular tunneling junction using a laterally-actuated cantilever. This approach is not suitable for the formation of molecular junctions made of PEG self-assembled layer. The cantilever design requires vapor-phase growth of the molecules and in the current form cannot accommodate solution-based assembly. The solution-based assembly can cause collapse of the cantilever structure due to capillary action and induce structural degradation depending on the solvents involved in the growth process. Therefore, an alternative design based on a vertically-actuated junction with Au bottom electrode, PEG-dithiol spacer and graphene top electrode is utilized. The fabrication process is selected such that damage to the molecules can be avoided to form well-defined compressible tunneling junctions.

To avoid the need for making electrical connections to the top electrode to ease fabrication, and to avoid damage to the graphene and the nanometer-thin molecular layer, the design is selected such that two bottom electrodes are bridged by a mechanically and electrically floating top electrode. In this case, an applied voltage across the two bottom electrodes induces an electrostatic force in this capacitive structure such that the top electrode is attracted towards the bottom, compressing the molecules to modulate the tunneling gap. A variation of this design can also incorporate interdigitated bottom electrodes.

7.2 Two-Terminal Squitch Fabrication Flow

The fabrication scheme is shown in Figure 7-2. The bottom electrode is formed through top-down lithography and lift-off using thermally evaporated Cr and Au (5 nm and 50-100 nm, respectively). The molecular layer is formed through thiol-based self-assembly of PEG-dithiol. The molecular weight is selected to acquire a self-assembled layer of the desired thickness. Molecular weight of 2000 g/mol with 22 repeat units in the polymer chain yields a self-assembled layer of ~3 nm as shown in the transmission electron micrograph of Figure 5-2. To promote self-assembly, the patterned bottom-electrodes are immersed in a 5 mM solution of PEG-dithiol in ethanol inside a nitrogen-filled glovebox at room temperature. After 24 hours, the substrates are removed from the PEG-dithiol solution, thoroughly rinsed in ethanol and gently dried under a stream of nitrogen.

To avoid damage to the molecular layer due to the top electrode deposition and in an attempt to achieve a well-defined switching gap, a graphene layer is used as the top electrode and transferred onto the molecular layer through an additive process. The atomically smooth surface of graphene with sub-nm localized roughness, as shown in Figure 7-2b, provides the desired uniformity to form a well-defined switching gap. The graphene is first synthesized through a chemical vapor deposition (CVD) technique [103]. To transfer the graphene onto the molecular layer, first the CVD-grown graphene on copper (Cu) foil is spun with poly(methyl-methacrylate) (PMMA) on one side and baked at 80°C for 10 min. The graphene on the back side of the Cu foil is then removed with an O_2 plasma etch. The Cu/graphene/PMMA stack is then placed in Cu etchant for 15 min, allowing the Cu to dissolve. The remaining graphene/PMMA film which floats at the water-air interface is rinsed in deionized water thoroughly and finally removed from the water using the receiving substrate which contains the bottom electrodes and the assembled molecules [104].

As seen in Figure 7-2b, despite graphene's local smooth topography, it exhibits surface nonuniformities over larger areas due to roughness of the underlying Cu foil used in the growth process and the wrinkles produced through the large-area transfer. This roughness can influence the device reproducibility and stability and can contribute to device-to-device variation in performance. Thus, to realize the squitch's optimal performance and enhance the fabrication yield, further improvements in the graphene transfer process are necessary.

In a variation of the transfer process outlined in scheme II of Figure 7-2d, to help define smaller devices which would enhance uniformity of the tunneling junction and performance, the graphene layer is lithographically patterned prior to the transfer onto the molecular layer. In this approach, graphene layer is first transferred onto a SiO_2 substrate using the process outlined above. Then, using lithography and lift-off, thermally-evaporated Au features with the desired form and dimensions of the graphene top electrode are patterned on the graphene surface. The Au then serves as a mask to etch the exposed graphene using O_2 plasma, leaving behind patterned graphene covered with Au to be used as the top electrode. To form the switching gap, the patterned top electrodes need to be aligned to the bottom electrodes prior to the transfer. In addition to serving as the etch mask, the Au covering the patterned graphene helps with the alignment process as it enhances graphene monolayer's visibility under an optical microscope. The Au also enhances the robustness and conductivity of monolayer graphene while the interface uniformity of the top electrode is still dominated by the sub-nm smoothness of the graphene layer. An example device is shown in Figure 7-3.

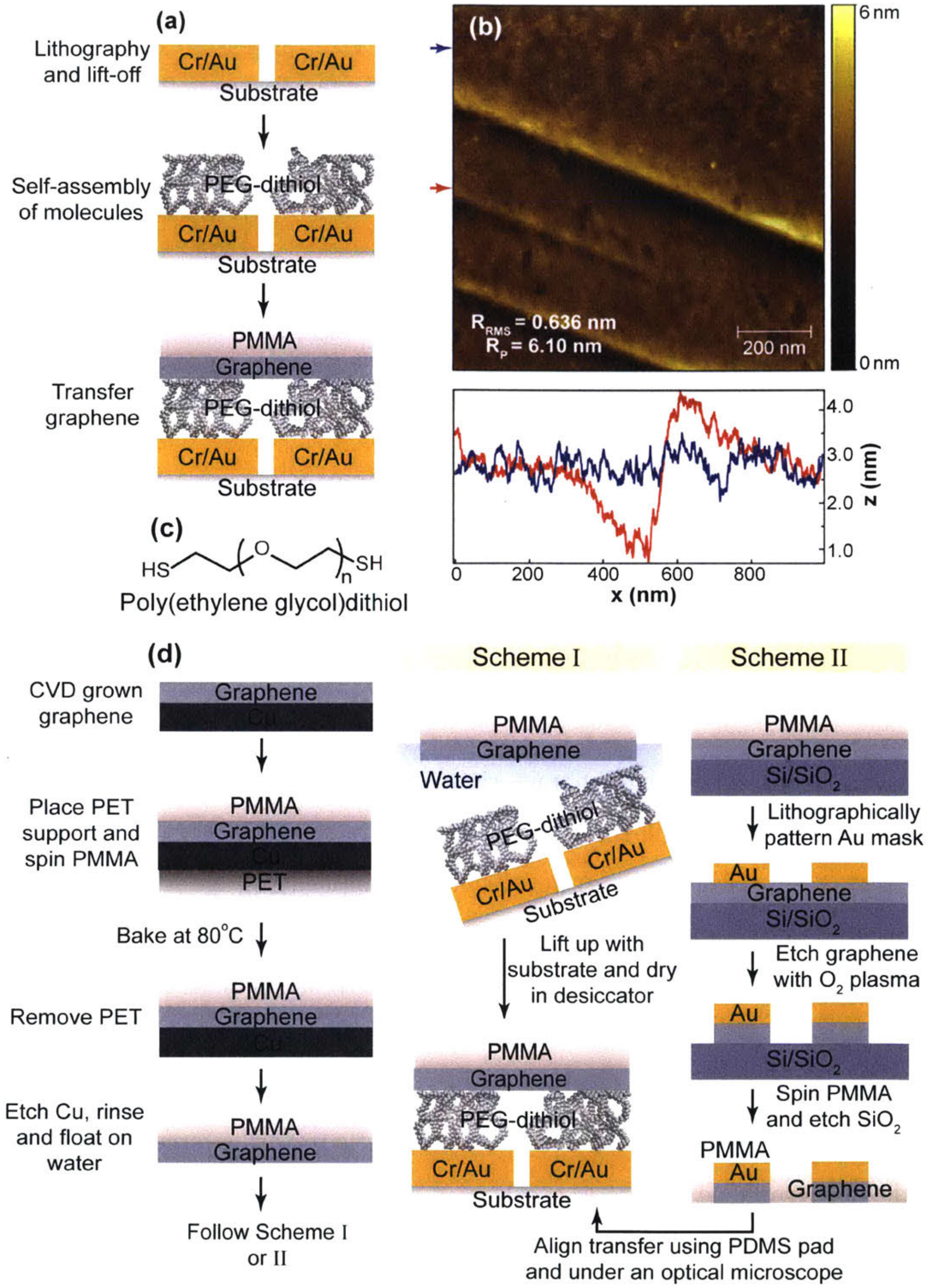
(a)
Lithography and lift-off
Cr/Au
Cr/Au
Substrate
Self-assembly of molecules
PEG-dithiol
Cr/Au
Cr/Au
Substrate
Transfer graphene
PMMA
Graphene
PEG-dithiol
Cr/Au
Cr/Au
Substrate
(b)
R_{RMS} = 0.636 nm
R_P = 6.10 nm
200 nm
6 nm
0 nm
4.0
3.0
2.0
1.0
z (nm)
0
200
400
600
800
x (nm)
(c)
HS
O
n
SH
Poly(ethylene glycol)dithiol
(d)
CVD grown graphene
Graphene
Cu
Place PET support and spin PMMA
PMMA
Graphene
Cu
PET
Bake at 80°C
Remove PET
PMMA
Graphene
Cu
Etch Cu, rinse and float on water
PMMA
Graphene
Follow Scheme I or II
Scheme I
PMMA
Graphene
Water
PEG-dithiol
Cr/Au
Cr/Au
Substrate
Lift up with substrate and dry in desiccator
PMMA
Graphene
PEG-dithiol
Cr/Au
Cr/Au
Substrate
Scheme II
PMMA
Graphene
Si/SiO_2
Lithographically pattern Au mask
Au
Graphene
Si/SiO_2
Etch graphene with O_2 plasma
Au
Si/SiO_2
Spin PMMA and etch SiO_2
PMMA
Au
Graphene
Align transfer using PDMS pad and under an optical microscope

Figure 7-2: (a) Fabrication scheme for a two-terminal squitch with Au-(PEG-dithiol)-graphene switching gaps. (b) AFM topography of CVD-grown graphene transferred on a substrate showing sub-1 nm local roughness. (c) Chemical structure of PEG-dithiol used for the spacer layer. (d) The technique used to transfer the top graphene electrode onto the molecular layer. The transfer can either be done without an alignment over the entire substrate as a single sheet (Scheme I), or, the graphene can be first lithographically patterned into smaller features and transferred onto the bottom electrodes locally using an aligned transfer technique under an optical microscope (Scheme II).

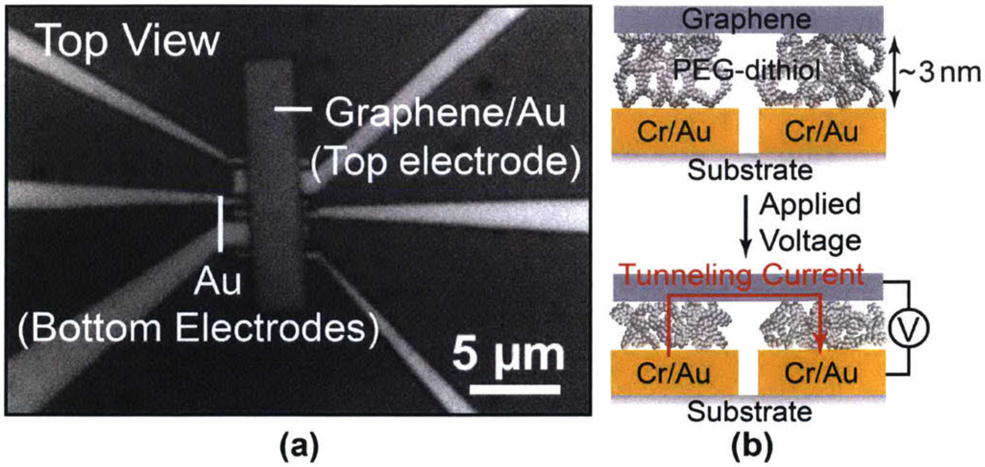

Figure 7-3: (a) Optical image of an example two-terminal squitch. (b) Schematic cross-section of a two-terminal squitch with graphene top electrode, PEG-dithiol spacer layer and Au bottom electrodes. An applied voltage across the bottom electrodes induces an electrostatic force to compress the molecular layer and tune the tunneling gap through which the tunneling current is modulated.

7.3 Results and Discussions

The measured current-voltage characteristics of three example squitches fabricated based on Au-PEG-graphene tunneling junctions are shown in Figure 7-4a. Two operating regimes are observed. An increase in the applied voltage results in an initial exponential increase in the tunneling current followed by an abrupt jump. The point of abrupt increase corresponds to the pull-in. Prior to pull-in, current increases exponentially as the tunneling gap is reduced by electrostatically induced compression of the molecular layer. Once the pull-in distance is reached, where the combined electrostatic and van der Waals forces overwhelm the elastic restoring force of the molecular layer, the top graphene electrode accelerates rapidly towards the bottom electrodes causing an abrupt decrease in the electrode-electrode distance and an increase in the tunneling current. The current saturation is due to the compliance set to the measurement instrument. The performance variations between devices may be attributed to differences in the molecular layer thickness and packing density, roughness of the electrodes which may result in variations in the effective width of the gap, and the properties of the Au-molecule or graphene-molecule junctions.

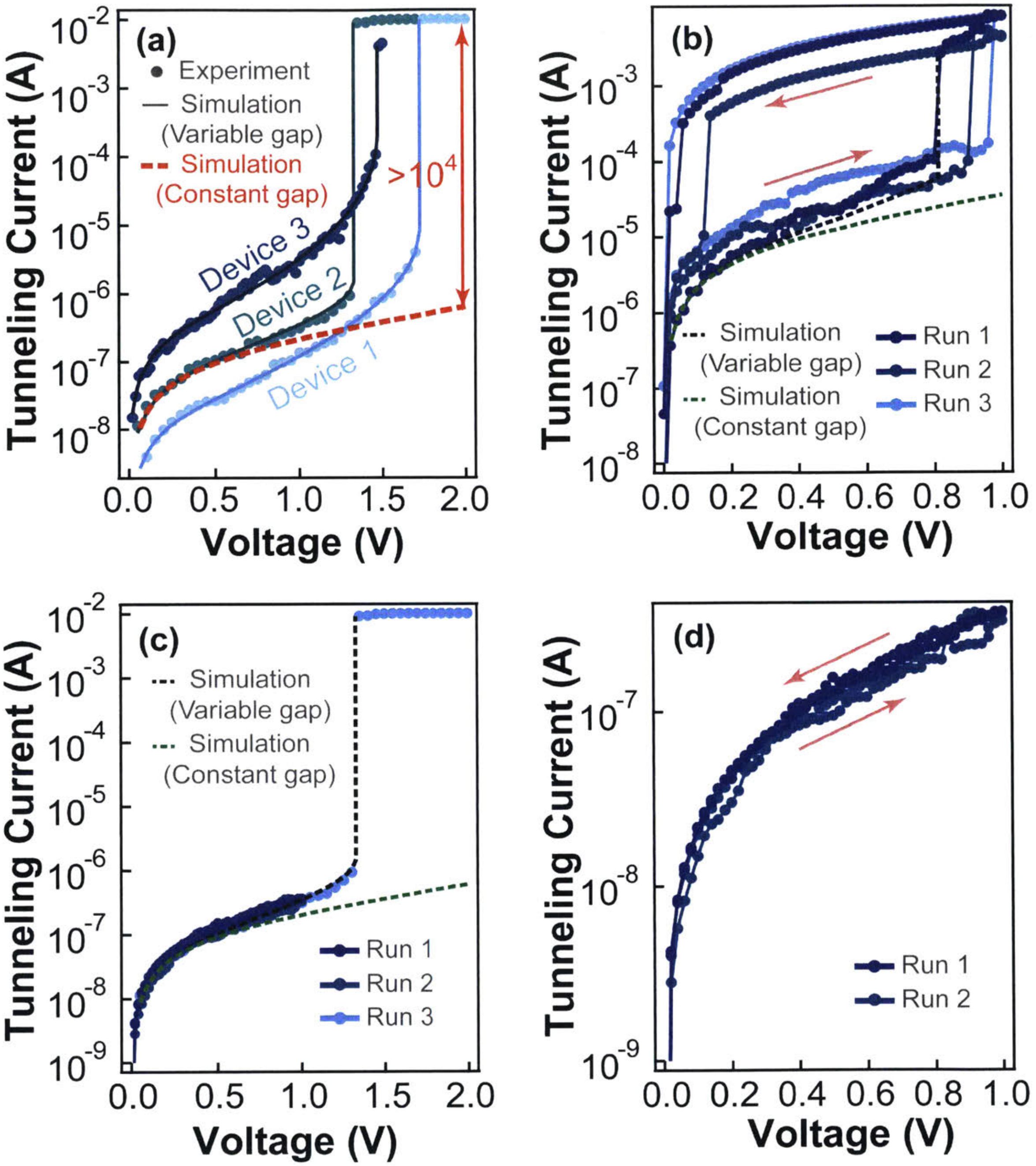

Figure 7-4: Current-voltage characteristics of two-terminal squitches. (a) I-V characteristics for three example squitches fitted to the theoretically simulated behavior. The following parameters were used to achieve the simulated best-fit curves: Device 1: $\phi = 1.6$ eV, $\alpha = 0.46$, $L = 3.1$ nm, $G_{pull-in} = 2.2$ nm, $\epsilon_r = 2.2$, $Y = 11$ MPa; Device 2: $\phi = 1.2$ eV, $\alpha = 0.43$, $L = 2.2$ nm, $G_{pull-in} = 1.6$ nm, $\epsilon_r = 1.4$, $Y = 17$ MPa; and Device 3: $\phi = 4.4$ eV, $\alpha = 0.41$, $L = 2.6$ nm, $G_{pull-in} = 1.9$ nm, $\epsilon_r = 2.9$, $Y = 16$ MPa. (b) Three consecutive measurement sweeps show hysteresis associated with the operation. (c) Three consecutive measurement sweeps for another device with the first 2 runs executed in the pre-pull-in regime and the third showing device pull-in. (d) The first two sweeps show no significant hysteresis when the device is operating in the pre-pull-in regime.

To further study the current conduction mechanism, the experimental results are fitted against the simulated performance. Taking the point of sudden increase in the current as the pull-in, the pull-in voltage in each device is used to extract the expected tunneling gap change with each applied voltage through solving the equation of motion (Equation 6.2). The evaluated tunneling gaps are then used with the Simmons tunneling model (Equation 6.1) to simulate the expected current modulation. In fitting the experimental data, a Monte Carlo approach is implemented where the tunneling barrier height (ϕ), tunneling barrier shape (α), initial thickness of the molecular film (L) and the pull-in point are the unknown parameters selected randomly within a predefined range to simulate the device performance and extract the expected dielectric constant and Young's modulus. In this analysis, the Hamaker constant is set to be 3×10^{-19} J. A detailed overview of the simulation approach and analysis is provided in Appendix C.

It should be noted that due to the large number of unknown parameters present in the model, many combinations of values for α, ϕ and L can yield a close fit to the experiment. Nevertheless, within the possible results, combinations of unknown parameters exist that are within physically reasonable bounds while strongly agreeing with experimentally extracted values of ϵ_r and Y. With α constrained to 0.7 ± 0.3, $\phi = 3 \pm 2$ eV and $\epsilon_r = 3 \pm 2$, the Young's modulus extracted for a self-assembled layer of PEG-dithiol (2000 g/mol) based on the three devices is within the 5 MPa to 40 MPa range (Appendix C). The pull-in gap for these devices is determined to be in the range of 0.71L to 0.74L where L is the initial thickness of the PEG self-assembled layer. A more precise determination of the parameters requires further information regarding the specifics of the tunneling junction, mechanical properties of the molecular layer, and dynamics of molecular layer electromechanical deformation which necessitates further experimentation. Acquiring the added information though is challenged by the inadequate characterization tools and experimental approaches currently available to independently extract each unknown component, in particular influenced by the extremely small dimensions being investigated. As a result, alternative metrology tools are also needed. The squitch concept augmented by a plasmonic ruler can be a suitable characterization platform as will be briefly discussed in Chapter 9.

The best-fit curves simulated for each device along with the corresponding parameters and extracted material properties are shown in Figure 7-4a. The close fit between the simulated and experimental results supports the proposed tunneling switching mechanism of squitches where electromechanical modulation of the tunneling current arises due to the controlled compression of the molecular film. This is compared to the theoretically simulated performance with no compression of the molecular layer in Figure 7-4a. Comparing the two scenarios, the experimental results show $>10^4$ current modulation with actuation voltage <2 V. With relatively low actuation voltage and an abrupt switching, the tunneling switching mechanism provides a promising platform for low-voltage and low-sticiton NEM switches. To achieve such optimal performance however, the device design and mechanics of the molecular layer and its dynamics need to be optimized.

A limitation of the prototype squitch design investigated here is that the operation in the pull-in regime is accompanied by a hysteresis. Figure 7-4b which depicts three consecutive current-voltage measurements of a squitch shows electromechanical modulation of the tunneling current and the associated hysteresis. Such hysteresis is undesirable as it causes unreliable performance over repeatable actuation and limits the energy efficiency of the device by adding to the active power consumption. In an ideal design, precise balancing of the surface adhesive forces through use of the elastic properties of the molecular layer is expected to help minimize hysteresis. The hysteresis observed in this example may be attributed to the non-ideal balance of forces due to the non-optimal morphology and mechanics of the molecular layer, intermolecular interactions, adhesion between the electrodes or the molecules and the electrodes, and presence of capillary forces. This hysteresis is not observed in the pre-pull-in regime. Figure 7-4c shows three consecutive current-voltage measurements of another squitch with the first two measurements performed prior to the pull-in while the third shows the pull-in at $\sim$1 V.

It should be noted that the concept squitches introduced here serve as preliminary efforts towards the demonstration of tunneling current modulation as the main switching mechanism in an electromechanical switch. In particular, PEG-dithiol is selected as a model material with a low Young's modulus, and a wide variety of other material systems and engineered thin-films can be designed for an improved performance. As well, alternative fabrication approaches and device architectures can be implemented. In the current design, despite the sub-nm smoothness of the top graphene electrode, the bottom electrode still has a roughness inherent to the lithography and deposition techniques utilized. The roughness of the underlying electrode can contribute to device instability. Development of an optimal squitch with sub-1 V actuation and reliable switching performance requires engineering of molecular layers with tailored mechanical properties, characterization of molecular layer's electromechanical performance, and practical integration of the molecular layer into optimized device geometries. Furthermore, extension of two-terminal squitches to more complex multi-terminal designs with gate-control is desired to render them more practical for applications in integrated systems, a topic of discussion in Chapter 8.

7.4 Summary

This chapter proposes NEM switches that operate through electromechanical modulation of tunneling current across a switching gap composed of a compressible molecular layer sandwiched between conductive contacts. In this design, electrostatic actuation of the switching gap results in the mechanical compression of the molecules as the two contacts approach each other. The decrease in the tunneling distance leads to an exponential increase in the tunneling current which defines the switching performance. Presence of the molecules provides a means of controlling surface adhesive forces while avoiding direct contact between the electrodes helping alleviate stiction. Concurrently, molecular films which can be precisely controlled in thickness help define switching gaps much smaller than allowed by conventional fabrication techniques to lower the actuation voltage. An example device in a two-terminal form is shown here using a Au-PEG-graphene tunneling junction with actuation voltage <2 V and current conduction modulation $>10^4$. Further optimization of the molecular layer and device architecture are needed to realize the optimal performance feasible through this tunneling switching mechanism.

Chapter 8

Multi-Terminal Tunneling Nanoelectromechanical Switches

Incorporating the tunneling-based switching mechanism within multi-terminal device architectures allows gated modulation of current. Such device resembles a conventional transistor in operation, extending squitch application as components of integrated systems. With increase in design complexity in multi-terminal devices to accommodate the desired performance parameters, however, fabrication becomes more demanding. An example design of a multi-terminal squitch and the corresponding fabrication procedure is presented here to demonstrate the possibility of the gated switching performance.

8.1 Multi-Terminal Squitch Design

Figure 8-1 shows a proposed design of a multi-terminal squitch. In this example, an applied voltage between gate electrodes 1 and 2 provides an electrostatic force to attract the top electrode towards the bottom to reduce the switching gap size and modulate the source-to-drain tunneling current. Similar to the two-terminal architecture, the sub-5 nm switching gap is composed of a compressible molecular layer. In the multi-terminal design though, to avoid an on-state tunneling leakage current, the gate electrodes should be recessed relative to the source and the drain by a few nanometers. With a goal of minimizing switching energy, in an optimal design, the recess should be sufficiently large to avoid leakage without inducing unnecessary increase in the actuation voltage. Such precisely defined surface topography with nanometer height variations between neighboring structures while maintaining <1 nm surface and edge uniformity is challenging to achieve through conventional techniques. Consistent with previously discussed examples, a hybrid top-down and bottom-up process would accommodate the design needs – developing electromechanically active switching gaps with nanometer precision, control and uniformity.

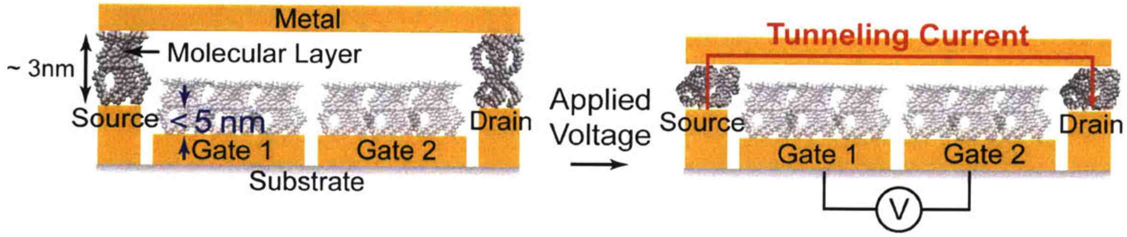

Figure 8-1: An example design of a multi-terminal squitch. An applied voltage across gate electrodes 1 and 2 provides an electrostatic force to compress the molecular layer to tune the tunneling gap between the top electrode and the source/drain electrodes and consequently modulate the drain current (I_D).

8.2 Multi-Terminal Squitch Fabrication Flow

Multi-terminal squitches consists of three components: bottom electrodes, molecular layer and the top electrode. In forming the bottom electrodes controlling the surface topography is necessary to achieve nanometer uniformity of surfaces and edges while acquiring the precise spatial profile needed between the electrodes. In this approach which is summarized in Figure 8-2a, two-dimensional materials, such as graphene, are lithographically patterned to be used as the sacrificial layer defining the recessed region. Two-dimensional materials are in particular suitable as their layered structure provides nanometer precision in thickness while also possessing atomically smooth surfaces. Once the sacrificial layer is formed, electrodes and interconnects are patterned using electron-beam lithography followed by thermal evaporation of Au and lift-off. Then, a technique similar to that discussed in Chapter 4 is implemented to peel the structures off the original substrate exposing the side originally in contact to the SiO_2 for further processing. The exposed sacrificial layer is then etched, revealing a recessed profile corresponding to the thickness of the two-dimensional material template. Figure 8-3 shows neighboring electrodes fabricated with ~4 nm height difference, illustrating the versatility of the peeling technique to achieve nanometer vertical resolution.

As shown through the atomic force micrographs of Figure 8-4, significant reduction is also observed in the edge and surface roughness that is otherwise inherent to the top-down fabrication techniques. The surface exposed through peeling assumes the roughness of the underlying flat SiO_2 substrate. Therefore, the edge defects are eliminated to achieve coplanar structures (Figure 8-4a and b). Additionally, the surface roughness is reduced from ~4 nm common to a thermally evaporated Au film to less than 1 nm on the peeled surface (Figure 8-4c and d). With sub-nm surface uniformity and resolution in defining the surface profile, a desired platform emerges to fabricate squitch bottom electrodes but is also broadly applicable to engineering other structures at the few-nanometer regime.

Once the bottom electrodes are fabricated, the molecular layer is formed through self-assembly in liquid phase using thiol-chemistry. Similar to the two-terminal devices, poly(ethylene glycol)thiol (PEG-thiol) is used as the compressible molecular layer. To promote the self-assembly, the bottom electrodes are placed in a 5 mM solution of PEG-thiol in deionized (DI) water for ~12 hours in a nitrogen-filled glovebox. Upon completion of the growth process, the substrate is then rinsed thoroughly in DI water and dried under a stream of N_2. Alternatively, the molecular layer can be self-assembled on the top electrode prior to the placement on the bottom contacts. A combination of molecular layer growth on both the bottom and top electrodes can also be implemented to achieve the desired thickness (8-2b).

Lastly, the top electrode needs to be added to the design without inducing damage to the molecular film. Direct deposition of the top contact in particular would be inadequate as it would lead to electrical shorting and nonuniform molecular junctions. To ensure achieving a well-defined switching gap with the desired surface uniformity,

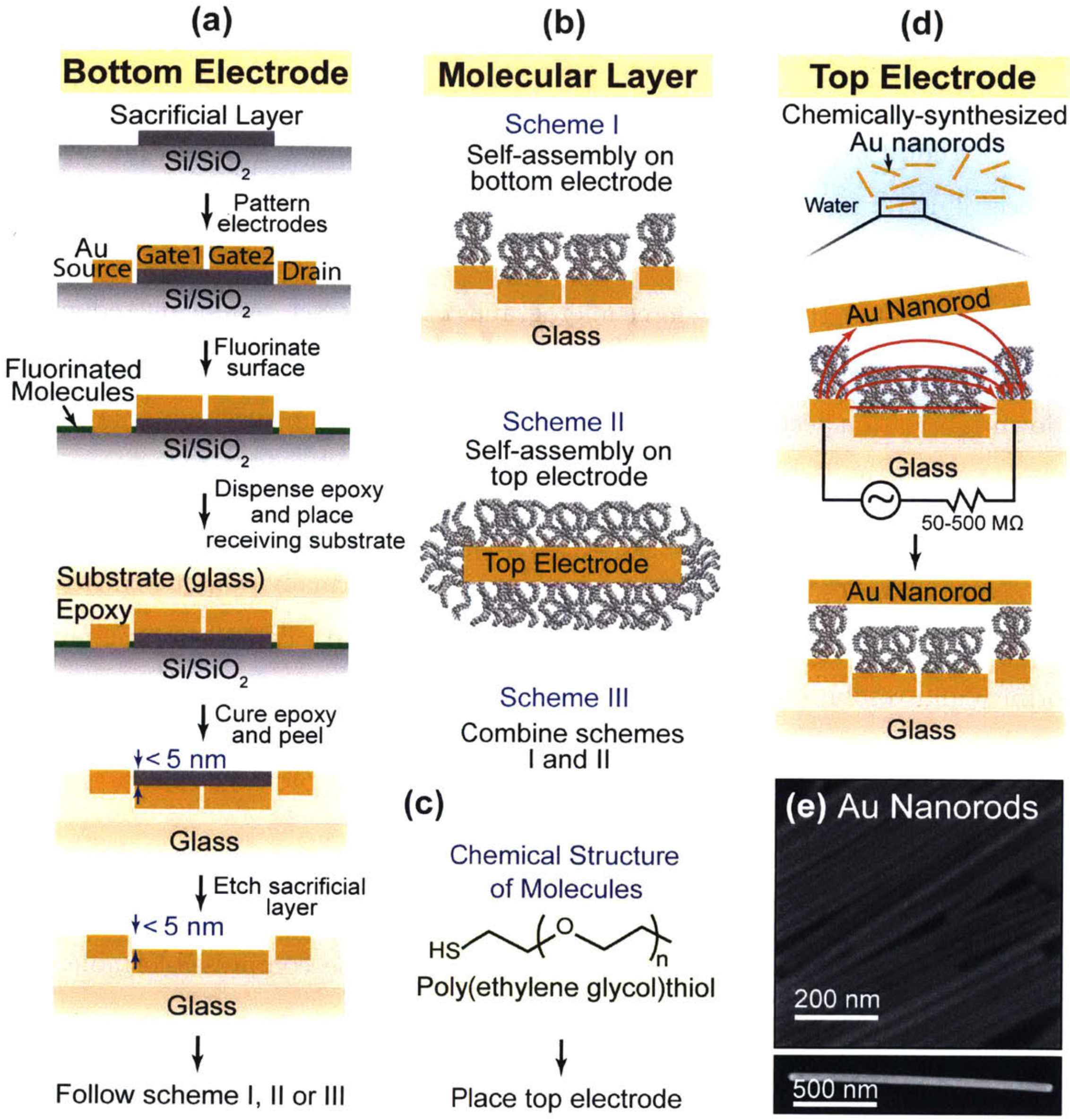
(a)
Bottom Electrode
Sacrificial Layer
Si/SiO$_2$
Pattern electrodes
Au
Source
Gate1
Gate2
Drain
Si/SiO$_2$
Fluorinate surface
Fluorinated Molecules
Si/SiO$_2$
Dispense epoxy and place receiving substrate
Substrate (glass)
Epoxy
Si/SiO$_2$
Cure epoxy and peel
< 5 nm
Glass
Etch sacrificial layer
< 5 nm
Glass
Follow scheme I, II or III
(b)
Molecular Layer
Scheme I
Self-assembly on bottom electrode
Glass
Scheme II
Self-assembly on top electrode
Top Electrode
Scheme III
Combine schemes I and II
(c)
Chemical Structure of Molecules
HS
O
n
Poly(ethylene glycol)thiol
Place top electrode
(d)
Top Electrode
Chemically-synthesized Au nanorods
Water
Au Nanorod
Glass
50-500 MΩ
Au Nanorod
Glass
(e) Au Nanorods
200 nm
500 nm

Figure 8-2: Fabrication scheme for multi-terminal squitches. (a) Bottom electrode fabrication: A sacrificial layer made out of two-dimensional materials such as graphene is lithographically patterned to define the surface topography. Electrodes and interconnects are formed using electron-beam lithography. The substrate surface is fluorinated. Using an epoxy adhesive layer and a glass receiving substrate the structures are peeled off the surface. Sacrificial layer is etched, using O_2 plasma in the case of graphene, revealing the bottom electrode with the desired topography. (b) Molecular layers are self-assembled either on the bottom electrodes (Scheme I), top electrode (Scheme II) or a combination of the two (Scheme III). (c) Chemical structure of PEG-thiol used as the molecular spacer layer. (d) Top electrode is formed using chemically synthesized Au nanorods. The nanorod is precisely positioned on the bottom electrodes using a dielectrophoretic trapping approach. (e) SEM image of chemically-synthesized Au nanorods.

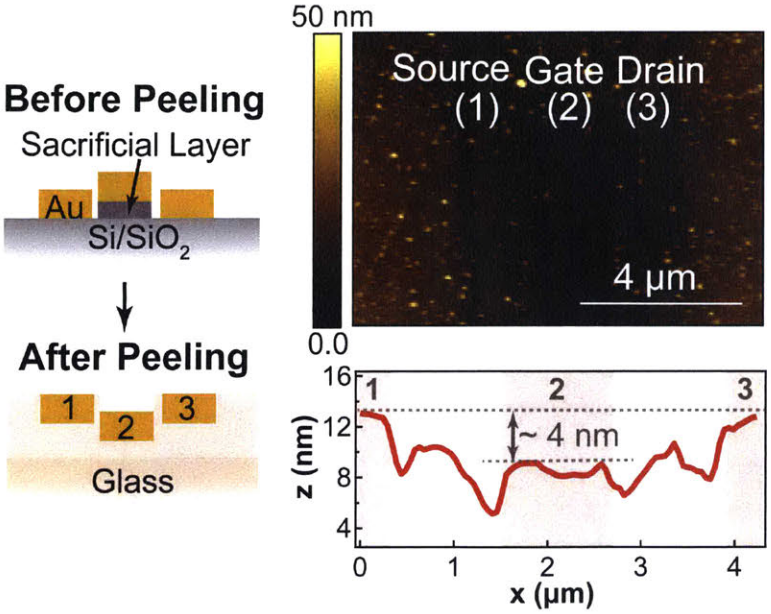

Figure 8-3: An example three-terminal bottom electrode formed using the fabrication technique of Figure 8-2a with Electrode 2 being recessed by ~4 nm relative to Electrodes 1 and 3 using graphene as the sacrificial material, and evaporated Au as electrodes.

chemically synthesized Au nanorods are utilized as the top contact. The scanning electron micrograph of the nanorods is shown in Figure 8-2e. These nanorods can be made with the desired length and diameter through an approach summarized in Appendix B [105]. The Au nanorods lack order as-synthesized. To allow device fabrication, individual nanorods need to be precisely positioned over the source-drain electrodes. To accommodate such precise manipulation of the nanoparticle, a dielectrophoretic approach is implemented (Figure 8-2d) [74–77]. A 10 μL droplet of the Au nanorod solution in water is placed on the electrodes. An AC voltage is applied between the source and drain electrodes (2-5 V peak to peak depending on the electrode design at 100 KHz - 1 MHz frequency). The applied voltage induces an electric field attracting the nanorod to the region of highest field intensity. As the rod aligns with the field it bridges the source to drain gap creating the desired squitch design. To limit the trapping to a single nanorod, a voltage dividing resistor is placed in series with the electrodes with a resistance intermediate to that of the nanogap with and without the bridged rod.

The transmission electron micrograph of Figure 8-5 shows the cross-section of a

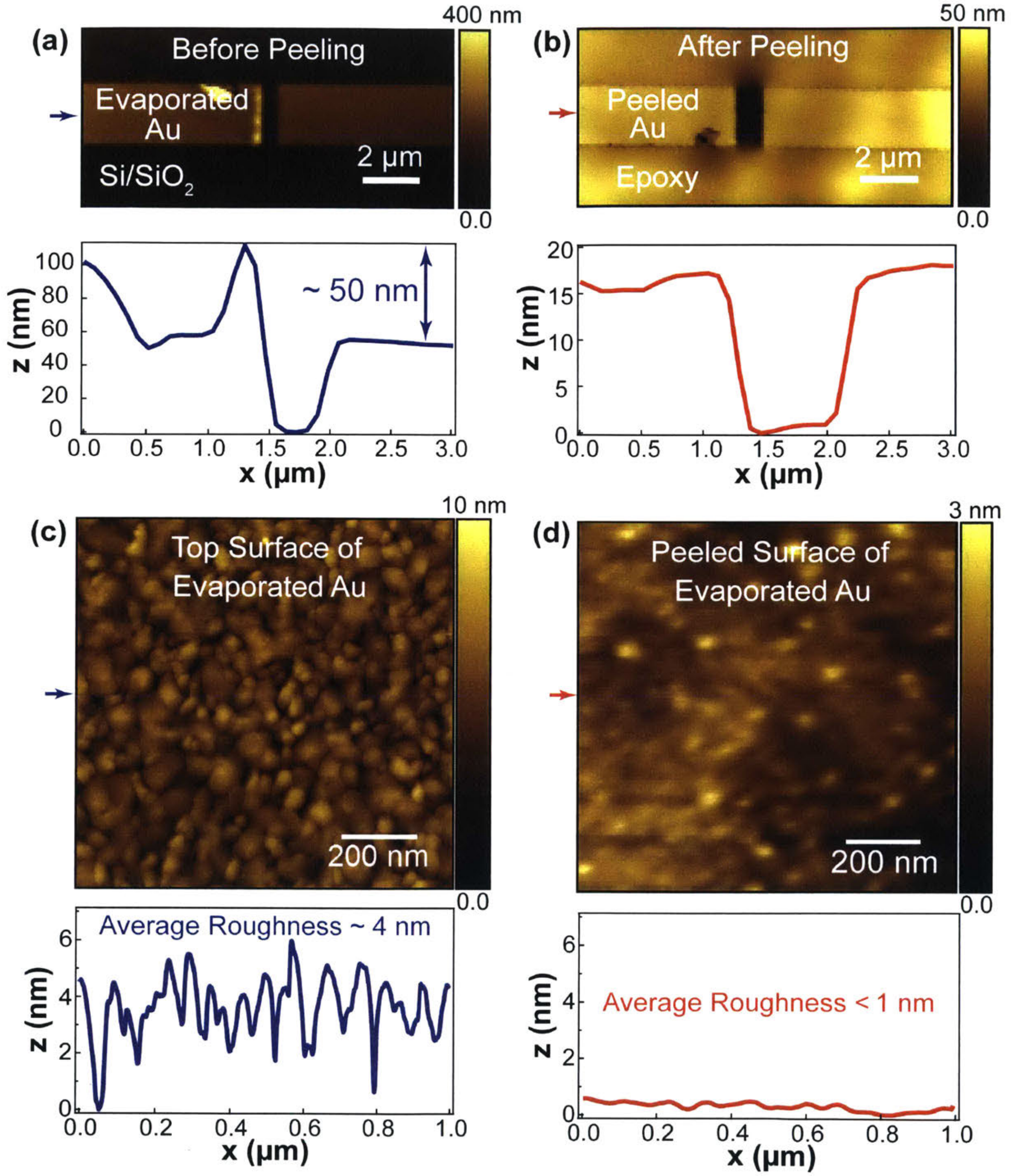

Figure 8-4: The peeling technique helps eliminate the edge defects imposed by the lift-off process. Here, an edge roughness ~50 nm caused by the lift-off process (a) is eliminated through the peeling technique (b). The peeling also minimizes the surface roughness, achieving <1 nm average surface roughness on the peeled surface (d) compared to ~4 nm roughness expected for the surface of an evaporated thin-film of Au (c).

representative molecular junction formed through the aforementioned process. The cross-section shows ~6 nm molecular gap formed between the atomically smooth facet of the top nanorod electrode and the peeled bottom electrode which has a sub-1 nm surface roughness. This cross-section clearly illustrates the benefit of the peeling technique in enhancing surface uniformity. The bottom edge of the evaporated electrode (Surface 1) shows a roughness ~4 nm consistent with the roughness expected for an evaporated Au film. However, the top peeled surface (Surface 2) shows a drastic decrease in roughness to <1 nm which promotes formation of a well-defined molecular gap. In addition to allowing formation of precisely defined molecular junctions, the proposed hybrid bottom-up and top-down technique can also lead to large-area device fabrication.

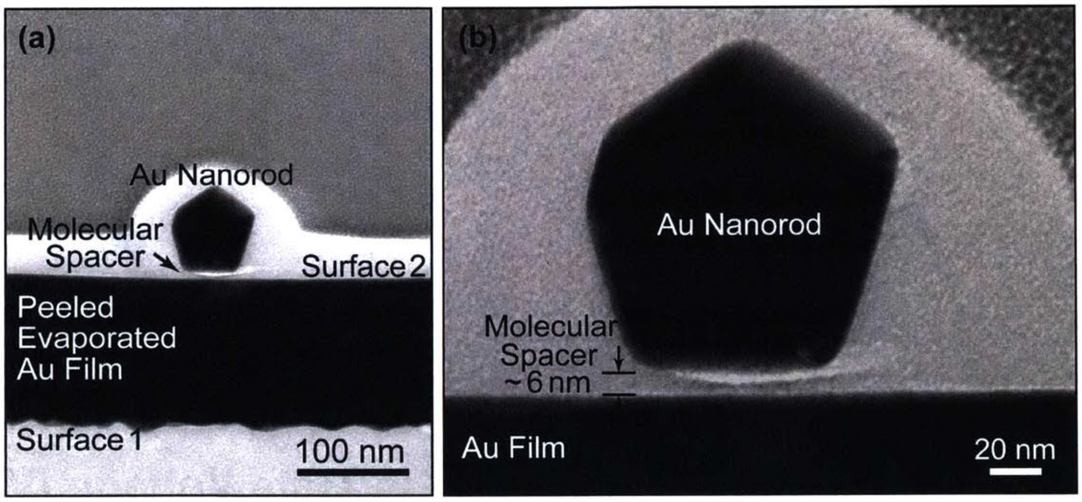

Figure 8-5: (a) TEM image of the cross-section of a molecular gap with Au nanorod top electrode and peeled evaporated Au film as the bottom electrode. (b) The magnified image shows the well-defined uniform molecular layer formed between the Au nanorod facet and the peeled electrode, both surfaces exhibiting roughness <1 nm.

8.3 Results and Discussions

The electrical characterization of the multi-terminal squitches suggests the gated-modulation of the tunneling current as shown in Figure 8-6. Similar to the case of two-terminal devices, two main sections are observed in the device operation. First, an exponential increase in the drain current (I_D) with an applied gate voltage corresponds to the decrease in the tunneling gap between the bottom electrodes and the top contact due to the induced electrostatic force. This is followed by an abrupt increase in I_D corresponding to pull-in at which point the combined electrostatic and van der Waals forces overwhelm the restoring force of the molecular layer such that the top electrode rapidly approaches the bottom leading to an abrupt decrease in the tunneling gap and consequently an abrupt increase in the current. The saturation region is due to the compliance set to the measurement tool.

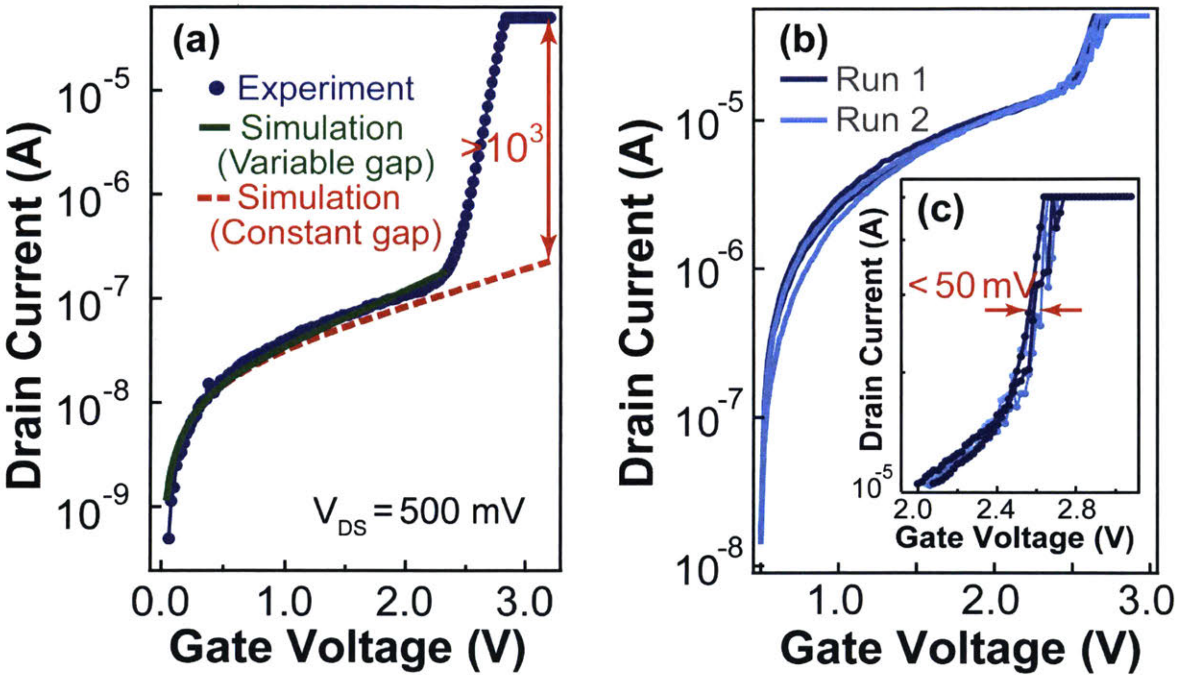

Figure 8-6: Current-voltage characteristics of an example multi-terminal squitch showing gated modulation of drain current. The experimental measurement is compared against the theoretically simulated performance showing a good fit when considering compression of the switching gap. To achieve the best-fit curve it is deduced that PEG-thiol layer has a Young's modulus of ~20 MPa. (b) Consecutive measurements of another device shows <50 mV hysteresis.

Assuming a pull-in voltage of 2.4 V, using the modified Simmons model in an approach similar to that discussed in Chapter 7, the experimental results are fitted against the theoretical simulation. Compared to the theoretical case where no compression of the molecular layer would be expected, electrostatically-induced compression of PEG-thiol molecular layer in this device results in $>10^3$ modulation of the current. Repeatable measurements also show <50 mV hysteresis associated with the devices, much smaller than that common in conventional contact-based NEM switches.

The results presented here are based on preliminary designs and more in-depth understanding of the device operation requires further experimentation. With the potential for low-voltage and abrupt switching with low hysteresis, squitches appear as a promising platform for energy-efficient NEM switches. To achieve ideal performance, optimization of device design and molecular layer chemical and mechanical properties are necessary. Beyond switches, the proposed tunable molecular gaps can also be applied to other mechanically-active nanoscale devices where control of surface adhesive forces is required for reliable and reversible operation.

8.4 Summary

An example design of a multi-terminal squitch is proposed where gated modulation of the tunneling current – resembling the operation of a conventional transistor – is achieved. To experimentally demonstrate this concept, a hybrid bottom-up and top-down fabrication is developed where nanometer precision, control and uniformity is achieved in forming well-defined molecular switching gaps. This technique leads to <1 nm uniformity of edges and surface roughness while providing nanometer resolution in defining surface topography with height variations between neighboring electrodes <5 nm. With the potential for low-voltage and abrupt switching with low hysteresis, tunable molecular gaps can serve as a promising platform towards more energy-efficient NEM switches. However, ideal operation requires further optimization of the device design and molecular layer chemical and mechanical properties. The fabrication and tunability techniques discussed here for multi-terminal squitches can also serve to form other building units of nanoscale devices and systems that require nanometer precision and uniformity.

Chapter 9

Summary and Outlook

9.1 Summary

Engineering at the limits of the nanoscale, dimensions in the few-nanometers regime, necessitates nanoscale precision, control and uniformity beyond those commonly possible through conventional techniques. In addition to precise fabrication, controlled placement of nanostructures relative to one another is challenging, in particular if mechanically active. The large surface adhesive forces hinder structural stability often causing adhesion between components or permanent collapse of structures. Therefore, when engineering at the limits of the nanoscale, beyond developing alternative fabrication techniques, devising approaches for nanoscale force control are essential. These challenges are investigated in this thesis while focusing on developing a new platform for energy-efficient NEM switches. With the goal of reducing actuation voltage and stiction, NEM switches require miniaturization of the electromechanically tunable switching gaps to <10 nm while controlling surface adhesion. Engineering such tunable nanogaps pushes the limits of nanoscale processing.

To achieve active nanoscale devices, such as electromechanically tunable nanogaps, with nanometer precision, control and uniformity, this thesis emphasizes hybrid top-down and bottom-up fabrication methodologies. This leads to techniques where chemistry, and surface and force engineering are integrated with conventional fabrication processes to enhance the resolution attainable while maintaining versatility. Utilizing this principle, two approaches are developed for controlled fabrication of electrically active nanogaps. In one, top-down fabricated nanostructures reconfigure through bottom-up engineering of surfaces and forces to achieve dimensions <10 nm much smaller than that readily feasible through the top-down approach. In an alternative technique, bottom-up assembly of nanogaps <10 nm is complemented by the lithographic patterning of electrical contacts and interconnects. These approaches facilitate nanoscale engineering by developing new fabrication processes and re-envisioning conventional ones while bridging the boundaries between different disciplines. The key is achieving integrative methodologies that provide the versatility needed to readily accommodate the more diverse material systems and unique capabilities that emerge as dimensions approach a few nanometers.

As is discussed in this thesis, controlling surface adhesive forces is another challenge of engineering at the limits of the nanoscale. Such control is in particular necessary for mechanically-active devices such as NEM switches. Dominating surface adhesive forces complicate device fabrication as dimensions are miniaturized, and impede reversible and reliable operation. In the case of a NEM switch, the surface adhesion also induces a hysteresis in performance setting a limit on the energy efficiency of the device. In this thesis, molecules are proposed as suitable building blocks to help minimize surface adhesion effects through use of their tailored chemical and mechanical properties. It is shown that molecules can serve as anti-stiction coatings lowering the surface energy of structures coming into contact with each other in a NEM switch, thus, minimizing the surface adhesive forces experienced. This scheme is schematically shown in Figure 9-1b. Furthermore, the molecules can serve as interconnects between the electrodes forming the switching gap. In this scheme, the molecules not only assist precise formation of nanometer-thin gaps by controlling molecular lengths through chemical synthesis but serve as nanoscale springs to tune the relative spacing in a controlled and reversible manner. The molecular layer can undergo controlled mechanical compression in response to an applied external force, for example an electrostatic force due to an applied voltage. As the molecules compress, the surfaces sandwiching the molecular film approach one another. The elastic restoring force of the molecules help balance the increasing surface adhesive forces. Once the applied force is removed, this elastic restoring force overcomes the surface adhesive forces to ensure that the movable surface transitions to its original position for a reversible operation, overcoming stiction. This principle is used to develop an electromechanically tunable metal-molecule-metal tunneling junction, where presence of the molecules helps formation of nanometer thin gaps with controlled and reversible tunability.

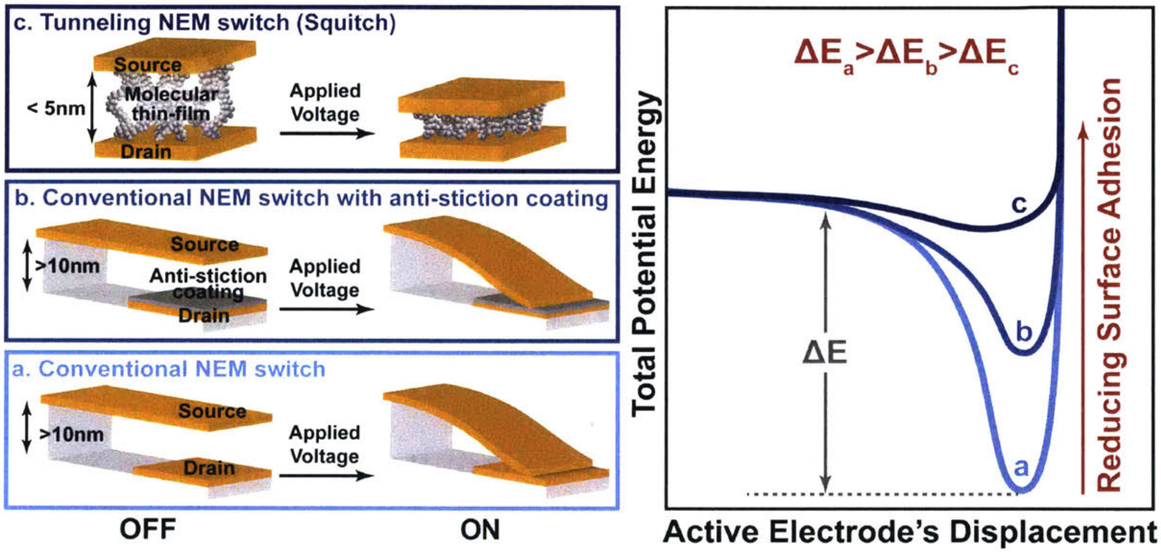
c. Tunneling NEM switch (Squitch)
Source
< 5nm
Molecular thin-film
Drain
Applied Voltage
b. Conventional NEM switch with anti-stiction coating
>10nm
Source
Anti-stiction coating
Drain
Applied Voltage
a. Conventional NEM switch
>10nm
Source
Drain
Applied Voltage
OFF
ON
ΔE_a>ΔE_b>ΔE_c
Total Potential Energy
c
b
a
ΔE
Reducing Surface Adhesion
Active Electrode's Displacement

Figure 9-1: Schematic representation of strategies toward low-energy stiction-free NEM switches utilizing molecular layers. (a) In a conventional contact-based NEM switch, the elastic restoring force should exceed the surface adhesive forces to overcome the energy barrier (ΔE) to break the contact. (b) Low surface energy molecular layers reduce the surface adhesive forces at contact, decreasing the potential for stiction. (c) Additional minimization of stiction can be achieved using a metal-molecule-metal switching gap which further lowers the surface adhesive forces and allows nanoscale force control through compression of the molecular layer, while enabling formation of a few nanometer-thick gap for sub-1 V operation [102].

A decrease in the tunneling gap leads to an increase in the tunneling current. The tunneling current modulation in an electromechanically tunable molecular nanogap is proposed as a switching mechanism for NEM switches, devices referred to as squitches. Implementing hybrid fabrication techniques, example squitches are demonstrated in this thesis in two-terminal form with <2 V actuation voltage and $>10^4$ current modulation. Extension to multi-terminal designs utilizing newly developed hybrid fabrication techniques suggests gated modulation of the tunneling current resembling operation of conventional transistors necessary for use in integrated systems. These devices also show <50 mV hysteresis, among lowest reported for NEM switches. With the potential to miniaturize the switching gap to much smaller than conventionally feasible while providing nanoscale force control, a platform for low-voltage and low-stiction energy-efficient switches emerges (Figure 9-1c). However, realizing optimal performance and full understanding of the switching mechanism require further improvements in device architecture, and chemical and mechanical properties of the molecular layer beyond the proof-of-concept designs explored here. Even though applied to tunneling-based NEM switches, the nanoscale processing toolsets developed here can also be broadly applicable to other active devices with critical features a few nanometers in size.

9.2 Outlook

9.2.1 Tunneling NEM Switches - Squitches

The squitch designs presented in this thesis demonstrate the feasibility of the proposed tunneling-based switching mechanism towards low-voltage and stiction-free NEM switches. The switching mechanism however, is not limited to the example designs and model material systems used. As mentioned previously, to realize an optimal switching performance in accordance to the desired application, optimizing the device architecture and molecular layer structural, mechanical and chemical properties are necessary. Further experimentation is also needed to investigate the device stability and lifetime. Stability of molecular layer under continuous high frequency mechanical deformation with electrical actuation is necessary to ensure long term device integrity and is a topic of future studies. Furthermore, future work will emphasize experimental characterization of the switching parameters including the switching speed and energy in various designs of squitches and corresponding circuits to identify performance limits and ideal designs.

Maintaining uniformity and precision is important in defining the sub-5 nm molecular switching gaps to maintain device stable operation. However, the need for uniformity extends beyond individual devices. Integration into circuits for practical applications requires large-area and high-density fabrication of such nanoscale devices which can be challenged by presence of device-to-device variations. Given the small dimensions and exponential dependence of the tunneling current on changes in the switching gap, minute conformational variations may lead to drastic discrepancies in performance. The sensitivity of squitch performance at a systems level to such structural variations should be evaluated and appropriate measures put in place to provide the necessary compensations to maintain consistency. When designing squitches, as considered in this thesis, new fabrication techniques are required to allow for the desired precision and uniformity. The fabrication techniques and device designs though are not limited to those introduced here. The concept can be implemented in a versatile set of device designs accommodated by various integrative fabrication methodologies. In some cases even conventional contact-based NEM switches can be modified to accommodate the tunneling-based switching mechanism through post-fabrication processing utilizing engineering of surfaces and forces.

The molecular layer's mechanical properties and time-dependent mechanical response defines the switching performance. Numerically simulated switching parameters of a simplified two-terminal design represent this dependence in Figure 9-2. As discussed in Chapter 5, the mechanical properties of the molecular layers can be engineered at two levels: 1) inherent properties of the molecules tuned through chemical synthesis, and 2) effective properties of the layer by using a combination of different molecular species. Furthermore, the mechanical tunability of the switching gap can be imposed by the use of responsive molecules that can undergo conformational changes in response to an external stimulus. Engineering of the molecular layer with the desired mechanics and dynamics though requires an in-depth understanding of these properties which have only been subject of minor studies in the past with limited reports in the literature. These properties are challenging to probe using conventional metrology tools, which are mainly based on scanning probe techniques, as they face limitations in resolution and accuracy given the small dimensions under consideration. These techniques are also largely inadequate in dynamic device characterization during active operation which would otherwise be useful in elucidating performance principles. Thus, alternative metrology techniques are necessary to study dynamic device operation, nanoscale motion and mechanical properties of the molecular layers to acquire the much needed knowledge-base to engineer molecular films with designer nanomechanics.

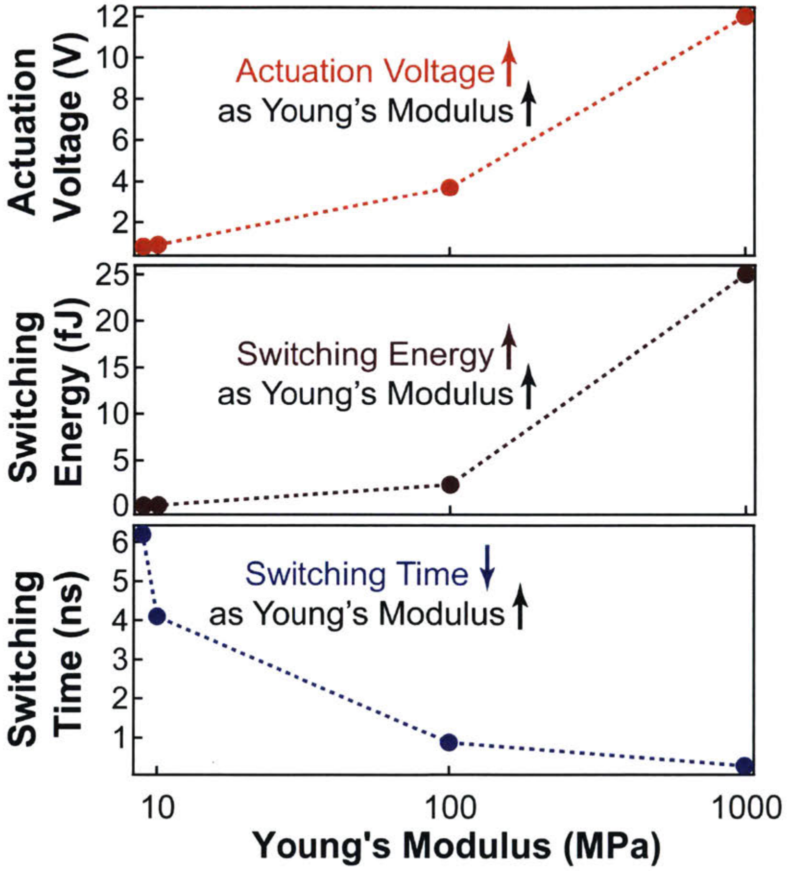

Figure 9-2: Switching parameters including actuation voltage, switching energy and switching time change as a function of the mechanical properties of the molecular spacer.

To concurrently allow performance control, it is desired for the characterization technique to be integrated within the active device design – a feature beneficial in particular for devices only few nanometers in size where any structural variations could lead to drastic performance inconsistencies. The methodology should also provide the much needed sensitivity where sub-nm conformation changes can be detected. To this end, a scheme that we propose involves use of plasmonic properties of metallic nanostructures. A metallic nanostructure in close proximity of an underlying metal film can plasmonically couple with a distance-dependent resonance red shift in its peak plasmon wavelength as it approaches the film [106–108]. The shift in plasmon resonance due to changes in the gap width has high spectral sensitivity. Thus, minute structural changes, even in the Å regime, can be detected through the output optical response by monitoring the far-field scattering spectrum. In the molecular nanogaps, changes in the gap size are imposed by electrostatically-induced compression of the molecules. As the two electrodes approach each other, a shift in resonance can be detected. Figure 9-3 shows this in two structures composed of a plasmon resonant Au nanoparticle coupled to Au film at two different molecular spacings. Collectively, the foundation for a metrology tool is provided where nanoscale motion and mechanical properties of molecules are characterized. The need for such alternative characterization means emphasizes the importance of developing metrology tools concurrent to processing techniques to push the boundaries of engineering at the limits of the nanoscale.

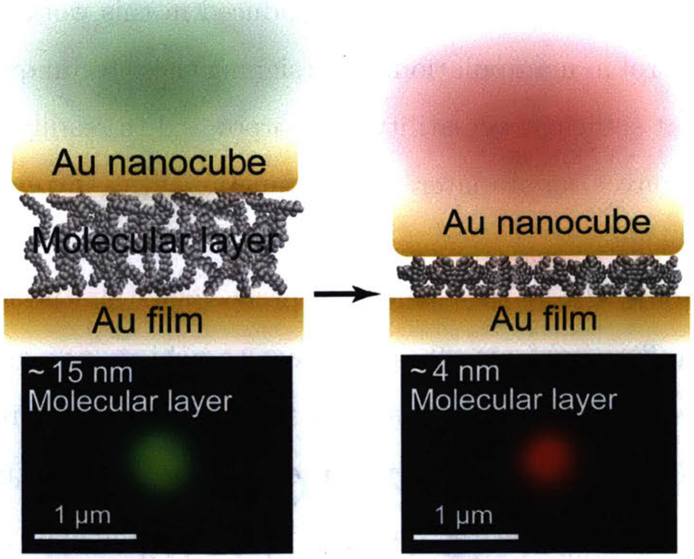

Figure 9-3: In a Au-molecule-Au nanogap, the plasmon resonance shifts as the metal-metal gap decreases. Dark-field microscope images of Au nanocubes spaced from an underlying Au film at different distances using molecular layers show the gap-dependent resonance.

9.2.2 Engineering at the Limits of the Nanoscale - Beyond Squitches

Squitches are just an example device platform made feasible by the ability to precisely manipulate dimensions, surfaces and forces at the few-nanometer regime. With the need for sub-5 nm and mechanically tunable molecular gaps, the challenges faced in the design of a squitch exemplify limitations broadly expected when engineering at such small dimensions. These are dominated by the lack of resolution and precision in defining nanoscale features, and the lack of control over surface interactions and adhesive forces. As discussed in this thesis, conventional fabrication techniques alone are insufficient to provide the unprecedented resolution, control and uniformity essential. When engineering devices with critical dimensions in the few-nanometer regime, such as the sub-5 nm width of the switching gap in a squitch, surface irregularities on the nanometer scale even though conventionally considered small can be detrimental for the device performance. To overcome the challenges, alternative approaches to fabrication are necessary – approaches that can be fundamentally new in functionality but also those that complement the conventional techniques to redefine their limits. Multidisciplinary methodologies leveraging the opportunities offered through chemistry and materials science, such as those introduced in this work, provide the much desired sub-nm control in manipulation. In designing these techniques, care should be taken to ensure that sufficient versatility is incorporated to readily accommodate the broad range of unconventional materials and functionalities involved in the evolving field of nanotechnology.

Beyond developing alternative nanoscale processing, this thesis also emphasizes the need for controlling surface adhesive forces to achieve not only fabrication by controlled and reversible tunability essential for mechanically-active structures. By achieving nanoscale force control, dynamic alteration of nanostructure's physical conformation allows modulation of the structural form and inherent properties beyond the electronic transport. The tunability in operation is dependent on the mechanical performance of the structures involved. Through use of nanomechanics, and by controlled and reversible modulation of the related properties, mechanically-active nanoscale devices with applications beyond conventional NEMS can emerge, with dimensions <10 nm being feasible. Such devices are not readily feasible conventionally. However, through use of alternative fabrication and implementing appropriate force control methodologies, the emerging nanoscale mechanically-active architectures can lead not only to the conventional devices of improved performance but those with fundamentally unique operating principles otherwise not attainable at larger dimensions.

The importance of molecules as nanoscale building blocks is also demonstrated in this thesis. Molecules which can precisely be defined in structure, chemical composition and mechanical properties do not only accommodate the fabrication of nanoscale features but help control surface interactions and forces. The versatility provided through chemical synthesis then leads to an extensive library of molecular components that can be integrated into nanoscale devices formed through the alternative fabrication methodologies introduced here. This allows a wide range of molecular device platforms. These devices can help advancements in the field of molecular electronics but also serve to expand device functionalities beyond those dependent on electronic transport.

"There's plenty of room at the bottom", an idea introduced by Richard Feynman in 1959. Decades later, even after tremendous improvements in nanotechnology engineering, we have yet to exploit the full potential of the field and there still remains plenty of room for scientific and technological advancements at the bottom. Currently, a limitation is in the ability to readily gain access to, control and tune such small dimensions. By implementing a multidisciplinary approach, techniques necessary to allow precise nanoscale manipulation and control are developed. This results in a wide range of active nanoscale structures with critical dimensions <10 nm in size and with the potential to uniquely manipulate excitonic, optical, mechanical, electronic, magnetic and/or spintronic properties (Figure 9-4). An example in reference to this thesis is shown in Figure 9-5. Precise manipulation of these properties leads to unique physical phenomena based on which a platform for the development of next generation nanodevices emerge, forming an ongoing interdisciplinary area of research.

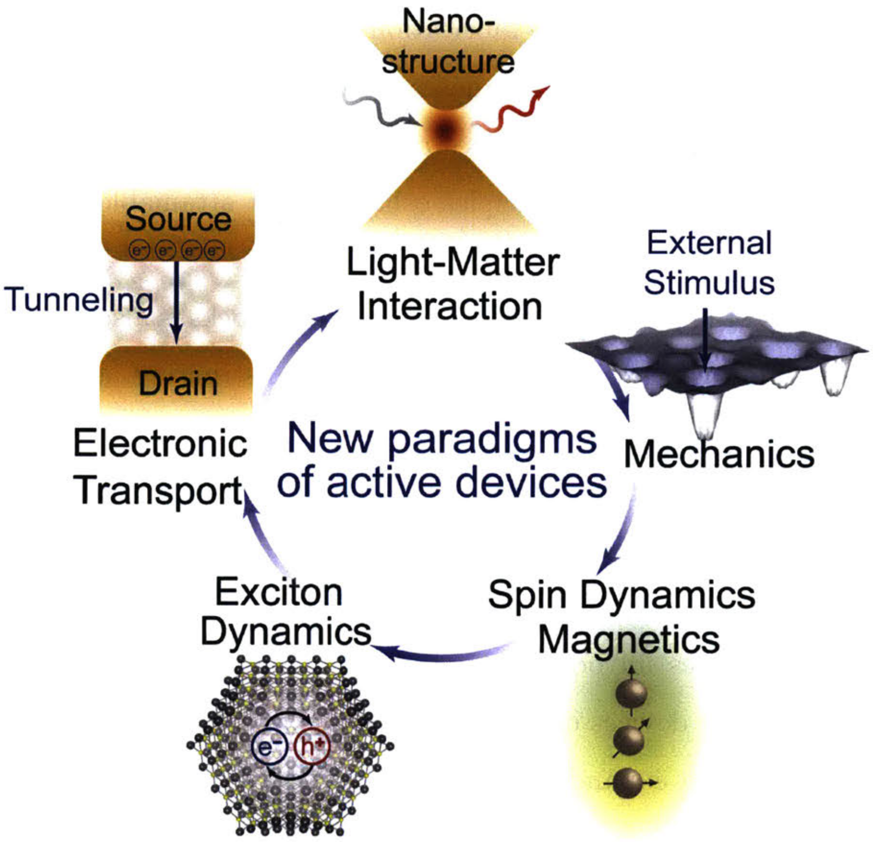
Nano-
structure
Light-Matter
Interaction
Source
e⁻ e⁻ e⁻ e⁻
Tunneling
Drain
Electronic
Transport
External
Stimulus
Mechanics
New paradigms
of active devices
Exciton
Dynamics
e⁻ h⁺
Spin Dynamics
Magnetics

Figure 9-4: Engineering at the limits of the nanoscale, enabled through development of alternative fabrication techniques and by achieving control over surfaces and forces, makes feasible unique manipulation of properties including electronic transport, light-matter interactions, mechanics, magnetics, exciton and spin dynamics that can lead to new paradigms of active devices.

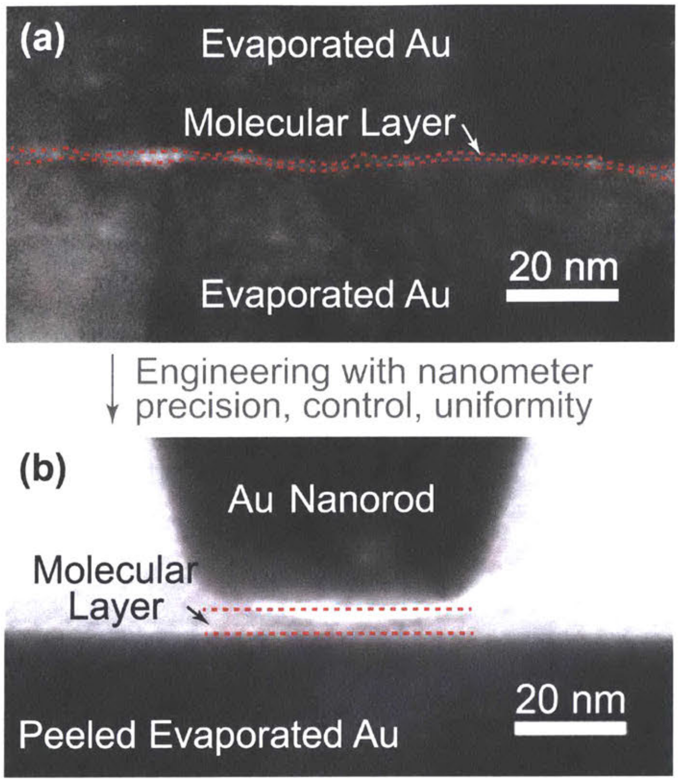
(a)
Evaporated Au
Molecular Layer
20 nm
Evaporated Au
Engineering with nanometer precision, control, uniformity
(b)
Au Nanorod
Molecular Layer
20 nm
Peeled Evaporated Au

Figure 9-5: Alternative fabrication methodologies are needed to achieve resolution, control and uniformity required to promote engineering of active devices at the limits of the nanoscale. For the example of electromechanically tunable molecular junctions, conventional top-down lithography and thermal evaporation commonly lead to nonuniform molecular junctions with metal penetration through the molecular layer inducing damage (a) while hybrid top-down and bottom-up techniques help formation of well-defined molecular nanogaps with sub-nm precision, control and uniformity (b). The molecular junctions are outlined in dotted red lines.

Appendix A

An Overview of NEM Switches

Table A.1: Representative electrostatic NEM switches - design and performance.

Structure (no. of Terminals)	**Primary Material**	**Fabrication Technique**	**Switching Gap (nm)**	**Actuation Voltage (V)**	**Hysteresis Voltage (V)**	**ON-OFF Ratio**
Pipe clip (2T) [8]	W, TiW	Spacer litho.	>4	>0.4	—	$>10^5$
Cantilever (2T) [9, 10]	TiN	Dep., Litho.	15	13	5	$>10^5$
Clamped plate (4T, 6T) [11, 12]	Poly-SiGe, W, PFDTES	Dep., Litho.	160 (Actuation) 60 (Contact)	0.05 ($\sim$17V body bias)	<0.05	$>10^6$
Vertical CNT (3T) [13, 14]	CNT	EBL, Growth	30	4.5	—	$>10^4$
In-plane cantilever (5T) [15, 16]	Pt	Dep., Litho.	—	8	$\sim$2	$>10^5$
In-plane cantilever (3T) [17]	WN_x	EBL	150	>0.8	$\sim$1	$>10^4$
In-plane cantilever (3T) [18, 19]	SiC	Dep., EBL	<500	15	$\sim$7	$>10^4$
Clamped-clamped wire (3T) [20]	SiC	EBL	$\sim$30	$\sim$1.5	$\sim$1	$>10^3$
Curved cantilever (3T, 4T) [21, 22]	a-C	Dep., EBL	60	7	0.5	$>10^8$
Clamped-clamped beam (3T) [23]	Ru	Dep., Litho., EBL	30-70 (Actuation) 20-50 (Contact)	>4	1	$>10^8$
Graphene membrane (2T) [24]	Graphene	Dep., EBL	>25	>2.7	—	$>10^4$
Cantilever (3T) [25]	TiN, Oil	Dep., Litho.	40 (Actuation) 20 (Contact)	>4	<1	$>10^4$

Litho.: Lithography; EBL: Electron-beam lithography; a-C: Amorphous carbon; CNT: Carbon nanotube; Dep.: Deposition; PFDTES: Perfluorodecyltriethoxysilane; Actuation: Actuation gap; Contact: Contact gap.

Appendix B

Synthesis of Au Nanoplates and Nanorods

B.1 Au Nanoplate Synthesis

The Au nanoplates are sythesized following a modified procedure reported by Gu *et al.* [73]. A solution of 0.054 mmol of $HAuCl_4.4H_2O$ is heated to 65^oC in a water bath for 20 min. Then, 0.1 M aniline solution in ethylene glycol is added to the heated $HAuCl_4$ solution under mild stirring to acquire a 2:1 molar ratio of aniline to Au. This reaction is allowed to proceed for 3 hours without stirring, leading to formation of triangular and hexagonal Au nanoplates with spherical nanoparticles as byproducts. The nanoplates precipitate at the bottom of the vial while the red supernatant mainly contains the spherical particles. The supernatant is gently removed without disturbing the precipitant and replaced with fresh ethanol. The vial is sonicated for about 10 s in pulses to disperse the Au nanoplates in ethanol. Note that a long sonication step will induce damage to the plates. The particles are allowed to settle and the supernatant is replaced with fresh ethanol. This is repeated 3 times to ensure the spherical particles are mainly removed. The cleaning can also be done through several centrifugation cycles instead of precipitation. In an alternative approach, upon addition of aniline, 900 μL of 1 mol/L polyvinylpyrrolidone (PVP) in ethylene glycol is added dropwise to the solution under gentle stirring before allowing the growth reaction to proceed for 3 hours. Addition of PVP leads to formation of smaller nanoplates with a tighter size distribution. Example scanning electron micrographs of the nanoplates are shown in Figure B-1.

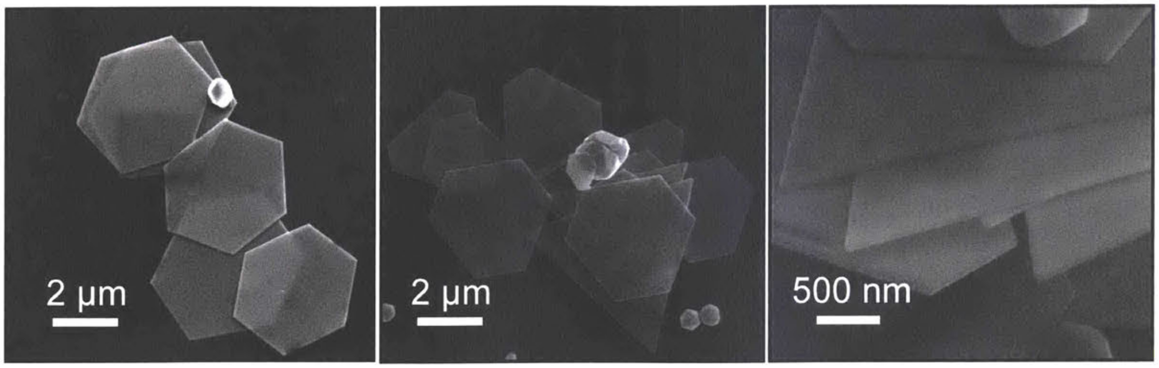

Figure B-1: SEM images of Au nanoplates synthesized in presence of PVP capping agent.

B.2 Au Nanorod Synthesis

Au nanorods are synthesized using a seeded growth method reported by Wang *et al.* [105]. In this process seed and growth solutions are prepared as follows.

Au seed solution preparation. A 10 mL solution of 0.25 mM $HAuCl_4$ and 0.1 M CTAB is prepared in deionized water. Then, 450 μL of 0.02 M ice-cold sodium borohydride ($NaBH_4$) solution is injected into the CTAB-$HAuCl_4$ solution while stirring vigorously. Once stirred for 5 min, the solution is then left undisturbed at 27^{o}C for 2 hours resulting in gold nanopartices a few nanometers in size.

Au growth solution preparation. Depending on the length of the nanorods desired, the growth solution will be slightly different. First, 180 mL aqueous solution of 0.1 M CTAB and 0.175 mM $HAuCl_4$ is prepared, and aliquoted into 3 flasks: flasks A and B contain 2.5 mL of solution and C holds 25 mL. Then, different amounts of 0.5 M nitric acid as per the amounts outlined in Table B.1 are added to flask C. Lastly, 10 μL, 10 μL, and 100 μL of 0.1 M ascorbic acid are added to flasks A, B, and C respectively and shaken gently until they become colorless.

Au nanorod synthesis. To form the Au nanorods, first 200 μL of seed solution is added to Flask A and shaken for 10 seconds. This is followed by immediately adding 200 μL of this solution to flask B and gently shaking the solution for 10 seconds. Then, a volume of this solution is added to flask C as per the amounts summarized in Table B.1 with reference to the desired particle size, and gently shaken for 5 seconds. The solution in flask C is then left undisturbed for 12 hours at 27^{o}C. After incubation, the purple-pink colored supernatant is carefully removed, leaving nanorods precipitated at the bottom of the vial. The rods are re-dispersed in 10 mL of deionized water. To remove excess reagents and nanoparticles of undesired shapes, the solution is cleaned twice by centrifuging it at 2000 rpm, removing the supernatant, and re-dispersing the particles in fresh deionized water. Scanning electron micrographs of example nanorods with two different lengths are shown in Figure B-2. It should be noted that the nanorod synthesis contains Au nanoplates and spherical nanoparticles as byproducts. The number of Au nanoparticles of undesired shapes and the rod's size distribution increase for the longer nanorods.

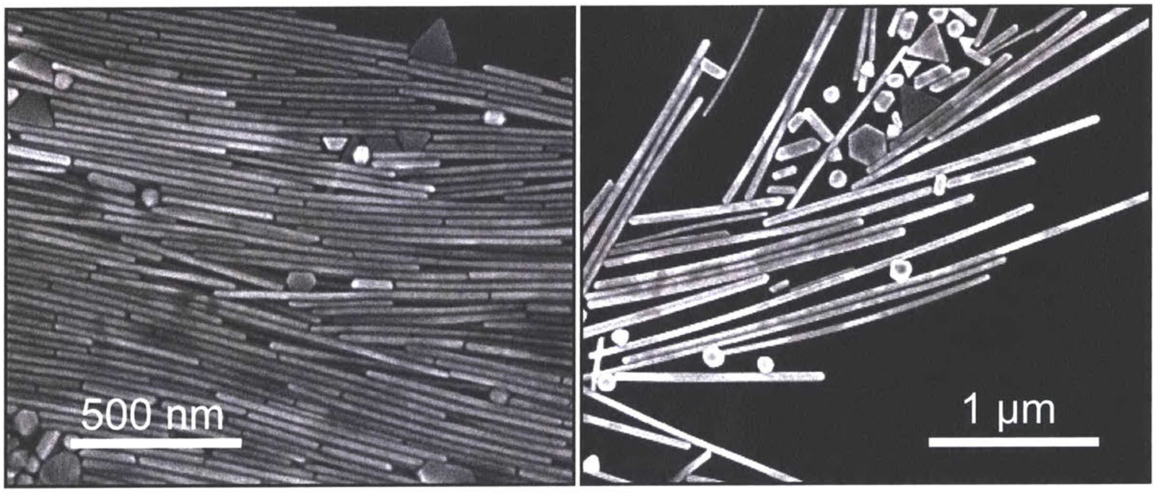

Figure B-2: SEM images of Au nanorods of two different lengths with the length modified by the reaction conditions according to the procedure outlined in this section.

Table B.1: The amounts of nitric acid (HNO_3) and solution B used in the synthesis of different nanorods and their corresponding average lengths.

Sample Number	**Volume of HNO_3 (μL)**	**Volume of B added to C (mL)**	**Nanorod Average Length (nm)**
1	50.4	2	530
2	252	2	654
3	50.4	0.2	665
4	550	2	1111
5	252	0.2	1255
6	1100	0.2	2469

Appendix C

Theoretical Simulation and Fitting of Experimental Results

The experimental results were fitted using the Simmons tunneling model while taking into account the switching gap compression by the applied voltage. In the analysis performed, several fitting parameters including the tunneling barrier shape (α), tunneling barrier height (ϕ), Hamaker constant (A_H), Young's modulus (Y) and dielectric constant (ϵ_r) of the molecular layer are unknown. Thus, to achieve a more cohesive overview of the fit to the experiment, we implemented a Monte Carlo approach. In this technique, values of α, ϕ, the initial thickness of molecular layer (L) and the normalized pull-in gap (Δ) are randomly selected within a pre-defined range to execute the model and extract ϵ_r and Y while optimizing the fit to the experiment. The process is outlined below.

For this analysis, the applied voltage corresponding to an abrupt increase in the measured current is considered to be the pull-in voltage of the device. Utilizing this voltage value, the normalized equation of motion is solved to simulate the expected tunneling gap modulation and the current conduction behavior. The equation of motion (Equation 6.2) at equilibrium can be written in the normalized form,

---

Appendix C is reprinted with permission from [F. Niroui, A. I. Wang, E. M. Sletten, Y. Song, J. Kong, E. Yablonovitch, T. M. Swager, J. H. Lang and V. Bulović, Tunneling nanoelectromechanical switches based on compressible molecular thin films, *ACS Nano*, 9(8): 7886-7894, 2015]. Copyright 2015 American Chemical Society.

$$\delta^4 - \delta^3 + \frac{\epsilon_r \epsilon_0 V^2}{2YL^2}\delta + \frac{A_H}{6\pi Y L^3} = 0 \tag{C.1}$$

where L is the thickness of the uncompressed molecular film, $\delta = g/L$ is the normalized tunneling gap, ϵ_0 is the permittivity of free space, ϵ_r is the dielectric constant of the molecular layer, Y is the material's Young's modulus, and A_H is the Hamaker constant set to be 3×10^{-19} J in this analysis. Equation C.1 can be rearranged in the form of Equation C.2 with lumped parameters K_0 and K_1,

$$\delta^4 - \delta^3 + K_1 V^2 \delta + K_0 = 0 \tag{C.2}$$

$$K_0 = \frac{A_H}{6\pi Y L^3} = 3\Delta^4 - 2\Delta^3, \text{and } K_1 = \frac{\epsilon_0 \epsilon_r}{2YL^2} = \frac{2\Delta^3 - \Delta^2 - \frac{2}{\Delta}K_0}{V^2{}_{Pull-in}} \tag{C.3}$$

where Δ is the normalized pull-in gap which can range between 2/3, if pull-in is purely electrostatically driven, to 3/4, when pull-in is induced purely by van der Waals forces.

Setting Δ values within the range 2/3 to 3/4, L in the range of 2 to 4 nm and pull-in voltage ($V_{pull-in}$) extracted from experimental data, Equation C.2 is solved to determine the tunneling gap at each applied voltage. The calculated gap thicknesses are then utilized with α constrained in the range of 0.4 to 1, and ϕ between 1 eV to 5 eV in the Simmons tunneling model to simulate expected current-voltage characteristics. The corresponding values of ϵ_r and Y are then calculated based on Equations C.3. The model is executed for a large number of randomly selected points and the case leading to the smallest discrepancy between the experiment and theory is determined.

Due to the large number of unknown parameters, determining a unique fit to the experimental data is not feasible. Other sets of numerical parameters can also lead to a good agreement with the measured results. However, amongst these value sets exist parameter combinations that are within physically viable bounds. Constraining the dielectric constants of the molecular layer to within 1 to 5, a reasonable range for organic materials, the Young's modulus of the material extracted from the three devices presented in Figure 7-4a are deduced to be approximately 5 MPa to 40 MPa with higher density of points in the 5 MPa to 15 MPa regime (Figure C-1). The mechanical properties of PEG self-assembled thin-films have not been previously studied, however, reports of bulk PEG material properties suggest that the Young's modulus range we deduce here satisfies that of the experimentally measured values for similar material sets. For example, the Young's modulus of PEG 600 g/mol is reported to be about 5 MPa [109]. More conclusive analysis of the experimental results require further knowledge of the mechanical properties of the molecular layer, the specifics of the tunneling junctions and the dynamics of the tunneling gap electromechanical modulations.

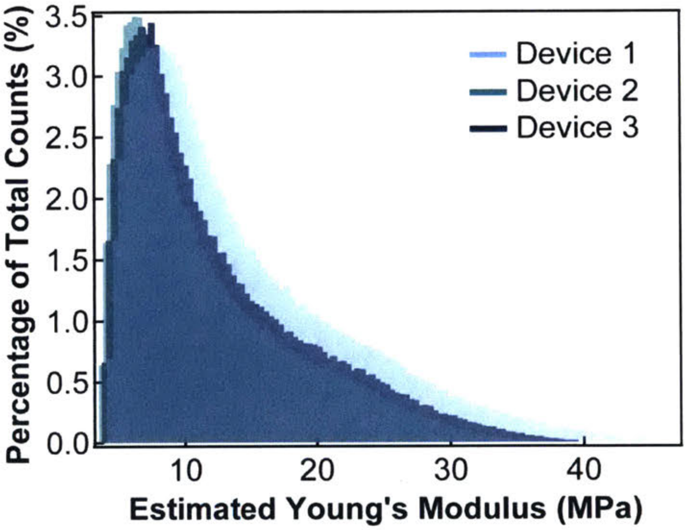

Figure C-1: The distribution of Young's moduli extracted from modeling the three squitches of Figure 7-4a over 1 million simulation runs with the possible dielectric constant values being constrained to the range 1 to 5. The values of α and ϕ leading to this distribution are in the range of 0.4 to 1, and 1 to 5 eV, respectively.

Bibliography

[1] O. Y. Loh and H. D. Espinosa. Nanoelectromechanical contact switches. *Nature Nanotechnology*, 7(5):283–295, 2012.

[2] A. Peschot, C. Qian and T.-J. King Liu. Nanoelectromechanical switches for low-power digital computing. *Micromachines*, 6(8):1046–1065, 2015.

[3] R. Maboudian and R. T. Howe. Critical review: Adhesion in surface micromechanical structures. *Journal of Vacuum Science & Technology B: Microelectronics and Nanometer Structures Processing, Measurement, and Phenomena*, 15(1):1–20, 1997.

[4] W. M. van Spengen, R. Puers and I. De Wolf. A physical model to predict stiction in MEMS. *Journal of Micromechanics and Microengineering*, 12(5):702–713, 2002.

[5] C. H. Mastrangelo. Adhesion-related failure mechanisms in micromechanical devices. *Tribology Letters*, 3(3):223–238, 1997.

[6] A. Hariri, J. W. Zu and R. Ben Mrad. Modeling of dry stiction in micro electromechanical systems (MEMS). *Journal of Micromechanics and Microengineering*, 16(7):1195–1206, 2006.

[7] U. Zaghloul, G. Papaioannou, B. Bhushan, F. Coccetti, P. Pons and R. Plana. On the reliability of electrostatic NEMS/MEMS devices: Review of present knowledge on the dielectric charging and stiction failure mechanisms and novel characterization methodologies. *Microelectronics Reliability*, 51(9):1810–1818, 2011.

[8] J. O. Lee, Y. Song, M. Kim, M. Kang, J. Oh, H. Yang and J. Yoon. A sub-1-volt nanoelectromechanical switching device. *Nature Nanotechnology*, 8(1):36–40, 2013.

[9] W. W. Jang, J. O Lee, J.-B. Yoon, M.-S. Kim, J.-M. Lee, S.-M. Kim, K.-H. Cho, D.-W. Kim, D. Park and W.-S. Lee. Fabrication and characterization of a nanoelectromechanical switch with 15-nm-thick suspension air gap. *Applied Physics Letters*, 92(10):103110, 2008.

[10] W. W. Jang, J.-B. Yoon, M.-S. Kim, J.-M. Lee, S.-M. Kim, E.-J. Yoon, K.-H. Cho, S.-Y. Lee, I.-H. Choi, D.-W. Kim and D. Park. NEMS switch with

30nm-thick beam and 20nm-thick air-gap for high density non-volatile memory applications. *Solid-State Electronics*, 52(10):1578–1583, 2008.

[11] B. Osoba, B. Saha, L. Dougherty, J. Edgington, C. Qian, F. Niroui, J. H. Lang, V. Bulović, J. Wu and T.-J. King Liu. Sub-50 mV NEM relay operation enabled by self-assembled molecular coating. *Electron Devices Meeting (IEDM), IEEE International*, 26.8.1–26.8.4, 2016.

[12] Y. Chen, R. Nathanael, J. Jeon, J. Yaung, L. Hutin and T.-J. King Liu. Characterization of contact resistance stability in MEM relays with tungsten electrodes. *Journal of Microelectromechanical Systems*, 21(3):511–513, 2012.

[13] J. E. Jang, S. N. Cha, Y. Choi, G. A. J. Amaratunga, D. J. Kang, D. G. Hasko, J. E. Jung and J. M. Kim. Nanoelectromechanical switches with vertically aligned carbon nanotubes. *Applied Physics Letters*, 87(16):163114, 2005.

[14] J. E. Jang, S. N. Cha, Y. Choi, T. P. Butler, D. J. Kang, D. G. Hasko, J. E. Jung, Y. W. Jing, J. M. Kim and G. A. J. Amaratunga. Nanoelectromechanical switch with low voltage drive. *Applied Physics Letters*, 93(11):113105, 2008.

[15] R. Parsa, W. S. Lee, M. Shavezipur, J. Provine, R. Maboudian, S. Mitra, H.-S. P. Wong and R. T. Howe. Laterally actuated platinum-coated polysilicon NEM relays. *Journal of Microelectromechanical Systems*, 22(3):768–778, 2013.

[16] R. Parsa, W. S. Lee, M. Shavezipur, J. Provine, R. Maboudian, S. Mitra, H.-S. P. Wong and R. T. Howe. Nanoelectromechanical relays with decoupled electrode and suspension. *Micro Electro Mechanical Systems (MEMS), IEEE 24th international conference*, 1361–1364, 2011.

[17] A. M. Mayet, A. M. Hussain and M. M. Hussain. Three-terminal nanoelectromechanical switch based on tungsten nitride – an amorphous metallic material. *Nanotechnology*, 27(3):035202, 2015.

[18] T. Lee, S. Bhunia and M. Mehregany. Electromechanical computing at 500°C with silicon carbide. *Science*, 329(5997):1316–1318, 2010.

[19] T. He, R. Yang, V. Ranganathan, S. Rajgopal, M. A. Tupta, S. Bhunia, M. Mehregany and P. X.-L. Feng. Silicon carbide (SiC) nanoelectromechanical switches and logic gates with long cycles and robust performance in ambient air and at high temperature. *Electron Devices Meeting (IEDM), IEEE International*, 4.6.1–4.6.4, 2013.

[20] X. L. Feng, M. H. Matheny, C. A. Zorman, M. Mehregany and M. L. Roukes. Low voltage nanoelectromechanical switches based on silicon carbide nanowires. *Nano letters*, 10(8):2891–2896, 2010.

[21] D. Grogg, C. L. Ayala, U. Dreschsler, A. Sebastian, W. W. Koelmans, S. J. Bleiker, M. Fernandez-Bolanos, C. Hagleitner, M. Depont and U. T.

Duerig. Amorphous carbon active contact layer for reliable nanoelectromechanical switches. *Micro Electro Mechanical Systems (MEMS), IEEE 27th International Conference*, 143–146, 2014.

[22] C. L. Ayala, D. Grogg, A. Bazigos, M. Fernandez-Bolanos Badia, U. T. Duerig, M. Despont and C. Hagleitner. A 6.7 MHz nanoelectromechanical ring oscillator using curved cantilever switches coated with amorphous carbon. *Solid State Device Research Conference (ESSDERC), 44th European*, 66–69, 2014.

[23] D. A. Czaplewski, G. A. Patrizi, G. M. Kraus, J. R. Wendt, C. D. Nordquist, S. L. Wolfley, M. S. Baker and M. P. de Boer. A nanomechanical switch for integration with CMOS logic. *Journal of Micromechanics and Microengineering*, 19(8):085003, 2009.

[24] J. Sun, M. E. Schmidt, M. Muruganathan, H. M. H. Chong and H. Mizuta. Large-scale nanoelectromechanical switches based on directly deposited nanocrystalline graphene on insulating substrates. *Nanoscale*, 8(12):6659–6665, 2016.

[25] J.-O. Lee, M.-W. Kim, S.-D. Ko, H.-O. Kang, W.-H. Bae, M.-H. Kang, K.-N. Kim, D.-E. Yoo and J.-B. Yoon. 3-terminal nanoelectromechanical switching device in insulating liquid media for low voltage operation and reliability improvement. *Electron Devices Meeting (IEDM), IEEE International*, 9.5.1–9.5.4, 2009.

[26] M. Liao, S. Hishita, E. Watanabe, S. Koizumi and Y. Koide. Suspended single-crystal diamond nanowires for high-performance nanoelectromechanical switches. *Advanced Materials*, 22(47):5393–5397, 2010.

[27] N. Mojarad, J. Gobrecht and Y. Ekinci. Beyond EUV lithography: A comparative study of efficient photoresists' performance. *Scientific Reports*, 5:9235, 2015.

[28] G. Tallents, E. Wagenaars and G. Pert. Optical lithography: Lithography at EUV wavelengths. *Nature Photonics*, 4(12):809–811, 2010.

[29] C. Wagner and N. Harned. EUV lithography: Lithography gets extreme. *Nature Photonics*, 4(1):24–26, 2010.

[30] A. Biswas, I. S. Bayer, A. S. Biris, T. Wang, E. Dervishi and F. Faupel. Advances in top–down and bottom–up surface nanofabrication: Techniques, applications & future prospects. *Advances in Colloid and Interface Science*, 170(1):2–27, 2012.

[31] X. Shi, P. Prewett, E. Huq, D. M. Bagnall, A. P. G. Robinson and S. A. Boden. Helium ion beam lithography on fullerene molecular resists for sub-10nm patterning. *Microelectronic Engineering*, 155:74–78, 2016.

[32] V. R. Manfrinato, L. Zhang, D. Su, H. Duan, R. G. Hobbs, E. A. Stach and K. K. Berggren. Resolution limits of electron-beam lithography toward the atomic scale. *Nano Letters*, 13(4):1555–1558, 2013.

[33] V. R. Manfrinato, A. Stein, L. Zhang, C.-Y. Nam, K. G. Yager, E. A. Stach and C. T. Black. Aberration-corrected electron beam lithography at the one nanometer length scale. *Nano Letters*, 17(8):4562–4567, 2017.

[34] X.-M. Zhao, Y. Xia and G. M. Whitesides. Soft lithographic methods for nano-fabrication. *Journal of Materials Chemistry*, 7(7):1069–1074, 1997.

[35] B. D. Gates, Q. Xu, M. Stewart, D. Ryan, C. G. Willson and G. M. Whitesides. New approaches to nanofabrication: molding, printing, and other techniques. *Chemical reviews*, 105(4):1171–1196, 2005.

[36] D. Qin, Y. Xia and G. M. Whitesides. Soft lithography for micro-and nanoscale patterning. *Nature Protocols*, 5(3):491–502, 2010.

[37] M. Geissler, H. Wolf, R. Stutz, E. Delamarche, U.-W. Grummt, B. Michel and A. Bietsch. Fabrication of metal nanowires using microcontact printing. *Langmuir*, 19(15):6301–6311, 2003.

[38] A. Quist, E. Pavlovic and S. Oscarsson. Recent advances in microcontact printing. *Analytical and Bioanalytical Chemistry*, 381(3):591–600, 2005.

[39] J. Zaumseil, M. A. Meitl, J. W. P. Hsu, B. R. Acharya, K. W. Baldwin, Y.-L. Loo and J. A. Rogers. Three-dimensional and multilayer nanostructures formed by nanotransfer printing. *Nano Letters*, 3(9):1223–1227, 2003.

[40] Y. L. Loo, D. V. Lang, J. A. Rogers and J. W. P. Hsu. Electrical contacts to molecular layers by nanotransfer printing. *Nano Letters*, 3(7):913–917, 2003.

[41] J. W. Jeong, S. R. Yang, Y. H. Hur, S. W. Kim, K. M. Baek, S. Yim, H. Jang, J. H. Park, S. Y. Lee, C.-O. Part and Y. S. Jung. High-resolution nanotransfer printing applicable to diverse surfaces via interface-targeted adhesion switching. *Nature Communications*, 5:5387, 2014.

[42] S. Y. Chou, P. R. Krauss, W. Zhang, L. Guo and L. Zhuang. Sub-10 nm imprint lithography and applications. *Journal of Vacuum Science & Technology B: Microelectronics and Nanometer Structures Processing, Measurement, and Phenomena*, 15(6):2897–2904, 1997.

[43] S. Y. Chou, P. R. Krauss and P. J Renstrom. Nanoimprint lithography. *Journal of Vacuum Science & Technology B: Microelectronics and Nanometer Structures Processing, Measurement, and Phenomena*, 14(6):4129–4133, 1996.

[44] A. A. Tseng. Recent developments in nanofabrication using focused ion beams. *Small*, 1(10):924–939, 2005.

[45] J.-S. Huang, V. Callegari, P. Geisler, C. Bruning, J. Kern, J. C. Prangsma, X. Wu, T. Feichtner, J. Ziegler, P. Weinmann, M. Kamp, A. Forchel, P. Biagioni, U. Sennhauser and B. Hecht. Atomically flat single-crystalline gold nanostructures for plasmonic nanocircuitry. *Nature Communications*,1:150, 2010.

[46] Y. Chen, K. Bi, Q. Wang, M. Zheng, Q. Liu, Y. Han, J. Yang, S. Chang, G. Zhang and H. Duan. Rapid focused ion beam milling based fabrication of plasmonic nanoparticles and assemblies via "sketch and peel" strategy. *ACS Nano*, 10(12):11228–11236, 2016.

[47] A. Cui, Z. Liu, H. Dong, Y. Wang, Y. Zhen, W. Li, J. Li, C. Gu and W. Hu. Single grain boundary break junction for suspended nanogap electrodes with gapwidth down to 1–2 nm by focused ion beam milling. *Advanced Materials*, 27(19):3002–3006, 2015.

[48] W. Lu and C. M. Lieber. Nanoelectronics from the bottom up. *Nature Materials*, 6(11):841–850, 2007.

[49] L. Cademartiri and K. J. M. Bishop. Programmable self-assembly. *IEEE Control Systems*, 27(4):43–56, 2007.

[50] G. M. Whitesides and B. Grzybowski. Self-assembly at all scales. *Science*, 295(5564):2418–2421, 2002.

[51] R. P. Goodman, I. A. Schapp, C. F. Tardin, C. M. Erben, R. M. Berry, C. F. Schmidt and A. J. Turberfield. Rapid chiral assembly of rigid DNA building blocks for molecular nanofabrication. *Science*, 310(5754):1661–1665, 2005.

[52] P. W. K. Rothemund. Folding DNA to create nanoscale shapes and patterns. *Nature*, 440(7082):297–302, 2006.

[53] M. R. Jones, N. C. Seeman and C. A. Mirkin. Programmable materials and the nature of the DNA bond. *Science*, 347(6224):1260901, 2015.

[54] V. Flauraud, M. Mastrangeli, G. D. Bernasconi, J. Butet, D. Tl. L. Alexander, E. Shahrabi, O. J. F. Marin and J. Brugger. Nanoscale topographical control of capillary assembly of nanoparticles. *Nature Nanotechnology*, 12(1):73–80, 2017.

[55] S. Ni, J. Leemann, I. Buttinoni, L. Isa and H. Wolf. Programmable colloidal molecules from sequential capillarity-assisted particle assembly. *Science Advances*, 2(4):e1501779, 2016.

[56] A. Bezryadin, C. Dekker and G. Schmid. Electrostatic trapping of single conducting nanoparticles between nanoelectrodes. *Applied Physics Letters*, 71(9): 1273–1275, 1997.

[57] A. H. J. Yang, S. D. Moore, B. S. Schmidt, M. Klug, M. Lipson and D. Erickson. Optical manipulation of nanoparticles and biomolecules in sub-wavelength slot waveguides. *Nature*, 467(7225):71–75, 2009.

[58] B. K. Teo and X. H. Sun. From top-down to bottom-up to hybrid nanotechnologies: road to nanodevices. *Journal of Cluster Science*, 17(4):529–540, 2006.

[59] C. A. Ross, K. K. Berggren, J. Y. Chen, Y. S. Jung and J.-B. Chang. Three-dimensional nanofabrication by block copolymer self-assembly. *Advanced Materials*, 26(25):4386–4396, 2014.

[60] H. Im, K. C. Bantz, N. C. Lindquist, C. L. Haynes and S. H. Oh. Vertically oriented sub-10-nm plasmonic nanogap arrays. *Nano Letters*, 10(6):2231–2236, 2010.

[61] T. Li, W. Hu and D. Zhu. Nanogap electrodes. *Advanced Materials*, 22(2): 286–300, 2010.

[62] D. E. Johnston, D. R. Strachan and A. T. C. Johnson. Parallel fabrication of nanogap electrodes. *Nano Letters*, 7(9):2774–2777, 2007.

[63] H. B. Akkerman and B. de Boer. Electrical conduction through single molecules and self-assembled monolayers. *Journal of Physics: Condensed Matter*, 20(1):013001, 2007.

[64] F. Streller, G. E. Wabiszewski, F. Mangolini, G. Feng and R. W. Carpick. Tunable, source-controlled formation of platinum silicides and nanogaps from thin precursor films. *Advanced Materials Interfaces*, 1(3):1300120, 2014.

[65] D. J. Beesley, J. Semple, L. K. Jagadamma, A. Amassian, M. A. McLachlan, T. D. Anthopoulos and J. C. deMello. Sub-15-nm patterning of asymmetric metal electrodes and devices by adhesion lithography. *Nature Communications*, 5:3933, 2014.

[66] V. Dubois, F. Niklaus and G. Stemme. Crack-defined electronic nanogaps. *Advanced Materials*, 28(11):2178–2182, 2016.

[67] X. Chen, H.-R. Park, M. Pelton, X. Piao, N. C. Lindquist, H. Im, Y. J. Kim, J. S. Ahn, K. J. Ahn, N. Park, D.-S. Kim and S.-H. Oh. Atomic layer lithography of wafer-scale nanogap arrays for extreme confinement of electromagnetic waves. *Nature Communications*, 4:2361, 2013.

[68] C. Thiele, H. Vieker, A. Beyer, B. S. Flavel, F. Hennrich, D. M. Torres, T. R. Eaton, M. Mayor, M. M. Kappes, A. Golzhauser, H. v. Lohneysen and R. Krupke. Fabrication of carbon nanotube nanogap electrodes by helium ion sputtering for molecular contacts. *Applied Physics Letters*, 104(10):103102, 2014.

[69] A. Cui, H. Dong and W. Hu. Nanogap electrodes towards solid state single-molecule transistors. *Small*, 11(46):6115–6141, 2015.

[70] F. Niroui, E. M. Sletten, P. B. Deotare, A. I. Wang, T. M. Swager, J. H. Lang and V. Bulović. Controlled fabrication of nanoscale gaps using stiction. *Micro Electro Mechanical Systems (MEMS), 28th IEEE International Conference*, 85–88, 2015.

[71] M. Toda, A. Yokoyama, N. Van Toan, M. Inomata and T. Ono. Fabrication of nano-gap structures based on plastic deformation of strained Si springs by stiction effects. *Microsystem Technologies*, 21(3):649–654, 2015.

[72] F. Niroui, M. Saravanapavanantham, T. M. Swager, J. H. Lang and V. Bulović. Fabrication of nanoscale structures with nanometer resolution and surface uniformity. *Micro Electro Mechanical Systems (MEMS), 30th IEEE International Conference*, 659–662, 2017.

[73] Z. Guo, Y. Zhang, Y. DuanMu, L. Xu, S. Xie and N. Gu. Facile synthesis of micrometer-sized gold nanoplates through an aniline-assisted route in ethylene glycol solution. *Colloids and Surfaces A: Physicochemical and Engineering Aspects*, 278(1):33–38, 2006.

[74] A. Barik, X. Chen and S.-H. Oh. Ultralow-power electronic trapping of nanoparticles with sub-10 nm gold nanogap electrodes. *Nano Letters*, 16(10):6317–6324, 2016.

[75] S. I. Khondaker, K. Luo and Z. Yao. The fabrication of single-electron transistors using dielectrophoretic trapping of individual gold nanoparticles. *Nanotechnology*, 21(9):095204, 2010.

[76] A. Bezryadin, C. Dekker and G. Schmid. Electrostatic trapping of single conducting nanoparticles between nanoelectrodes. *Applied Physics Letters*, 71(9):1273–1275, 1997.

[77] S. Strobel, R. A. Sperling, B. Fenk, W. J. Parak and M. Tornow. Dielectrophoretic trapping of DNA-coated gold nanoparticles on silicon based vertical nanogap devices. *Physical Chemistry Chemical Physics*, 13(21):9973–9977, 2011.

[78] M. Ratner. A brief history of molecular electronics. *Nature Nanotechnology*, 8(6):378–381, 2013.

[79] D. Xiang, X. Wang, C. Jia, T. Lee and X. Guo. Molecular-scale electronics: from concept to function. *Chemical Reviews*, 116(7):4318–4440, 2016.

[80] H. Jeong, D. Kim, D. Xiang and T. Lee. High-yield functional molecular electronic devices. *ACS Nano*, 11(7):6511–6548, 2017.

[81] A. Vilan, D. Aswal and D. Cahen. Large-area, ensemble molecular electronics: motivation and challenges. *Chemical Reviews*, 117(5):4248–4286, 2017.

[82] J. Chen, T. Lee, J. Su, W. Wang, M. A. Reed, A. M. Rawlett, M. Kozaki, Y. Yao, R. C. Jagessar, S. M. Dirk, D. W. Price, J. M. Tour, D. S. Grubisha and D. W. Bennet. Molecular electronic devices. *Molecular Nanoelectronics*, 40114, 2003.

[83] N. J. Tao. Electron transport in molecular junctions. *Nature Nanotechnology*, 1(3):173–181, 2006.

[84] S. V. Aradhya and L. Venkataraman. Single-molecule junctions beyond electronic transport. *Nature Nanotechnology*, 8(6):399–410, 2013.

[85] J. C. Love, L. A. Estroff, J. K. Kriebel, R. G. Nuzzo and G. M. Whitesides. Self-assembled monolayers of thiolates on metals as a form of nanotechnology. *Chemical Reviews*, 105(4):1103–1170, 2005.

[86] R. Maboudian, W. R. Ashurst and C. Carraro. Self-assembled monolayers as anti-stiction coatings for MEMS: characteristics and recent developments. *Sensors and Actuators A: Physical*, 82(1):219–223, 2000.

[87] W. R. Ashurst, C. Yau, C. Carraro, R. Maboudian and M. T. Dugger. Dichlorodimethylsilane as an anti-stiction monolayer for MEMS: a comparison to the octadecyltrichlorosilane self-assembled monolayer. *Journal of Microelectromechanical Systems*, 10(1):41–49, 2001.

[88] M. Emanuela, P. Strobel, M. M. Asmar, M. Seifert, J. Li, M. Sachsenhauser, O. Ceylan, C.-A. Palma, J. V. Barth, J. A. Garrido, A. Cattani-Scholz, S. E. Ulloa and J. J. Finley. Emergence of photoswitchable states in a graphene–azobenzene–Au platform. *Nano Letters*, 14(12):6823–6827, 2014.

[89] T. A. Su, H. Li, M. L. Steigerwals, L. Venkataraman and C. Nuckolls. Stereoelectronic switching in single-molecule junctions. *Nature chemistry*, 7(3):215–220, 2015.

[90] B. Xu, X. Xiao and N. J. Tao. Seed-mediated growth of ultralong gold nanorods and nanowires with a wide range of length tunability. *Journal of the American Chemical Society*, 125(52):16164–16165, 2003.

[91] H. Song, H. Lee and T. Lee. Intermolecular chain-to-chain tunneling in metal-alkanethiol-metal junctions. *Journal of the American Chemical Society*, 129(13):3806–3807, 2007.

[92] F. W. DelRio, C. Jaye, D. A. Fischer and R. F. Cook. Elastic and adhesive properties of alkanethiol self-assembled monolayers on gold. *Applied Physics Letter*, 94(13):131909, 2009.

[93] J. E. Houston and H. I. Kim. Adhesion, friction, and mechanical properties of functionalized alkanethiol self-assembled monolayers. *Accounts of chemical research*, 35(7):547–553, 2002.

[94] F. Niroui, P. B. Deotare, E. M. Sletten, A. I. Wang, E. Yablonovitch, T. M. Swager, J. H. Lang and V. Bulović. Nanoelectromechanical tunneling switches based on self-assembled molecular layers. *Micro Electro Mechanical Systems (MEMS), 27th IEEE International Conference*, 1103–1106, 2014.

[95] J. R. Niskala, W. C. Rice, R. C. Bruce, T. J. Merkel, F. Tsui and W. You. Tunneling characteristics of Au-Alkanedithiol-Au junctions formed via nanotransfer

printing (nTP). *Journal of the American Chemical Society*, 134(29):12072–12082, 2012.

[96] W. Wang, T. Lee, and M. A. Reed. Mechanism of electron conduction in self-assembled alkanethiol monolayer devices. *Physical Review B*, 68:035416, 2003.

[97] R. E. Holmlin, R. Haag, M. L. Chabinyc, R. F. Ismagilov, A. E. Cohen, A. Terfort, M. A. Rampi and G. M. Whitesides. Electron transport through thin organic films in metal-insulator-metal junctions based on self-assembled monolayers. *Journal of the American Chemical Society*, 123(21):5075–5085, 2001.

[98] J. G. Simmons. Electric tunnel effect between dissimilar electrodes separated by a thin insulating film. *Journal of applied physics*, 34(9):2581–2590, 1963.

[99] J. G. Simmons. Generalized formula for the electric tunnel effect between similar electrodes separated by a thin insulating film. *Journal of Applied Physics*, 1963.

[100] H. B. Akkerman, P. W. M. Blom, D. M. De Leeuw and B. de Boer. Towards molecular electronics with large-area molecular junctions. *Nature*, 441(7089):69–72, 2006.

[101] G. Palasantzad, P. J. van Zwol and J. Th. M. De Hosson. Transition from Casimir to van der Waals force between macroscopic bodies. *Applied Physics Letters*, 93(12):121912, 2008.

[102] F. Niroui, A. I. Wang, E. M. Sletten, Y. Song, J. Kong, E. Yablonovitch, T. M. Swager, J. H. Lang and V. Bulović. Tunneling nanoelectromechanical switches based on compressible molecular thin films. *ACS Nano*, 9(8):7886–7894, 2015.

[103] A. Reina, X. Jia, J. Ho, D. Nezich, H. Son, V. Bulović, M. S. Dresselhaus and J. Kong. Large area, few-layer graphene films on arbitrary substrates by chemical vapor deposition. *Nano Letters*, 9(1):30–35, 2008.

[104] G. B. Barin, Y. Song, I. de Fatima Gimenez, A. G. Souza Filho, L. S. Barreto and J. Kong. Optimized graphene transfer: Influence of polymethylmethacrylate (PMMA) layer concentration and baking time on graphene final performance. *Carbon*, 84:82–90, 2015.

[105] Y.-N. Wang, W.-T. Wei, C.-W. Yang and M. H. Huang. Seed-mediated growth of ultralong gold nanorods and nanowires with a wide range of length tunability. *Langmuir*, 29(33):10491–10497, 2013.

[106] R. T. Hill, J. J. Mock, A. Hucknall, S. D. Wolter, N. M. Jokers, D. R. Smith and A. Chilkoti. Plasmon ruler with angstrom length resolution. *ACS Nano*, 6(10):9237–9246, 2012.

[107] R. T. Hill, K. M. Kozek, An .Hucknall, D. R. Smit and A. Chilkoti. Nanoparticle–film plasmon ruler interrogated with transmission visible spectroscopy. *ACS Photonics*, 1(10):974–984, 2014.

[108] N. Liu, M. Hentschel, T. Weiss, A. P. Alivisatos and H. Giessen. Three-dimensional plasmon rulers. *Science*, 332(6036):1407–1410, 2011.

[109] S. A. Soule and K. V. Cashman. The mechanical properties of solidified polyethylene glycol 600, an analog for lava crust. *Journal of Volcanology and Geothermal Research*, 129(1):139–153, 2004.